Modeling Pseudomonas syringae metabolism to interrogate in planta infection dynamics

Philip John Tubergen

Charlottesville, Virginia

B.S. Biology and Biochemistry, Calvin University, 2017

A Dissertation presented to the Graduate Faculty

of the University of Virginia in Candidacy for the Degree of

Doctor of Philosophy

Department of Biology

University of Virginia

April, 2023

Thesis Abstract:

Plants have a complex innate immune system that conveys strong resistance to most microbial organisms. To maintain vitality, plants can respond to a wide range of potential threats with increases in phytohormones, secondary metabolites, and anti-microbials that successfully inhibit growth of non-pathogenic bacteria and fungus. Dysregulation of any number of mechanisms within a plant's defensive capabilities can lead to otherwise harmless bacteria becoming serious threats to plant health. *Arabidopsis thaliana* has been used for decades as a model plant due to its genetic tractability and simple lifestyle. It is related to many important agricultural species and thus serves as a model to understand defense mechanisms plant-kingdom-wide.

Pathogenic species of microbes evade or suppress defense responses of plants and produce infections, often leading to a loss of yield in important agricultural species. Pathogenic species like *Pseudomonas syringae* (Pst) utilize host-made metabolites to produce growth and infect other tissues. The exact metabolites Pst uses during infections remain relatively uncharacterized. Due to the complexity of studying a two-organism system, we have generated a metabolic model, iPst19, to predict how the pathogen Pst produces infections in *A. thaliana* and what plant-made metabolites Pst uses while invading the leaf. iPst19 highlighted the importance of branched-chain amino acid (BCAAs) catabolism as a part of Pst combatting *A. thaliana* defenses. The availability of BCAAs reduces the infective capabilities of Pst and prevents infections from proceeding normally. In media

designed to induce virulence factor synthesis, BCAAs are still able to suppress genes related to virulence.

iPst19 helped identify BCAA metabolism bacterial genes that could play a role in helping Pst express virulence during infection. Modulating these genes in Pst caused reduced infectivity in *A. thaliana* and reduced normal growth capabilities, suggesting these genes could be potential targets for anti-microbial development. Taken together, iPst19's predictive capabilities can be an effective tool for developing strategies to prevent yield-loss in important agricultural species.

Acknowledgements

I am immensely grateful for those who have supported me throughout my graduate studies and for everyone who contributed towards my education and passions leading here:

To my parents, who were the first to instill curiosity and provoke my learning, encouraging me at every step, and who modeled kindness, generosity and a love of learning.

To my brother, who challenged me to be better as a student, as a friend, and as a person.

To my friends, who have been with me through it all: every experiment, every failure, every success, and who are always willing to celebrate every accomplishment, big or small.

To Greg, for walking me through my first forays in the computational universe, and for answering every question I had with patience despite knowing full well the answer was somewhere on StackOverflow.

To my committee, for providing much needed advice, stability and clarity to see through the minutia of my project at the bigger picture.

And finally, to Colo, for fostering the scientific spirit in me. You have challenged me to think critically about my work and its implication, to learn new techniques and hone old skills, to delve into completely uncharted waters, and to utilize a passion for discovery. You have trained me to be a better scientist, for which I am deeply grateful.

Common Abbreviations

AS – antisense overexpression
BCAA – branched-chain amino acids
CEL – conserved effector locus
CFA – coronafacic acid
CMA – coronamic acid
COR – coronatine
ETI – effector triggered immunity
GEM – genome scale metabolic model
GENRE – genome scale network reconstruction
GO – gene ontology
HMM – hrp-inducing minimal medium
HPE – hours post elicitation
HPI – hours post infiltration
Hrp – hypersensitive response and pathogenicity
HR – hypersensitive response
JA – jasmonic acid
KB – King's B medium
LA – leaf apoplasm
Lrp – leucine responsive regulatory protein
MAMPs – microbe associated molecular patterns
mM9 – modified M9 minimal medium
ORF – open reading frame
OX - overexpression
Pae – Pseudomonas aeruginosa
Pst – Pseudomonas syringae pv. tomato DC3000
PTI – pattern triggered immunity
SA – salicylic acid
T3SS – type three secretion system

Chapter 1: Introduction

Plants have evolved as sessile, resilient organisms, in part due to a complex array of defense mechanisms. At the cellular level, plants respond dynamically to the presence of microbes and differentiate between non-pathogenic species and pathogenic species. The majority of microbes that find themselves in contact with a plant cell are recognized therein by molecular patterns such as flagellin or lipopolysaccharides that they express. Recognition of these highly conserved microbial features leads to a signal cascade and the induction of plant defense hormones, heightening the plant defenses and restricting further proliferation of the microbes. Pathogenic microbes engage in more sophisticated maneuvers to avoid plant recognition or dampen the signal cascade at the early stages of the infection.

1.1 Plant Immunity

Unlike humans, plants lack a circulating, active immune system. Yet, plants are not defenseless against invading pathogens. The innate immune system in plants is far more complex than the innate immune system in humans and other animals, which likely evolved as a result of lacking an adaptive immune system that produces antibodies. The complexity of innate immunity in plants lies in a two-tiered system of pattern-triggered immunity (PTI) and effector-triggered immunity (ETI). PTI and ETI were once thought to be sequential components of the innate immune system, where PTI was first triggered by an invading microbe while further on in the infection process ETI was initiated in response to bacterial virulence factors. This timeline of infection was unofficially dubbed the “zig-zag model” of

plant innate immunity (Tsuda & Katagiri, 2010). However, in recent years, the lines between PTI and ETI have become increasingly blurred, as evidence supporting the concerted and simultaneous effects of both immune functions continues to create support for parallel activation of both arms of immunity.

Foliar infections are characterized by pathogen entry into leaves, followed by subsequent recognition by plant cells. Under homeostatic conditions within the leaf, photosynthetically active mesophyll cells produce sugars and amino acids, which are exported into the extracellular space called the leaf apoplasm (LA). Within the leaf, the LA makes up only a small portion of the volume; the majority of volume (50%-90%) is air (Lohaus et al., 2001). The remaining volume of LA is comprised of water and macromolecules that can facilitate proliferation of a pathogen such as Pst (Rico & Preston, 2008).

1.1.A Pattern Triggered Immunity

The induction of PTI occurs at the plasma membrane (PM) level of a plant cell (Chinchilla et al., 2007). Surface receptors such as FLS2 span the PM with an extracellular recognition domain and an intracellular signaling domain. Molecular patterns are the primary microbial factors recognized that induce PTI (Tsuda et al., 2008); they are highly-conserved features common to most microbes and pathogens. These include the flagellum, chitin, lipopolysaccharides, and other virtually immutable microbial features that are shared across taxa, collectively called microbe associate molecular patterns (MAMPs) (Choi & Klessig, 2016).

Upon recognition, the plant surface recognition receptors (PRR) initiate a signaling cascade that leads to transcriptional reprogramming of the plant cell. This reprogramming results in lower photosynthetic activity, production of reactive oxygen species (ROS), accumulation of defense-related hormones, and modulation of metabolite transporters (Chinchilla et al., 2007; Daudi et al., 2012; Lu et al., 2010; Zeier, 2013). Collectively, these responses define PTI and are effective at preventing the progression of infections from most microbes. In *A. thaliana* researchers can induce PTI responses with a simple injection of a synthetic peptide flg22, the minimal epitope of the protein flagellin. Thus, flagellin is a useful tool for studying the effects of PTI on invading pathogens and nonpathogens alike in a model plant species. Upon elicitation with flg22, *A. thaliana* is able to suppress the progression of infections by more than two logs of bacterial growth (Zipfel et al., 2004).

The elicitation of PTI using microbial patterns including flg22 provides useful insights into the progression of infection and the efficacy of plant inducible defenses. By using MAMPs to elicit the plant defense response, we can interrogate important mechanisms without interference by the pathogen, as a host-pathogen system is never static. For the purposes of these studies *in planta*, we have used only flg22. There are other MAMPs, such as elf26 and flg18, which cause similar responses in the plant but are considered MAMPs from different bacteria (Chinchilla et al., 2007; Daudi et al., 2012).

Many of the previously described individual facets of PTI are necessary for preventing infection progression. Plants that lack the ability to increase the level of

the phytohormone salicylic acid (SA) are particularly susceptible to infection with both pathogenic and nonpathogenic strains of *Pseudomonas.* The isochorismate synthase (*ICS*) gene is critical for converting chorismate into SA, known because the corresponding *A. thaliana* knockout mutant moniker, *sid2,* has a severely susceptible infection phenotype to Pst infections (Wildermuth et al., 2002). Transcriptional changes of metabolite transporters are similarly critical for the defense of the plant, though these changes are less well-characterized, and the implications of modulation are still being elucidated. Sugar transporters in the *STP* family are induced upon flg22 perception. The upregulation of these transporters leads to a clear depletion of hexoses in the LA; when these transporters are knocked out, plants accumulate more hexoses in the LA and are more susceptible to infection akin to a plant that cannot perceive the presence of any bacteria (*fls2*) (Yamada 2016).

Amino acid transporters are similarly modulated in response to flg22 elicitation (Khadka, in prep, Zhang et al., 2023). While this may seem like a clear relationship between nutrient access and infection progression, where access to more nutrients allows the pathogen to produce a more robust infection, the story is complicated by the pathogen response to excess nutrients. Critically, access to growth-stimulating amino acids, such as glutamine and serine, decrease the induction of virulence markers by Pst during infection in *A. thaliana* (Zhang et al., 2022, 2023b). These amino acids are some of the most abundant in flg22 treated plants, suggesting flg22-induced amino acid modulation evolved as a broad-spectrum resistance mechanism against pathogens.

1.1.B Effector Triggered Immunity

Effector triggered immunity (ETI) is substantively different but intimately connected to PTI, and is equally important for pathogen defense in the plant. ETI is more specific than PTI. A necessary feature of ETI is the recognition of bacterial effector proteins by plant R-proteins (Tang et al., 2006). ETI can enhance PTI transcription and elicit a hypersensitive response (HR), leading to localized cell death. HR is effective at preventing the spread of an infection within the LA, as it essentially creates a desert in which the pathogen cannot survive (Guo et al., 2012; Morel & Dangl, 1997). Further, there is evidence to suggest that HR primes cells both locally and distally for further pathogen invasion, leading to systemic acquired resistance (SAR)(Backer et al., 2019).

Resistance genes (R genes) express resistance proteins (R proteins) which are a diverse set of intracellular receptors that recognize bacterial made proteins. The most common family of R proteins is the nucleotide-binding /leucine-rich-repeat effector recognition (NLR) family (Cui et al., 2015). NLR proteins are typified by three main domains: a nucleotide binding domain (NB), which binds ADP/ATP; a leucine rich repeat domain(LRR), which provides effector recognition specificity and is the most variable of the three domains; and either a toll-interleukin 1 receptor (TIR) or coiled coil (CC) domain (Cui et al., 2015). In terms of plant defense, HR is incredibly effective but costly. HR is characterized by the rapid onset of cell death upon pathogen recognition. Symptoms typically include lesions on the leaf that are devoid of chlorophyll and moisture, often appearing as brown puncta (Morel & Dangl, 1997). Localized cell death is costly due to the loss of

photosynthetically active tissue within the leaf, leading to decreased carbon fixation and nutrient production.

HR can be induced by all manner of pathogens, including fungal, viral and bacterial pathogens. Within a plant-pathogen interaction, HR is induced on a gene-for-gene system (I. C. Yu et al., 1998). A plant R protein must bind with a pathogen-specific avirulent (Avr) protein; upon binding, the R protein will initiate HR through gene expression and shifts in protein recycling (Ebel J. & Mithöfer A., 1998).

Due to the high cost of HR, it is tightly regulated to prevent spontaneous cell death. Several mutants without proper regulation of HR exhibit spontaneous lesion formation without pathogen induction, resulting in the costs of HR but without the need for the defense. Regulation of NLRs includes decoy binding, where plants bind their own R proteins with decoy proteins similar to the Avr proteins of the pathogen. This appropriately prevents constitutive HR and spontaneous lesion formation. *RIN4,* present in many terrestrial plants, serves this function for many different NLRs. When *RIN4* activity is abrogated, plants exhibit spontaneous lesion formation due to the hyperactivity of paired NLRs (Toruño et al., 2019).

1.2 Pathogenesis of Pseudomonas syringae

1.2.A Type-Three Secretion System

Several pathogens utilize protein secretion as a means of mitigating host defenses and obtaining nutrients to proliferate. These secretion systems allow pathogens to establish and maintain infections within the host and are required for survival; lacking components of a secretion system often leads to failed infections where

the pathogen is easily overcome by host defenses(Büttner & Bonas, 2010; Cornelis & Van Gijsegem, 2000; Diard et al., 2013).

Many plant pathogens utilize a type three secretion system (T3SS) wherein they inject effector proteins into plant hosts to modulate the plant's defense responses. The core structures of the T3SS form a syringe-like protein bridge through which effector proteins are shuttled into the plant cell (Tang et al., 2006). The formation of this pilus is metabolically taxing, as the structure requires several large protein components. Therefore, bacteria experience a metabolic tradeoff between synthesis of the T3SS and optimal growth exists within environments conducive to T3SS expression. In *Salmonella* species, strains unable to express the T3SS outgrow T3SS+ strains during competitive *in vitro* growth assessment, illustrating the growth penalty conveyed by T3SS expression where it is not necessary for survival (Sturm et al., 2011). Conversely, when Pst is exposed to a host plant, the T3SS is absolutely necessary for a successful infection (Deng et al., 1998; Gough et al., 1992).

The tight regulation of T3SS expression is absolutely critical for colonization of a host as well as survival in permissive conditions. For *P. syringae*, early onset of T3SS is critical for preventing the induction of defense responses in the plant. In strains that lack the ability to synthesize the *hrp* pilus (called Δ*hrcC*), the pathogen fails to initiate an infection from inoculation (Deng et al., 1998).

The predominant virulence component of most *P. syringae* strains is the T3SS and suite of effector molecules that interface with the plant cellular immunity. Pst contains HR and pathogenicity (Hrp) genes, which regulate and encode the pilus

of the T3SS, avirulence (Avr) genes and Hrp-dependent outer protein (Hop), which encode effector proteins that determine the specificity of host pathogen recognition (Collmer et al., 2000). The regulator of the Hrp operon is *hrpL,* an alternate sigma factor. Conversely, the expression of the Hrp operon is repressed through constitutive activation of *hrpV*, though this phenotype is overcome by constitutive expression of *hrpL*, suggesting *hrpV* to be the upstream of *hrpL* regulation (Collmer et al., 2000; Preston et al., 1998). Interestingly, *hrpL* expression is σ-54 dependent, suggesting an intersection with metabolism (Hendrickson et al., 2000).

In *P. syringae*, as well as *Salmonella* and *Yersinia*, all of which rely heavily on the T3SS for infectivity, the main virulence related genes are often arranged compactly in pathogenicity islands (Collmer et al., 2000; Song et al., 2004). The pathogenicity islands (PI) are reported to be transferred horizontally among species, leading to rapid evolution of pathogenicity among conjugants. In *P. syringae,* the PI that contains genes coding for the *hrp* pilus are considered the minimum pathogenicity requirement *in planta* (Collmer et al., 2000).

The recently created PSRnet (a model of transcriptional regulators of virulence in Pst) illustrated further the complex regulatory networks surround virulence in *P. syringae.* Shao and colleagues have described 16 different regulators of the T3SS which contribute to expression of 391 virulence-related genes in rich (KB) and hrp-inducing media (HMM)(Shao et al., 2021).

The T3SS does not interfere with the defenses of the plant itself; rather, it is used to transport effector proteins into the plant cell. Effector proteins interact with various signaling components within plant defense pathways, either adjusting the

responses or disrupting them completely. Again, many of these genes are located within pathogenicity islands, allowing for the rapid evolution of pathogenesis in strains previously found to be avirulent (Dillon et al., 2019). One such PI is the conserved effector locus (CEL) within Pst. The CEL contains six orfs that, when deleted, severely compromise the ability of Pst to infect either tomato or *A. thaliana* (Badel et al., 2003). Importantly, the induction of Pst loci containing virulence factor related genes is only beginning to be understood. Recent studies have characterized induction by organic acids and suppression by amino acids; further, plant exudates greatly induce virulence compared to phosphate buffered saline, suggesting plant made metabolites have strong inducing capabilities(Anderson et al., 2014a; Zhang et al., 2022, 2023b).

1.2.B Coronatine

The phytotoxin coronatine (COR) plays an important role in the progression of disease when plants are assaulted by *P. syringae* strains such as Pst and Psm (P. syringae pv maculicola). Coronatine is composed of two subunits, each synthesized independently from unique metabolite pools. Coronamic acid (CMA) is directly synthesized from L-isoleucine, which could be contributing function of coronatine in mimicking jasmonic acid – isoleucine (JA-Ile) conjugants or methyl jasmonate(Bender et al., 1999; Mitchell et al., 1994). The three-step process converts L-ile to allo-L-ile, followed directly by coronamic acid (Bender et al., 1999). Mitchell and colleagues demonstrate both exogenous and synthesized isoleucine act as precursor to CMA. Further, they show that accumulation of Cma does not

disrupt the activities of enzymes within the CMA pathway in Cor producing strains of *P. syringae* (Mitchell et al., 1994).

The other moiety in coronatine, coronfacic acid (CFA), is a polyketide formed through a several step process. Previous studies suggest CFA integrates one pyruvate, one butyrate and three acetate units to form the polyketide chain, which upon modification, is formed into CFA (Parry et al., 1994). Following formation, CFA and CMA are joined via an amide bond to form COR, catalyzed by the enzyme coronafacic acid ligase (cfl). Each of the Cor synthesis operons is regulated transcriptionally by *corR* and *corS*, each of which has also been shown to have regulatory impacts on *hrpL* (Tang et al., 2006).

Production of both subunits of coronatine are controlled by two operons: *cma* and *cfl/cfa* (Panchal et al., 2016). These operons also respond to temperature, as both promoters for CMA and CFA respond optimally at 18C, with decreasing expression as temperature rises. Maximal biosynthetic production of COR was also shown at 18C (Bender et al., 1999). Other factors that impact coronatine production *in vitro* include salts, carbon source, and availability of amino acids, suggesting a potential tie of phytotoxin production to metabolic state (Palmer & Bender, 1993).

Coronatine serves a wide variety of functions during the course of infection. As a structural mimic of JA-Ile, it promotes the association of JAZ and COI1, which initiates a signaling cascade of JA. Coronatine is vastly more efficient at promoting this association, leading to a robust JA response from susceptible plants (Khadka, in prep). Further, Cor has been demonstrated to lead to a global shift in the transcriptional profile of tomato plants, causing downregulation of photosynthesis

and likely the production of another immune-responsive phytohormone salicylic acid (SA) (Zhang et al., 2023b). Typical symptoms of COR toxicity in *A. thaliana* plants include chlorotic tissue, water-soaking, and necrosis.

A key function of Cor *in planta* is induction of stomatal opening; forcing stomata to remain open is thought to promote further exacerbation of infection. COR- strains of Pst show decreased colonization in *A. thaliana* plants when infiltrated directly into the leaves; however, when a leaf dip method of infection is used, Cor- strains show dramatically reduced colonization of the leaf, owed predominantly to the stomal-opening function of COR and failed transition from leaf surface to leaf apoplast (Mittal & Davis, 1995).

1.3 Metabolism-Virulence Crosstalk

1.3.A Environmental Queues impacting Virulence

It is well documented in many pathogenic prokaryotic species that virulence is partially impacted through sensing of the environment, including *P. syringae*. A study by Yu and colleagues highlighted the role of transcriptional regulators in the transition from epiphytic to endophytic environments. These two differ strongly; where the outside of the leaf is carbon restrictive with low humidity, the inside of the leaf is carbon rich and saturated. Yet, *P. syringae* is able to recognize both environments and initiate a transition from outside to inside the leaf using alternative sigma factors (X. Yu et al., 2013).

It has become clear that metabolic apoplastic markers are an important player in inducing virulence for Pseudomonas. Anderson and colleagues discovered an

array of virulence-inducing plant metabolites that contribute to the resistance phenotype of *A. thaliana* mutant *mkp1.* When a metabolic profile of *mkp1* plants was assembled in an attempt to explain this resistance phenotype to Pst, several organic and amino acids had decreased concentrations in mutant, resistant plants. In part, susceptibility seems to be correlated with accumulation of cAMP intracellularly, which *mkp1* cannot achieve. When Pst is co-infiltrated with citrate, aspartate, and 4-hydroxy-buteric acid (4hba), not only does cAMP levels rise to WT levels in *mkp1* plants, but CFU/cm^2 also returns to WT levels, suggesting a correlation between organic acids, intracellular cAMP, and T3SS induction (Anderson et al., 2014a).

Pst virulence is differentially induced in a carbon source specific manner. The bacteria seem to have preferred carbon sources for producing growth, such as amino acids and organic acids (Rico & Preston, 2008). Hexoses, like fructose and glucose, seem to readily induce virulence and do not sustain high growth rates (Anderson et al., 2014a; Stauber et al., 2012).

Amino acids have emerged as important regulators of virulence through various mechanisms. Amino acid supplementation into the LA during infection with Pst decreased long-term leaf colonization in an AA-specific manner. *Pst* shows decreased colonization of the leaf after 72 hours when co-infiltrated with either glutamine, serine, or valine (Zhang et al., 2022, 2023b). Branched-chain amino acids (BCAAs), including valine, have been shown to regulate virulence in gram-negative bacteria by modulating the activity of the global transcriptional regulator

Lrp (Kaiser & Heinrichs, 2018). *Lrp* activity responds to the bacterial nutritional state and regulates both virulence and the transition into the stationary phase.

1.3.B Leucine-responsive regulatory protein

Leucine-responsive regulatory protein (Lrp) acts as a global regulator of metabolism in gram-negative bacteria (Landgraf et al., 1996). Lrp has been extensively studied in *E. coli,* where it has been attributed with shifting expression of over 700 genes in a condition-specific manner (Kroner et al., 2019). Lrp and lrp-like proteins are conserved in prokaryotes, though the highest degree of conservation in form and function seems to be within the γ-proteobacteria group (Brinkman et al., 2003). Lrp and related transcriptional regulators often respond to specific substrates, notably amino acids such as leucine. Leucine seems to be an especially potent and important substrate, it is the most represented residue in proteins on average (at 9.1% of residues), suggesting a role as a nutrient and protein stability sensor (Brinkman et al., 2003).

In the case of *E. coli* Lrp, cytoplasmic Lrp forms hexadecamers, which have regulatory functions and can dissociate upon interaction with free L-leucine (Chen et al., 2001). As the concentration of leucine increases, either through uptake, biosynthesis, or proteolysis, the hexadecamers dissociate into leucine-bound octamers, which modulate the expression of genes (Chen et al., 2001). Lrp has been shown to repress and induce expression in the presence and absence of L-leucine (as well as other amino acids). Previous studies have suggested Lrp participates in the modulation of expression of the *ilv* branched-chain amino acid

biosynthetic operon, *gvc* glycine cleavage system, and *glt* glutamine biosynthetic operon. These three operons are important for maintaining proper levels of amino acids within the cell while efficiently providing building blocks for secondary metabolites and nitrogen moieties (Cho et al., 2008). The association of *leucine*-responsive regulatory protein with biosynthetic and catabolic operons utilizing other amino acids may not be apparent outright, however the interconnectedness of the metabolic network surrounding amino acid metabolism renders control at one locus a potential checkpoint for another amino acid.

The complexity of expression modulation by Lrp is not trivial. According to Cho and colleagues, six modes of Lrp expression modulation exist: independent induction or repression, concerted induction or repression, and reciprocal induction or repression (Cho et al., 2008) (Table 1.1). Independent modes require Lrp, but expression is modulated regardless of concentration of leucine. Concerted modes require leucine to induce modulation, while reciprocal modes require leucine to repress modulation (Cho et al., 2008). Because in many instances Lrp directly responds to the concentration of BCAAs intracellularly, it can be thought of as a BCAA sensor that alters transcription in response to changing levels of BCAAs (Figure 1.1A). Within the scope of the following studies, we leverage this facet of regulation to understand how BCAA levels or genetic alteration of Lrp levels, both of which disrupt the homeostatic equilibrium of [Lrp]/[BCAA] intracellularly and could impact transcriptional targets (Figure 1.1AB).

Lrp not only modulates expression of metabolic genes, but also virulence genes. In *Salmonella enterica*, when Lrp is constitutively active, virulence was severely

attenuated in a mouse infection model. Conversely, an Lrp deletion resulted in hypervirulence, suggesting Lrp functions as a switch regarding nutritional status and virulence induction (Baek et al., 2009). In *Xenorhabdous nematophila*, an insect pathogen and nematode mutualist, Lrp controls the different symbioses with these organisms. Lrp-null strains of *X. nematophila* were unable to exhibit the same extent of nodulation and did not produce a robust immune response in the larvae of *Manduca sexta,* both hallmarks of attenuated virulence. Interestingly, when the nematode *Stienernema carpocapsae* is grown on plates containing Lrp-null *X. nematophila,* the number of offspring produced falls dramatically. Both phenotypes of *X. nematophila* Lrp- mutants are attributed to loss of modulation of virulence factors and mutualism factors (Cowles et al., 2007). In *Vibreo cholerae*, Lrp-null organisms could not initiate expression of *aphA*, a transcription factor responsible for increasing expression of the cholera pathogenicity island (Lin et al., 2007). The contrasting roles of Lrp in *S. enterica* and *X. nematophila/V. cholerae* regarding virulence could suggest Lrp also plays a role in the virulence of *Pseudomonas syringae* while infecting *A. thaliana.*

Table 1.1

Mode	Gene/Operon	Functional Notes
Independent Inducing	gcvT	Glycine cleavage; releases ammonium moiety
Independent Repressing	ftsQ	Cell division protein
Concerted Inducing	fadJ	Involved in anaerobic fatty acid degradation
Concerted Repressing	livKJ	High- affinity leucine transport
Reciprocal Inducing	gltB	Glutamine synthase
Reciprocal Repressing	thrL	Biosynthesis of threonine

Table 1.1. Modes of regulatory action and transcriptional targets of Lrp in *E. coli*. Adapted from Cho et al, 2008. Functional notes obtained from Uniprot.

Figure 1.1

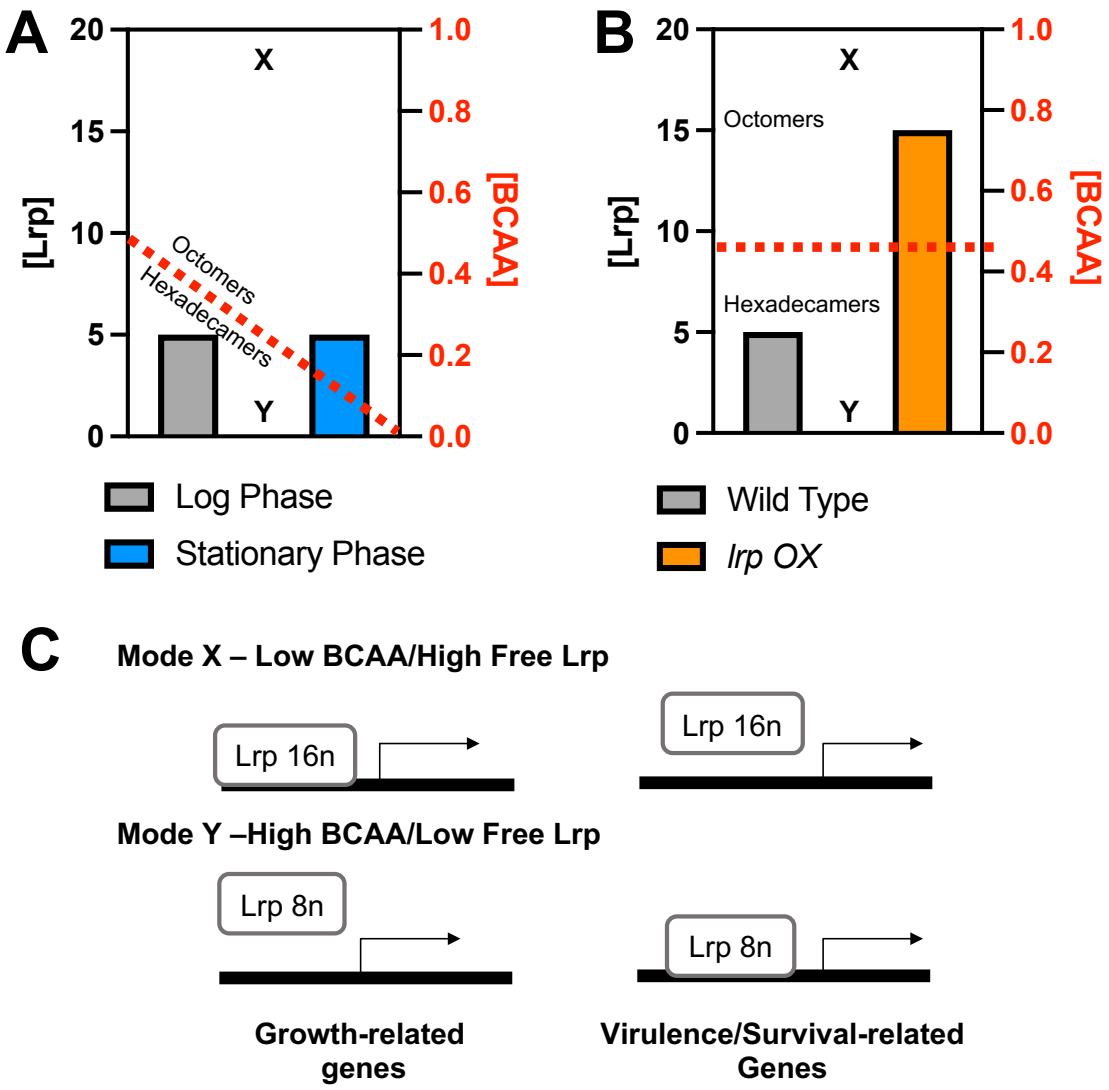
A
20
15
10
5
0
[Lrp]
1.0
0.8
0.6
0.4
0.2
0.0
[BCAA]
X
Y
Octomers
Hexadecamers
Log Phase
Stationary Phase
B
Octomers
Hexadecamers
Wild Type
Irp OX
C
Mode X – Low BCAA/High Free Lrp
Lrp 16n
Lrp 16n
Mode Y –High BCAA/Low Free Lrp
Lrp 8n
Lrp 8n
Growth-related genes
Virulence/Survival-related Genes

Figure 1.1. Schematic representations of Lrp and its response to concentrations of BCAAs. A. The concentrations for both Lrp (bars) and BCAAs (dotted line) in a non – genetically perturbed bacteria growing from log phase (gray bar) to stationary phase (blue bar), where over the growth period, the concentrations of BCAAs (red line) decrease. When the bar has a larger value than the line, the BCAA concentration is not high enough to keep Lrp in hexadecameric form and causes a transcriptional shift. B. Representation of genetically perturbing Lrp levels through overexpression. Regardless of the timepoint, the overexpression of Lrp forces Lrp concentrations higher than the BCAA threshold, thus causing dissociation into the octameric form and causing transcriptional shifts. C. Schematic representation of the transcriptional program of Lrp as it relates to A and B. Binding of Lrp to a promoter region can either support transcription or suppress transcription, as detailed by Cho et al, 2008. For the simplicity of this schematic, Lrp bound to the promoter is inducing transcription.

Chapter 2: Creating, validating and constraining of iPst19 predicts BCAA importance during foliar infection[1]

2.1 Summary

A. thaliana and Pst engage in a complex exchange of virulence and defense strategies that involve plant-made changes in metabolite composition in the LA during infection. Due to the technical challenges of isolating apoplastic washing fluid and the dynamic changes in composition imparted by both the pathogen and its host, the identity of important LA metabolites that Pst uses to propagate an infection has only begun to be characterized recently. Here, we have created a new tool for addressing these complexities. iPst19 is a metabolic model that we use to query metabolic changes Pst undergoes during the course of an infection. iPst19 predicts metabolites important for sustaining growth, such as hexoses and amino acids, but also highlights the most likely metabolic pathways used to convert available nutrients into biomass. Further, constraining iPst19 metabolic flow using global gene expression profiles from Pst actively infecting *A. thaliana*, we have predicted disproportionate flux through the BCAA catabolic pathway in Pst infecting defense-elicited plants, while auxiliary pathways to BCAA catabolism are predicted to carry less flux.

[1] This chapter was completed in collaboration with Gregory Medlock, PhD. PT and GM contributed to the design of the experiments. PT contributed to the writing of initial and final published code for creating the model and final experimental analyses and visualizations. GM contributed to the debugging of final code and initial integration of transcriptomic data.

2.2 Introduction

The LA complex composition and the dynamic concentration changes in metabolites that take place during the course of an infection makes it difficult to define which plant metabolites, and at which concentrations, would have a positive or a negative impact on Pst growth in planta. In an attempt to capture this complexity, recently published studies have used bacterial gene expression profiling as a means to understand how PTI affects Pst growth and virulence (Lovelace et al., 2018; Nobori et al., 2018a). These two studies hypothesized that PTI could suppress the expression of bacterial virulence genes through metabolite deprivation, as previously reported by Anderson and colleagues (Anderson et al., 2014a). In addition, Nobori and colleagues found that PTI also suppresses the expression of genes encoding ribosomal proteins, suggesting that PTI may affect Pst protein synthesis as well. Besides reaching similar conclusions with regard to Pst virulence suppression, these two studies reached dissimilar conclusions with regards to the plant metabolites that restrict Pst growth *in planta*. While Lovelace et al. proposed that sulfur may become limiting under PTI conditions, Nobori et al discovered that Pst iron uptake and iron metabolism pathways were indicative of iron starvation. This apparent discrepancy in addressing which plant metabolites are limiting under PTI conditions may stem from experimental differences across these studies. However, it is also possible that Pst transcriptomics analyses alone would be insufficient to capture the complexity of the metabolic changes that define Pst growth in planta. To address these potential limitations, we have generated an

ensemble **ge**nome-scale **n**etwork **re**constructions (GENREs) to assess multi-omics data with an “aerial” vantage point.

GENREs, and their corresponding modeling counterparts genome-based models (GEMs), have emerged as a powerful tool for predicting metabolic phenotypes and gene essentiality (Blazier & Papin, 2012). They have facilitated drug development and have contributed to better understanding the mechanisms driving evolution of antibiotic resistance in bacteria. GEMs consist of biochemical reaction pathways with associated genes (if known) that reflect the metabolism of an organism. They are originally built from genome annotations and are curated with various forms of evidence, including in vitro metabolic demands, organismal homology and literature research (Thiele & Palsson, 2010). Within a GEM, transport reactions facilitate movement of metabolites from one compartment (i.e. the outside environment) to another compartment (i.e. inside the cell). Gene expression data can be overlaid on top of a GEM framework to make integrative predictions of metabolic outcomes. Multiple algorithms for integrating gene expression data with GEMs have been developed, each of which make assumptions about the relationship between gene expression and reaction activity (Richelle et al., 2019). GENREs may be best thought of as a network of pipes. The pipes all have an input and output, and these pipes may initially start with a common diameter. The arrangement of the pipes may also determine how fast water can move from input to output. As water flows through the pipes, the rate of gallons of water is determined by the diameter of the pipe. In the context of an objective function like biomass production, the GENRE pipe network only has one output but many

nutritional inputs. Integration of transcriptomic data serves to change the diameter of the pipe, and thus the rate which water can flow through particular subnetworks (or metabolic pathways) of the whole pipe network. In this way, we can use transcriptomic data as a snapshot of how expression of upstream genes affects flow downstream in the pathway, giving us a better view of organismal response to different conditions.

2.3 Materials and Methods

Initial Reconstruction:

The Pst genome assembly used was originally contributed by Buell and colleagues (Buell et al., 2003). The draft GENRE was generated using ModelSEED (v2.1) (Seaver et al., 2021) and the RAST database (Aziz et al., 2008) and further optimized using the cobrapy toolbox. The Pst GENRE was refined using cross-species homologous comparisons with two *Pseudomonas aeruginosa* models, iPau1129 and iPae1146. Due to the high amount of protein comparisons being made between two species, we used the DIAMOND alignment software (Buchfink et al., 2014). DIAMOND is similar in sensitivity to BLASTn, yet runs considerable faster with less computational demand, thus it is suitable for large dataset queries. DIAMOND alignments were made between Pst annotated protein features and *P. aeruginosa* annotated protein features included in the respective GENREs. Comparisons that yielded a significant (e-value < 0.0001) were queried for associated reactions in the *P. aeruginosa* GENREs and subsequently added to the Pst GENRE with the significantly matching homolog if there was sufficient literature with supporting evidence for protein function. While the e-value threshold is relaxed compared to many studies regarding the evolution of homologs and protein sequence similarity, the purpose of this step was to generate a list of potential targets for inclusion in the model,

based on previously curated models. This targeted list was further manually curated by looking for functional evidence in the literature.

Bacterial Growth Conditions:

Pst was grown in liquid King's B culture at shaking at 230 RPM and 28C. Bacteria for growth rate assessment was taken from fresh LB agar plates and grown overnight in the liquid media, followed by sub-culturing 10% until mid-exponential phase.

Initial Reconstruction and Gap Filling

The draft was further curated through ensemble gap filling. A full schematic of the process is depicted in Figure 2.1. To gap fill and further curate the GENRE, we used an approach called Automated Metabolic Model Ensemble-Driven Elimination of Uncertainty with Statistical learning (AMMEDEUS) (Medlock & Papin, 2020). The inconsistencies in gap filled solutions between ensemble members that influence simulation uncertainty are identified using the resulting output of AMMEDEUS, generating a targeted curation list. Gap filled reactions that presented the most uncertainty were assessed for literature support in Pst and other Pseudomonas, specifically looking for evidence that supported the existence of a molecular function. This iterative process was completed 3 times to form the current 100-member iPst19 ensemble (Figure 2.1). Importantly, this is not only the first metabolic model create for Pst, but also, this model uses AMMEDEUS and the ensemble modelling approach to increase the predictive capabilities of the metabolic model. We have also leveraged the curation of two previous *Pseudomonas* models to aid in the rapid but accurate curation of iPst19.

In total, AMMEDEUS gap filling consistently added reactions until biomass production was satisfied; 16 of the added reactions fell within an "uncertain"

category. They included reactions related to arginine transport and synthesis, nitric oxide metabolism, and nitric oxide oxidoreduction reactions. In these cases, the gap filling process across the 100 ensemble members use two distinct reactions to complete a pathway; however, there was no obvious consensus among the members as to which reaction would be the most parsimonious addition. In these cases, we queried the contesting reactions for any supporting evidence in the literature. In the case where there was clear evidence for one pathway architecture over another, we added these reactions to the base model and performed AMMEDEUS again. In cases where the uncertainty could not be alleviated with literature support, neither pathway architecture was added to the base model.

Biomass quantification:

Pst was grown as previously described in bacterial growth conditions. Liquid cultures were centrifuged at 3500 RPM for 10 minutes. Growth media was removed, the pellet was washed twice using sterile water. The pellet was resuspended in 10 mL sterile water and immediately frozen. Samples were lyophilized. Samples were split for each quantification assay, ensuring the samples would be matched for the different quantification protocols. Dry weights of each fraction were recorded. Total protein was quantified using a standard Bradford's assay on lysed cells. DNA was extracted from lyophilized cells using the Cold Spring Harbor Laboratory DNA extraction from Gram negative bacteria protocol. RNA was extracted from lyophilized cells using the aforementioned RNA extraction protocol. Both RNA and DNA were quantified using spectrophotometry. All quantifications were normalized to the total dry weight of bacterial cells.

Ensemble Generation:

A full description of the ensemble process and justification was recently published by Medlock and Papin (Medlock & Papin, 2020). iPst19 was generated from the cross-species compared draft reconstruction with integration from single carbon source utilization data (see Biolog growth assays). Each substrate that produced positive growth as defined by significantly different maximum measured OD600nm from the negative control was compiled into a randomly-ordered list for use in gap-filling the draft reconstruction. The specific order of metabolites is important during the gap-filling process, as only the most parsimonious use of the metabolite will result in addition of reactions. If a metabolite can be utilized with the metabolic infrastructure already in place, no new reactions will be added; otherwise, the reactions that add the minimum amount of flux will be added to make use of the metabolite. Only when the draft reconstruction is gap filled and can satisfy the fixed-growth constraint of the biomass function and minimize the fluxes through all other reactions on all *in vitro* growth-producing metabolites (as empirically assessed with Biolog plates), it is then considered a member of the ensemble. The process repeats, starting with the draft reconstruction and a shuffled order of the growth-producing metabolites. All of the members have slightly different architectures and may produce different biomass fluxes on simulated medias. With each round of ensemble gap filling, the 20 most uncertain reactions (where members did not agree on the necessary inclusion of a reaction) introduced by AMMEDEUS we manually curated via literature research. This resulted in the addition of 16 reactions of previously high uncertainty with curated literature support for a particular architecture within the members. The full repository is available at https://github.com/gregmedlock/psy_recon.

Inclusion of Coronatine synthesis pathway

Considering the importance of coronatine for *P. syringae,* we also included the biosynthetic pathway for COR synthesis in iPst19. For simulating virulence

conditions, COR synthesis could be included as part of the objective function for iPst19. For the simulations in this work, included the active pathway, but did not require its activity to satisfy the objective function because the majority of our simulations would be in permissive, non-virulence inducing conditions. The architecture of the pathway is abbreviated due to the uncertainty specifically surrounding the synthesis of the CFA arm of COR production. The CMA arm of synthesis is fully included, starting with the production of allo-Ile from Ile, followed by the conversion of allo-Ile into CMA as annotated by Bender and colleagues (Bender et al., 1999). Conversely, the CFA arm of synthesis remains largely and mechanistically unknown. It is assumed that 3 acetate molecules, 1 butyrate and 1 pyruvate are used in conjunction with acyl-carrier proteins to synthesize CFA, therefore, these are the moieties that comprise the reaction used to simulate CFA synthesis in iPst19. Finally, CFA and CMA are joined with the release of 1 water molecule to form COR. The schematic representation of these pathways is depicted in Figure 2.3.

Biolog growth assays:

Biolog PM1 and PM2 plates were inoculated with 100uL of inoculating fluid 0 (IF0) (Biolog, Inc.) per well, in which Pst was suspended at 0.07 OD600 from fresh agar plates. Biolog plates were shaken at 7000 rpm and 28C for 60 hours. OD600 measurements were taken every 12 hours. Gas permeable film was secured to the plate to ensure gas exchange but prevent evaporation, but were removed prior to spectrophotometric reading. Baseline was subtracted before use in figures and in analysis. Metabolites that had been previously described as producing growth in the literature had more than 0.1 OD, while the baseline sat around 0.08. Metabolites that we knew from previous literature did not produce growth

never crossed the 0.1 threshold; therefore, this seemed like an appropriate threshold to set threshold that could easily distinguish between obvious growth and no growth.

Gene ontology assessment:

Genes included within iPst19 were ontologically assessed with PANTHER. The same was done for the whole genome of Pst. Results were normalized to the whole and compered.

Single carbon source simulations:

SCS growth simulations were performed by constraining the transport reactions for only one specific carbon source at a time. Other metabolites, such as water and salts present in Biolog IF-0, were not restricted to ensure simulated growth similar to *in vitro* growth in the Biolog plates.

Ensemble Transcriptomic Integration:

RNAseq global gene expression profiles of Pst exposed to mock and flg-22 elicited plants generated by Nobori and colleagues were integrated into iPst19 members using the GIMME algorithm modified from the Driven package (https://github.com/opencobra/driven). Genes are first stripped from the ensemble, after which they are iteratively added back into the ensemble as a function of expression and significance. The minimum framework needed to satisfy the objective function was assessed for fluxes across all reactions.

Ensemble Single Gene Deletions:

For each member in iPst19, every gene within the member was simulated as a loss of function. For reactions with only one gene association, flux of the reaction became zero. Reactions in which the gene deletion was part of an “and” association, the reaction flux also became zero. For reactions where the deleted gene was in an “or” association, the reaction flux was unaltered. Final readouts of objective function flux were assessed: if the reaction flux was zero or near zero (flux<10e-5), the gene was predicted to be an essential gene. The media compositions tested were similarly derived as the SCS media, excluding

"complete" media and "*in planta*" media. "Complete" media does not have any supplemental constraints; if there is a transporter present within the ensemble, iPst19 will have access to it. The "*in planta*" media was comprised of a rough estimation of carbon and nitrogen sources profiled from *A. thaliana* leaf apoplast by Anderson and colleagues (Anderson et al., 2014b).

Ensemble Multi-Carbon Growth Media Gene Essentiality:

Multi-carbon media simulations were made from L-leucine and D-glucose combinations as a percent of the total carbon atoms present in the media. Combinations included 100% glucose, 99% glucose:1% leucine, 90% glucose:10% leucine, 50% glucose:50% leucine, 10% glucose:90% leucine, 1% glucose:99% leucine, and 100% leucine.

2.4 Results

Biomass Equation

An essential part of GEMs is the objective function, often a simulation of growth or maximization of ATP production. For iPst19, we have generated a semi-species-specific biomass function, building off of the previously established biomass function for E. coli and Pseudomonas aeruginosa. We have experimentally determined total protein content, RNA content, and DNA content in exponential phase Pst in liquid culture. Amino acid and nucleotide fractions were determined from published genome content and CDS content (Buell et al., 2003). We further tailored the lipid, lipopolysaccharide, and polyamine pools quantified in other Pseudomonas species. The full set of coefficients for the biomass function can be found in Figure 2.2.

Comparison to other metabolic models

Basic metrics of a metabolic model include reactions, metabolites, and gene-product-rules (GPRs) which associate a gene with an enzymatic reaction. While there is no accepted threshold for a well-curated model, it is understandable that a more complete model will more closely reflect similar metrics (GPR numbers closer to the total number of genes, i.e. more genes are included in the model because more functions are known about these genes) for the organism itself. E. coli W and its corresponding model are considered to be one of the most well-studied organisms and well-curated models. The model contains 1372 GPRs and 2782 reactions, both of which are considerably higher than the most complete *Pseudomonas* model for strain PAO1. iPst19 is much more similar in size and coverage compared to PAO1, suggesting more curation is necessary, yet iPst19 is sufficient to make predictions (Table 1.1).

Carbon Utilization and Simulation

We performed single carbon source growth phenotyping using Biolog (Hayward, California) phenotype microarrays PM1 and PM2a. We grew Pst in each of 190 single carbon sources in quadruplicate and recorded the optical density at 600nm (OD600) at 0, 12, 24, 36, 48, and 60 hours (Figure 2.5). In order to only include high-confidence positive growth conditions for gap filling, we only considered conditions that resulted in a max OD600 greater than 0.1 as positive growth conditions (after subtraction of 0-hour baseline).

Many amino acids and sugars produced sufficient positive growth over 60 hours of incubation in Biolog plates. Figure 2.5A presents growth curves for all 190 carbon substrates, with metabolites previously shown to have an impact on infection dynamics between Pst and *A. thaliana* highlighted in color (Anderson et al., 2014a; Rico & Preston, 2008). GABA, a highly abundant amino acid in the apoplast of tomato plants, produced robust growth, as did L-glutamine, sucrose, and D-glucose (Figure 2.5A). We then assessed the *in silico* biomass production on single carbon sources to preliminarily validate the ensemble. Of the highlighted substrates in Figure 2.5A, all in silico simulations were able to predict the in vitro growth outcome (Figure 2.5B).

Predictive Gene Essentiality – Core

Within an ensemble, gene essentiality varies depending on the media composition and on the associated potential constraints of the ensemble. A list of essential genes needed for Pst to grow using various metabolites present in the LA as carbon sources was generated through iterative exclusion of genes and associated reactions from the models. A range of media conditions were tested including complete medium, simulated LA medium, as well as minimal medium supplemented with either L-aspartate, citrate, D-fructose, D-glucose, L-glutamine, L-leucine, sucrose, or γ -aminobutyric acid (GABA), all of which have been previously described in the LA as metabolites that support Pst growth. Due to the alternative configuration of pathways within each of the 100 ensemble members, some genes will be predicted as essential in one configuration but not in another,

resulting in “essentiality probability”. In order for a gene to be predicted as truly essential it has to meet the criteria of being called essential in all 100 ensemble members used in the simulation. From a total of 889 genes, our analysis identified 136 predicted essential genes necessary for biomass production on all tested media (Figure 2.6A). These can be considered the core essential genes; regardless of media type, these genes are necessary to fulfill the biomass objective function in the simulations. Genes included in this category fall within well-known metabolic pathways, such as glycolysis and the TCA.

In addition, the analysis identified 31 media-specific predicted essential genes (Figure 2.6B). The 31 conditionally essential genes consist of 21 genes that are common to all single C source media and 10 genes that are essential in some but not all single C source media. Interestingly, gene essentiality profiles are almost completely shared among different minimal media where L-amino acids are the only carbon source. However, the L-leucine minimal medium rendered three additional catalytic genes predicted to be essential: PSPTO_2736 (*liuD*), PSPTO_2738 (*liuB*) and PSPTO_2739 (*liuA*), each of which is involved in the branched-chain amino acid (BCAA) catabolic pathway. These genes are orthologous to those in the PA14 liu/gny operon (Dunphy et al., 2019).

Comparison between glucose and leucine alone

We highlighted the gene essentiality screen in three distinct media: complete media, glucose minimal media, and leucine minimal media, because of the clear essentiality patterns in Figure 2.6B and because sugar metabolism has been

previously implicated as an important factor during Pst infections in Arabidopsis. Similarly, BCAA metabolism has been previously identified as important for a range of pathogens, include Pseudomonas aeruginosa and Xanthamonas citri (Nelson et al., 2019a; Tomassetti et al., 2018). When queried only for glucose and leucine-containing media, the SCS gene essentiality looks almost identical to the previous visualization presented in Figure 2.6B. However, from a total of 889 genes, the analysis identified 136 predicted essential genes necessary for biomass production in complete media (Figure 2.7A). In addition, we identified 28 substrate-specific predicted essential genes (Figure 2.7B). Twenty-three genes were common to both glucose and leucine SCS media, and 5 were differentially essential to one or the other substrate.

Predictive Gene Essentiality – Semi-complex Defined Media

Single carbon substrate media provide valuable information regarding metabolite utilization but do not mimic the organism growth in its natural, more complex environment. We simulated biomass accumulation and generated a gene essentiality profile on media formulations with mixed carbon sources that introduce more complexity to metabolites available for biomass production. The simulated mixed media we used contained D-glucose and L-leucine in varying concentrations for each metabolite. These metabolites serve two functions: glucose alone is metabolite that produces robust growth experimentally yet lacks a nitrogen moiety, while L-leucine produces modest growth experimentally, but provides a nitrogen moiety as a part of the single carbon source, thus potentially relieving nitrogen

limitation. L-leucine minimal media also produced a distinct gene essentiality profile in silico when compared to other amino acids, allowing us to assess the impact of metabolite supplementation on predicted gene essentiality. Total availability of mixed substrates in the media was maintained at 10mM/gDW. In a mixed substrate with 99% glucose and 1% L-leucine, gene essentiality matches predicted gene essentiality in D-glucose alone. Similarly, in a mixed substrate with 1% D-glucose and 99% L-leucine, the essentiality profile resembles that of L-leucine alone. The essentiality profile of 50% D-glucose and 50% L-leucine, as well as those with 10% of the second substrate, included fewer genes than either single substrate (Figure 2.8A). The essentiality of genes was not a binary output immediately alleviated by introducing the secondary metabolite. Instead, there was a predicted threshold at which leucine alleviated glucose-only derived gene essentiality and *vice versa* (Figure 2.8AB).

Transcriptomics integration to assess differential metabolic states in mock or flg22 elicited plants

To understand the metabolic states the bacteria could develop over the course of infection, we conditionally restricted iPst19 by integrating gene expression data obtained from Pst 5h after inoculation of mock or flg22-treated wild-type Arabidopsis plants. Using the RIPTIDE integration method, we created differentially constrained ensembles that reflect the metabolic states of the bacteria in these conditions. Compression of flux variability of all shared reactions across the differentially constrained members using non-metric multidimensional scaling

(NMDS) revealed a broad swath of shared metabolism between the two conditions, with distinct patterning between conditions as well (Figure 2.9A). When the same flux variability samples were subjected to random forest machine learning, the most determinant reactions causing differences in the NMDS plot included many amino acid related reactions, of which BCAA related reactions were present.

Transcriptomics integration to assess BCAA catabolic differences

Because the genes within the *liu* cluster are uniquely essential in leucine minimal medium (Figure 2.6), have a relatively small threshold of essentiality (Figure 2.8AB), and several bacterial pathogens tightly regulate internal levels of BCAA during host invasion (Kaiser & Heinrichs, 2018; Subashchandrabose et al., 2009; Tomassetti et al., 2018), we hypothesized that these genes could provide useful insights into how BCAAs could be related to Pst pathogenesis. To understand if these genes contributed to the Pst pathogenesis during Arabidopsis infection, we conditionally restricted iPst19 by integrating gene expression data obtained from Pst 5h after inoculation of mock or flg22-treated wild-type Arabidopsis plants. By contextualizing the iPst19 with gene expression profiles, we were able to integrate not only information about how much a transcript is expressed, but also created a framework for understanding the potential additive effects of several genes in a metabolic pathway being only moderately induced.

We constrained the ensemble using a previously published *in planta* Pst gene expression data set (Nobori et al., 2018a) using the GIMME integration algorithm. For our interests, we focus only on gene expression profiles within this data set

from Pst exposed to mock or flg22 elicited plants for five hours, representing an early infection stage. To capture early events of the interaction between Pst and Arabidopsis that to prevent differences in bacterial population size in Pst-inoculated mock- *versus* flg22-pretreated plants, Nobori and colleagues used a high initial bacterial titer (OD_{600nm} 0.2) and a 6h inoculation time point to take samples for gene expression analysis. We integrated the gene expression data set into iPst19 using GIMME (Gene Inactivity Moderated by Metabolism and Expression). GIMME prunes reactions from iPst19 that do not meet an expression threshold for the associated annotated genes. This reduces the network reconstruction to an experimentally-based minimal model; typically, these models do not produce biomass, rendering growth simulation unattainable. Therefore, GIMME will systematically lower the threshold and add reactions back into iPst19 until the biomass function can be satisfied. Because there is relevant literature showing the importance of BCAA levels and pathogenesis, we directly assessed the fluxes of the BCAA catabolic pathway between mock and flg22 conditions (Figure 2.10). Overall, in the mock condition, there was more transport of leucine into ensemble members, yet the actual catabolism of leucine into 4-methyl-2-oxopenanoate (4MOP), isovaleryl-CoA, and methylcrotonyl-CoA was enriched in the flg22 condition. In mock-pretreated plants, the off-shoot metabolism (not directly related to BCAA catabolism) of Pst was enriched disproportionately. This included the conversion of 4MOP into 2-isopropyl-2-oxosucciante, which is ultimately converted into other amino acids. iPst19 did not predict any differential flux between mock and flg22 conditions for either leucyl-tRNA production or the

conversion of isovaleryl-CoA into isovaleryl-ACP. The contribution of leucine to the biomass objective is held constant, so no differential flux would have been expected.

GO Enrichment of Multiple Transcriptomic Datasets

The gene expression analysis of Pst colonization of mock or flg22-pretreated plants has shown major differences in the expression pattern of metabolism and virulence. When comparing Pst gene expression in mock- and flg22-pretreated plants to naïve plants, there were also substantial differences in the overall gene expression profile. Figure 2.11 illustrates the major changes using GO terms, where the differential expression of genes from mock or flg22 compared to naïve plants within a GO term are averaged. Within the top twenty most differentially expressed GO terms, some are shared between mock and flg22, such as calmodulin binding and activity.

2.5 Discussion

Our analysis of single carbon source utilization by Pst is one of the most extensive published to date. While we have only highlighted carbon sources of interest in this study, a total of 64 carbon sources produced significant Pst growth in liquid culture. This wide range of growth-producing metabolites is consistent with Pst lifestyle (Massey et al., 1976). Pseudomonas syringae is predominantly a hemi-biotrophic plant pathogen found in over 50 plant species and in a diverse range of environments (Xin et al., 2018). When comparing the carbon sources used by Pst

against the human pathogen Pseudomonas aeruginosa, both organisms can grow on a wide variety of substrates. However, the properties of the carbon sources are categorically different. Pst produces biomass on 14 amino acids and 20 organic acids compared to PA14, which produces biomass on 7 amino acids and 14 organic acids.

Studies assessing the infectivity of *P. aeruginosa* have revealed some overlap in hosts with Pst *(i.e. A. thaliana)* presumably due to the expression of highly conserved virulence factors. *P. aeruginosa* is an opportunistic human pathogen that infects the respiratory tract of immunocompromised patients, skin lesions of healthy patients and the lungs of cystic fibrosis patients (Bodey et al., 1983). A more recent study revealed the importance of *P. aeruginosa* trehalose biosynthesis for maintaining infections in planta, while simultaneously revealing the requirement of plant-made xyloglucan working in concert with trehalose to satisfy nitrogen needs of P. aeruginosa (Djonović et al., 2013). To our knowledge, a similar requirement for virulence does not exist in Pst, yet other metabolites have been previously shown to induce virulence and metabolic shifts. L-aspartic acid, in concert with fructose, has been shown to induce the T3SS, an essential step required to produce infections in *A. thaliana* (Anderson et al., 2014a; Turner et al., 2020). Conversely, both L-serine and L-glutamine suppress virulence *in planta*, likely through a completely unrelated regulatory mechanism (Zhang et al., 2022).

The predicted gene essentiality of Pst presented in Figure 2.6 reveals a large, core set of 130 essential genes that is common across all media types. Many of these genes are related to amino acid, nucleotide, and cofactor production, all of which

are part of the biomass objective function in iPst19.These findings are again supported by the study from Helmann and colleagues, who found the functional categories of “cofactor metabolism”, “amino acid transport and metabolism”, and nucleotide metabolism and transport” to be in the top six most essential functional categories, along with “translation”, “energy generation”, and ”no functional category” (Helmann et al., 2019). Further, genes that facilitate the transport of C sources in each media type become necessary, if not already predicted as essential in all media types. In media containing only carbohydrate carbon sources such as sucrose, the gene that codes for an ammonium transporter (PSPTO_0218) is predicted as essential due to the lack of nitrogen-containing metabolites in the medium. Without a nitrogen-containing carbon source, ammonium is essential for producing amino acids and polyamines among other N-containing metabolites. While ammonia freely diffuses across the cell membrane, the necessary amounts of nitrogen cannot be met by diffusion alone. Therefore, microbes will express ammonium transporters in nitrogen-depleted conditions to compensate, such as a sugar minimal media (Kim et al., 2012). Even small amounts of amino acids within the simulated medium do not alleviate the need for NH4 transport. In Figure 2.10, we have shown how the addition of 1% L-leucine is not sufficient for alleviating the predicted essentiality of the ammonium transporter. However, this small addition of L-leucine to a glucose media is sufficient to reduce the predicted essentiality of 3-isopropylmalate dehydrogenase (PSPTO_2175), a critical enzyme in the biosynthesis pathway of BCAAs (Wallon et al., 1997). This

reveals a potentially dynamic system that can respond to small changes in the concentrations of critical metabolites.

Transcriptomic integration into iPst19 has highlighted the potential importance of the BCAA catabolism during the course of infection in defense elicited plants, which has not been previously described in the literature for Pst, despite gene expression profiling showing induction of BCAA catabolic genes in two independent data sets. While flux through the biomass function remained constant between Pst in mock-treated plants and flg22-treated plants, the reactions associated with *liuA* and BCAA catabolism broadly carried disproportionate flux in defense elicited plants (Figure 2.10). Considering the connection of intracellular BCAA levels to virulence in other species of pathogens,

While the expression of these genes is driving the flux within the BCAA catabolic pathway, it is important to highlight the inclusion of significantly differentially expressed genes (DEG) within iPst19. In total, 251 genes are significant DEGs that are also included in iPst19. Both Nobori and colleagues, as well as Lovelace and colleagues, report clear patterns revolving around iron and sulfur metabolism as the highlights of early, *in planta* infections by Pst. Indeed, iPst19 is able to capture these changes based on transcriptomic integration with GIMME. Of the 251 DEGs in iPst19, 11 of them are related to sulfur metabolism and 9 to iron metabolism. Further, a large proportion of metabolic flux went through glycolysis and the TCA cycle when iPst19 was constrained with Pst gene expression data from mock-treated plants, which reflects what has previously been described by Yamada and colleagues. These findings reflect patterns already explored in the

literature, suggesting that iPst19 can highlight already known elements of host-pathogen interactions, as well as highlight new facets of the interaction such as the predicted importance of maintaining intracellular BCAA concentrations presented here.

These findings add support to the use of a metabolic model like iPst19 to contextualize gene expression data. While both the Nobori and Lovelace studies highlighted the importance of iron and sulfur metabolism during the onset of infection, respectively, they overlook other expression signatures present within their datasets that iPst19 was able to contextualize, such as BCAA metabolism, a finding that will be explored in further detail in this thesis. Herein lies the advantage of metabolic modeling: while there could be large changes in expression for a small subset of genes related to a type of metabolism (often highlights through GO enrichment) each of these genes could be the only gene within a given pathway that is highly upregulated. Similarly, there could be several genes, each of which contributes to the same pathway, that have only moderate changes in expression, yet the overall effect on the metabolism is additive and significant. Likely, moderate changes in expression with every gene in a pathway can contribute to a greater metabolic change that oen gene that is highly changed. Therefore, even if there are other signatures that are apparent in a transcriptional dataset, like sulfur and iron metabolism, iPst19 can be used to highlight patterns within transcriptional data that are not apparent without contextualization by a metabolic model.

2.6 Figures

Figure 2.1

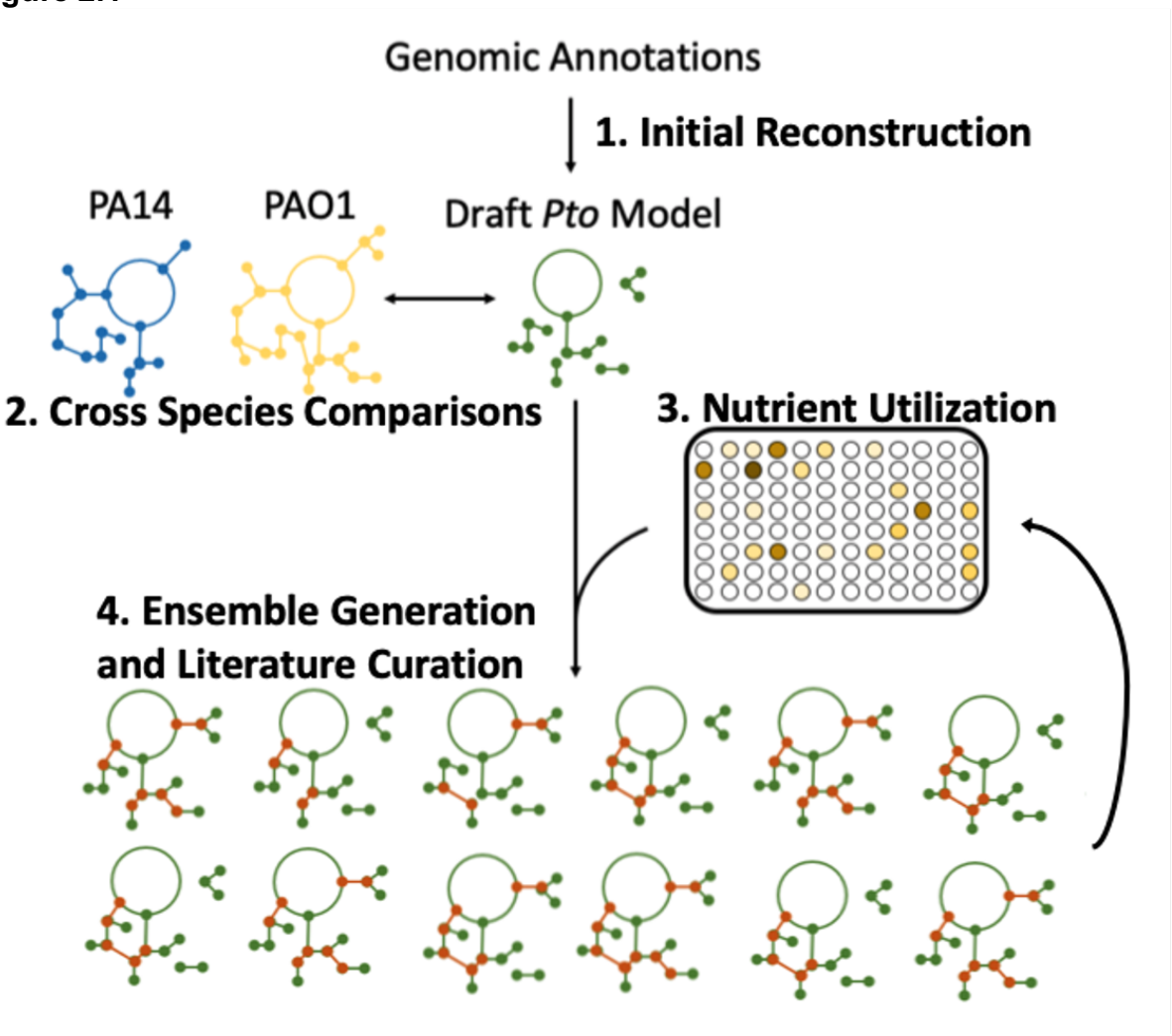

Figure 2.1. A schematic representation of the full reconstruction process for iPst19. Genome annotations were obtained from K.E.G.G., originally curated by Buell and collogues in 2003. **1.** The initial reconstruction was generated from the genome annotations using ModelSEED. **2.** This reconstruction was compared to two other GENREs for *Pseudomonas aeruginosa* strains PAO1 and PA14 (Bartell et al., 2017; Oberhardt, Puchałka, Fryer, Martins Dos Santos, et al., 2008). Homologs with significant similarity computed by DIAMOND between these strains and Pst that also have a curated reaction and functional evidence in the literature were added to iPst19 if missing. **3.** Single carbon source utilization was assessed (data presented in Figure 2.5) for Pst. For carbon sources that produce biomass, exchange reactions were added to the draft GENRE. **4.** Carbon sources that produce growth *in vitro* were assembled into a list of metabolites for gap-filling the GENRE. After a GENRE was gap filled, becoming a member of the ensemble, the order of the metabolites used was shuffled, and the draft GENRE was gap-filled again. Ensembles of 100-500 members were created, curated, and re-gap-filled with curated reactions.

Figure 2.2

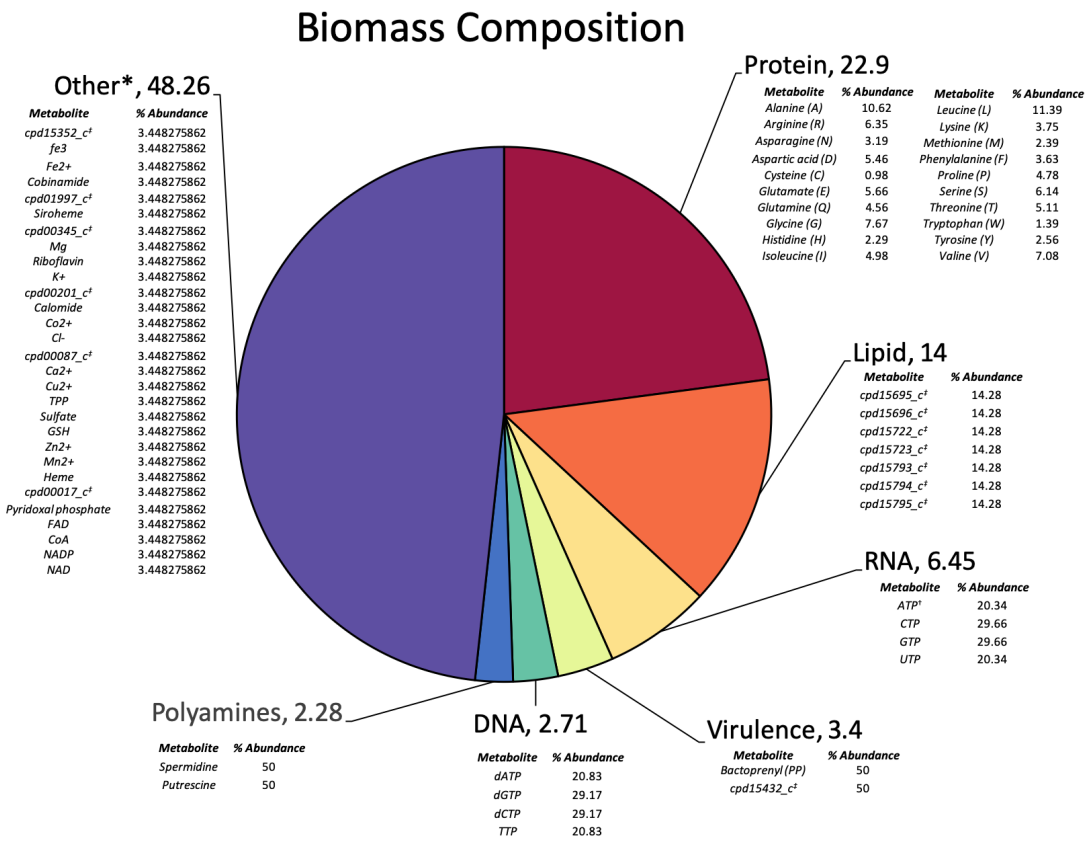
Biomass Composition
Other*, 48.26
Metabolite % Abundance
cpd15352_c‡ 3.448275862
fe3 3.448275862
Fe2+ 3.448275862
Cobinamide 3.448275862
cpd01997_c‡ 3.448275862
Siroheme 3.448275862
cpd00345_c‡ 3.448275862
Mg 3.448275862
Riboflavin 3.448275862
K+ 3.448275862
cpd00201_c‡ 3.448275862
Calomide 3.448275862
Co2+ 3.448275862
Cl- 3.448275862
cpd00087_c‡ 3.448275862
Ca2+ 3.448275862
Cu2+ 3.448275862
TPP 3.448275862
Sulfate 3.448275862
GSH 3.448275862
Zn2+ 3.448275862
Mn2+ 3.448275862
Heme 3.448275862
cpd00017_c‡ 3.448275862
Pyridoxal phosphate 3.448275862
FAD 3.448275862
CoA 3.448275862
NADP 3.448275862
NAD 3.448275862
Protein, 22.9
Metabolite % Abundance Metabolite % Abundance
Alanine (A) 10.62 Leucine (L) 11.39
Arginine (R) 6.35 Lysine (K) 3.75
Asparagine (N) 3.19 Methionine (M) 2.39
Aspartic acid (D) 5.46 Phenylalanine (F) 3.63
Cysteine (C) 0.98 Proline (P) 4.78
Glutamate (E) 5.66 Serine (S) 6.14
Glutamine (Q) 4.56 Threonine (T) 5.11
Glycine (G) 7.67 Tryptophan (W) 1.39
Histidine (H) 2.29 Tyrosine (Y) 2.56
Isoleucine (I) 4.98 Valine (V) 7.08
Lipid, 14
Metabolite % Abundance
cpd15695_c‡ 14.28
cpd15696_c‡ 14.28
cpd15722_c‡ 14.28
cpd15723_c‡ 14.28
cpd15793_c‡ 14.28
cpd15794_c‡ 14.28
cpd15795_c‡ 14.28
RNA, 6.45
Metabolite % Abundance
ATP† 20.34
CTP 29.66
GTP 29.66
UTP 20.34
Polyamines, 2.28
Metabolite % Abundance
Spermidine 50
Putrescine 50
DNA, 2.71
Metabolite % Abundance
dATP 20.83
dGTP 29.17
dCTP 29.17
TTP 20.83
Virulence, 3.4
Metabolite % Abundance
Bactoprenyl (PP) 50
cpd15432_c‡ 50

Figure 2.2. Composition of the biomass function of iPst19. Coefficients for the biomass function were either experimentally determined from four independent cultures in KB media or informed by literature and coefficients from other *Pseudomonas* species. Each macromolecular category is further subdivided to show the overall composition of each category, where possible.

Figure 2.3

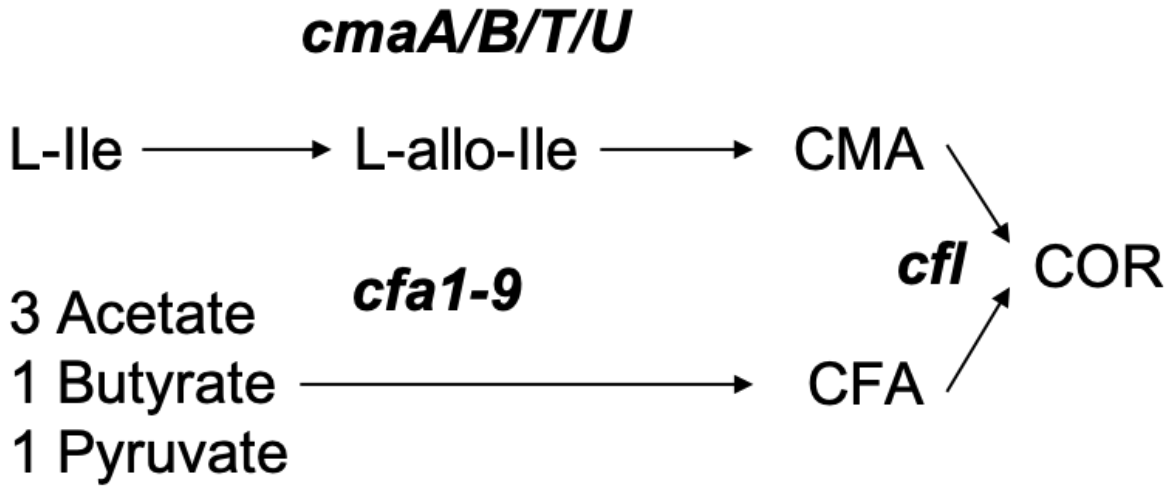
cmaA/B/T/U
L-Ile
L-allo-Ile
CMA
cfl
COR
cfa1-9
3 Acetate
1 Butyrate
1 Pyruvate
CFA

Figure 2.3. Schematic representation of the coronatine biosynthetic pathway included in iPst19. This pathway requires the starting metabolites of isoleucine, acetate, butyrate, and pyruvate to form CMA, CFA and finally COR. The genes predicted to be responsible for each arm of the pathway are depicted in bold above each segment. Adapted from Bender and colleagues (Bender et al., 1999).

Figure 2.5

A

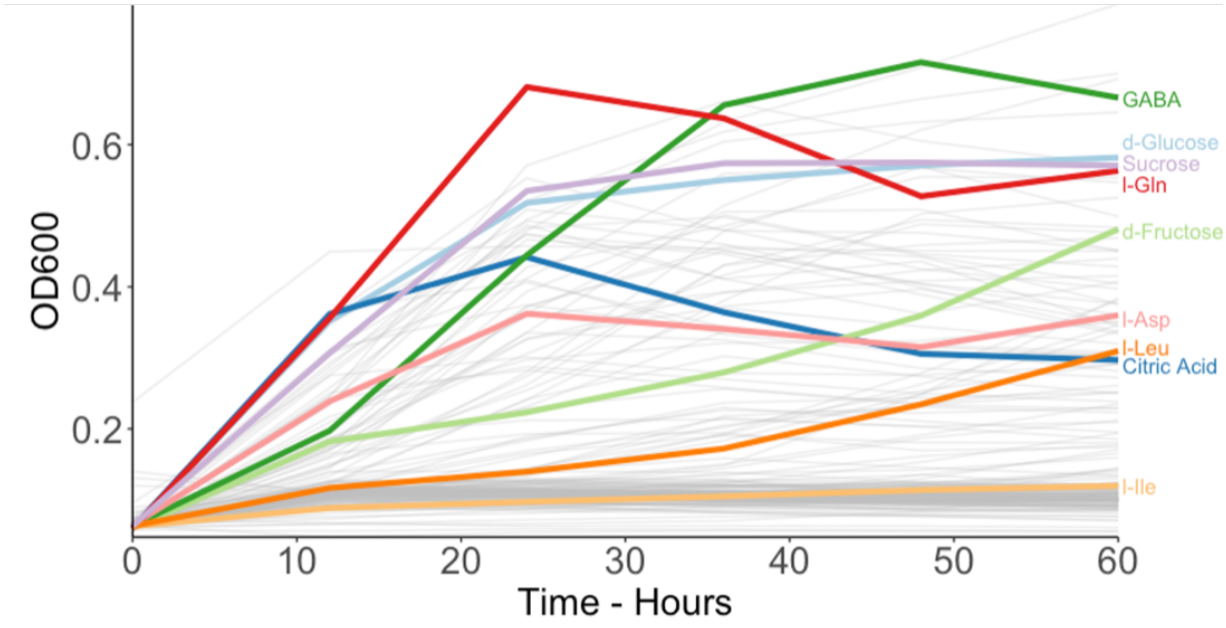

B

	Sucrose	D-Fructose	D-Glucose	L-Gln	GABA	L-Leu	L-Ile	Citrate
Growth Status	+	+	+	+	+	+	-	+

Figure 2.5. Single carbon source utilization of amino acids, sugars and organic acids *in vitro* and *in silico.* A. Optical density at 600 nm was assessed in 190 distinct carbon sources over 60 hours. Highlighted in color are metabolites shown to produce growth and virulence in previous works. In grey are the growth curves for the other 181 carbon sources. **B.** The highlighted metabolites in A were assessed for *in silico* utilization in iPst19. Presented is a binary of biomass production when uptake of the carbon source is limited to 10mM/g dry weight.

Figure 2.6

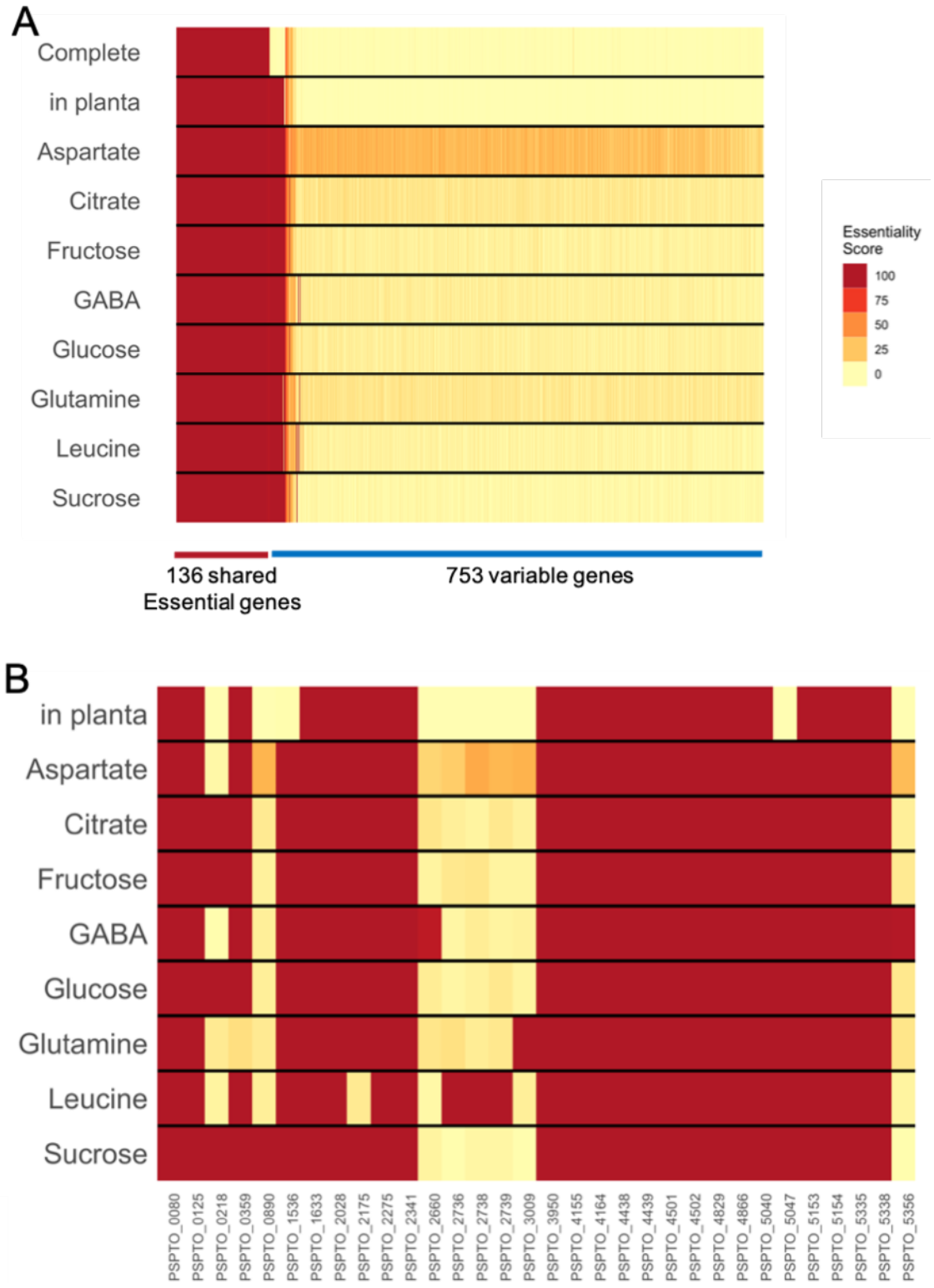
A
Complete
in planta
Aspartate
Citrate
Fructose
GABA
Glucose
Glutamine
Leucine
Sucrose
Essentiality Score
100
75
50
25
0
136 shared Essential genes
753 variable genes
B
in planta
Aspartate
Citrate
Fructose
GABA
Glucose
Glutamine
Leucine
Sucrose
PSPTO_0080
PSPTO_0125
PSPTO_0218
PSPTO_0359
PSPTO_0890
PSPTO_1536
PSPTO_1633
PSPTO_2028
PSPTO_2175
PSPTO_2275
PSPTO_2341
PSPTO_2660
PSPTO_2736
PSPTO_2738
PSPTO_2739
PSPTO_3009
PSPTO_3950
PSPTO_4155
PSPTO_4164
PSPTO_4438
PSPTO_4439
PSPTO_4501
PSPTO_4502
PSPTO_4829
PSPTO_4866
PSPTO_5040
PSPTO_5047
PSPTO_5153
PSPTO_5154
PSPTO_5335
PSPTO_5338
PSPTO_5356

Figure 2.6. Predicted gene essentiality across various media simulations. Each gene is removed from an ensemble one at a time and final biomass production was assessed. Each medium formulation was used for its suggested importance in the literature. **A.** Predicted essentiality in each media condition is given out of 100 ensemble members. An essentiality score of 100 indicates essentiality in all 100 ensemble members, while a score of 0 indicates non-essentiality in all members. Across all media conditions, there are 136 shared predicted essential genes. **B.** Predicted essential genes disparate from complete media. Twenty-one genes are shared across the different media, while eleven genes have varying degrees of essentiality corresponding to media type.

Figure 2.7

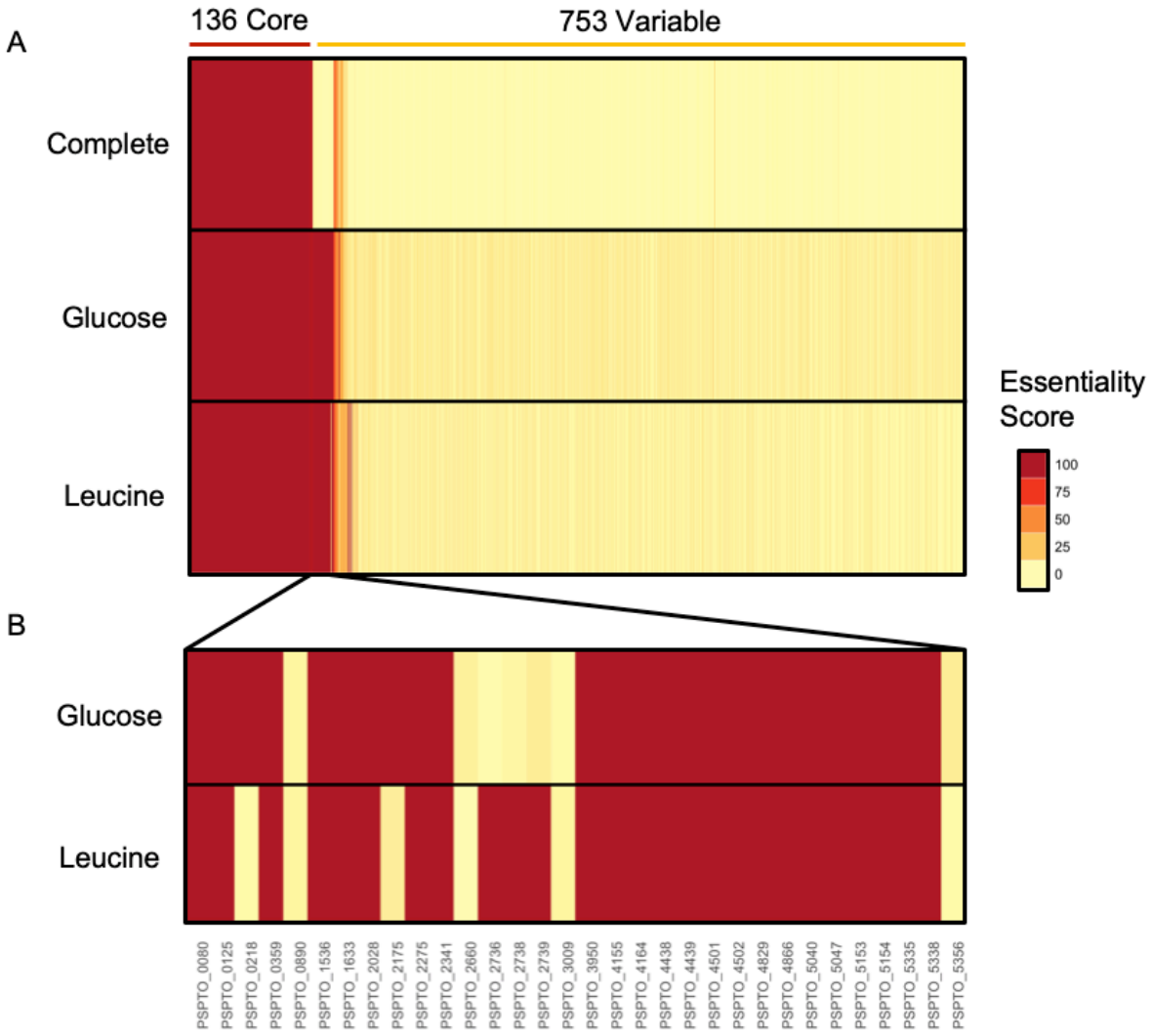
A
136 Core
753 Variable
Complete
Glucose
Leucine
Essentiality Score
100
75
50
25
0
B
Glucose
Leucine
PSPTO_0080
PSPTO_0125
PSPTO_0218
PSPTO_0359
PSPTO_0890
PSPTO_1536
PSPTO_1633
PSPTO_2028
PSPTO_2175
PSPTO_2275
PSPTO_2341
PSPTO_2660
PSPTO_2736
PSPTO_2738
PSPTO_2739
PSPTO_3009
PSPTO_3950
PSPTO_4155
PSPTO_4164
PSPTO_4438
PSPTO_4439
PSPTO_4501
PSPTO_4502
PSPTO_4829
PSPTO_4866
PSPTO_5040
PSPTO_5047
PSPTO_5153
PSPTO_5154
PSPTO_5335
PSPTO_5338
PSPTO_5356

Figure 2.7. Predicted gene essentiality across complete, glucose, or leucine media simulations. A. Predicted essentiality in each media condition is given out of 100 ensemble members. Across all media conditions, there are 136 shared predicted essential genes. B. Twenty-three predicted glucose- and leucine-specific essential genes are shown, five of which have varying degrees of essentiality depending on the carbon source used. Three genes of the liu operon (PSPTO_2736, PSPTO_2738, and PSPTO_2739) are essential to use leucine as the sole carbon source.

Figure 2.8

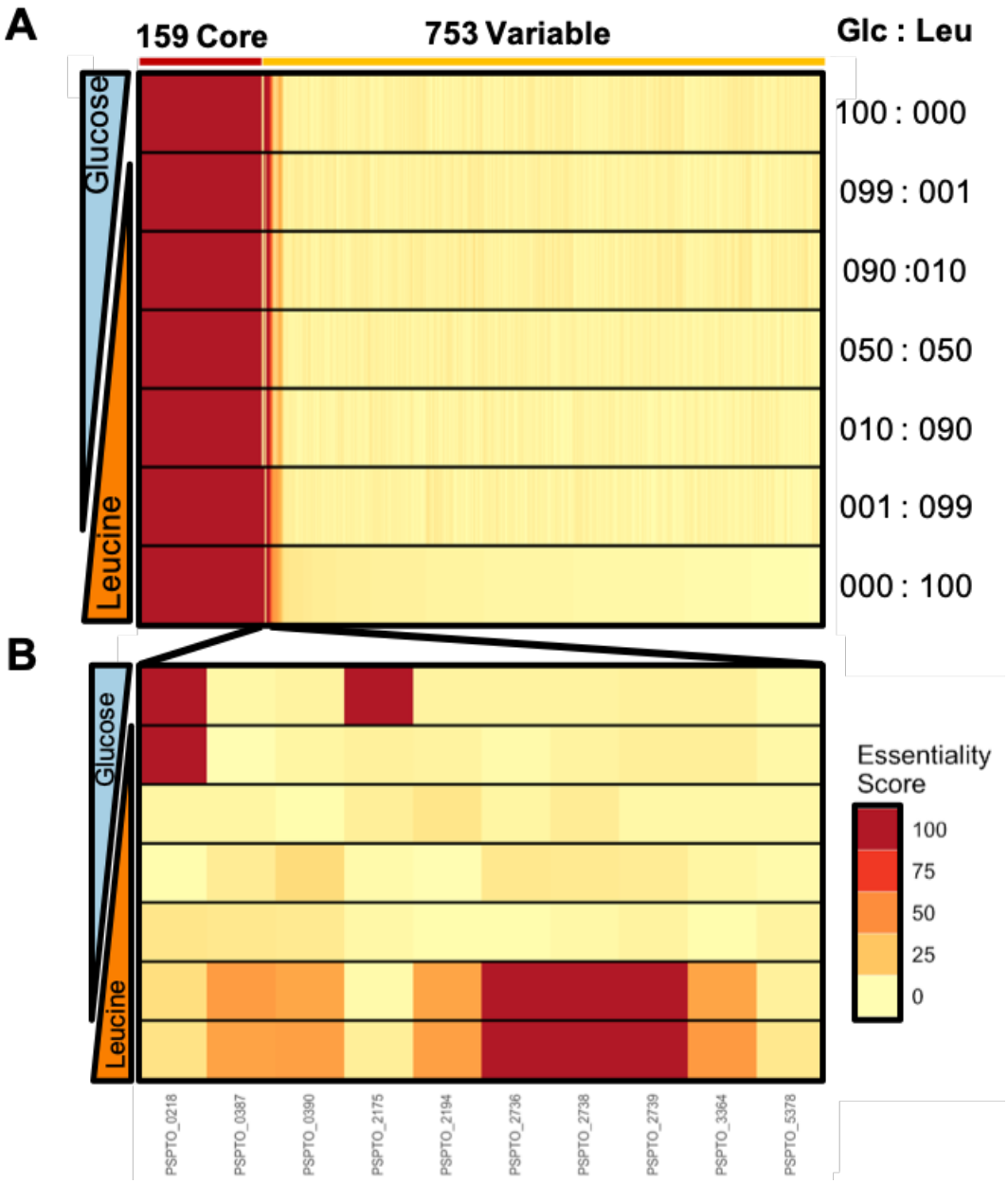
A
159 Core
753 Variable
Glc : Leu
Glucose
Leucine
100 : 000
099 : 001
090 :010
050 : 050
010 : 090
001 : 099
000 : 100
B
Glucose
Leucine
Essentiality Score
100
75
50
25
0
PSPTO_0218
PSPTO_0387
PSPTO_0390
PSPTO_2175
PSPTO_2194
PSPTO_2736
PSPTO_2738
PSPTO_2739
PSPTO_3364
PSPTO_5378

Figure 2.8. Predicted gene essentiality changes with mixed carbon sources. iPst19 growth was simulated in conditions where carbon sources were restricted to an uptake rate of 10 mM/g dry weight. The carbon composition of the Glc and Leu simulated media is indicated to the right. (A) All genes present in iPst19 were simulated for essentiality. (B) The most dissimilar essential genes in D-glucose and L-leucine simulated medium.

Figure 2.9

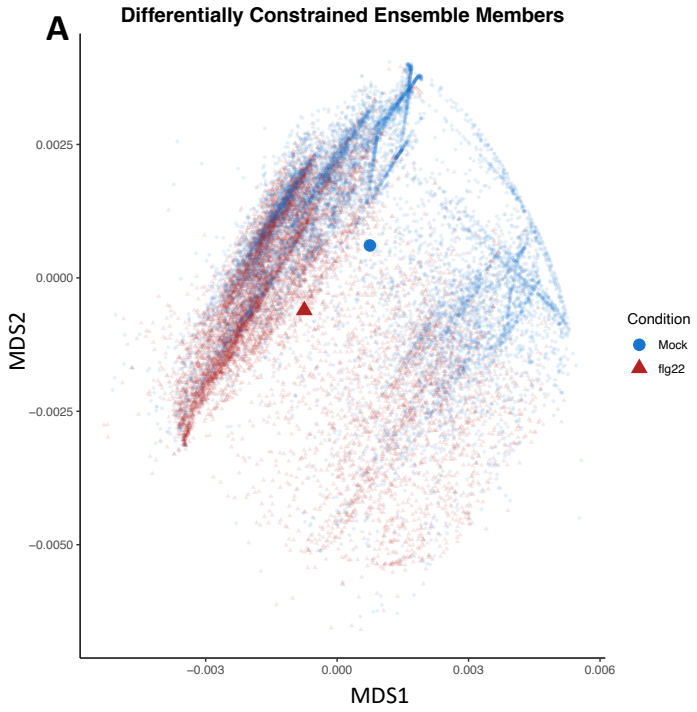
A
Differentially Constrained Ensemble Members
0.0025
0.0000
−0.0025
−0.0050
MDS2
−0.003
0.000
0.003
0.006
MDS1
Condition
Mock
flg22

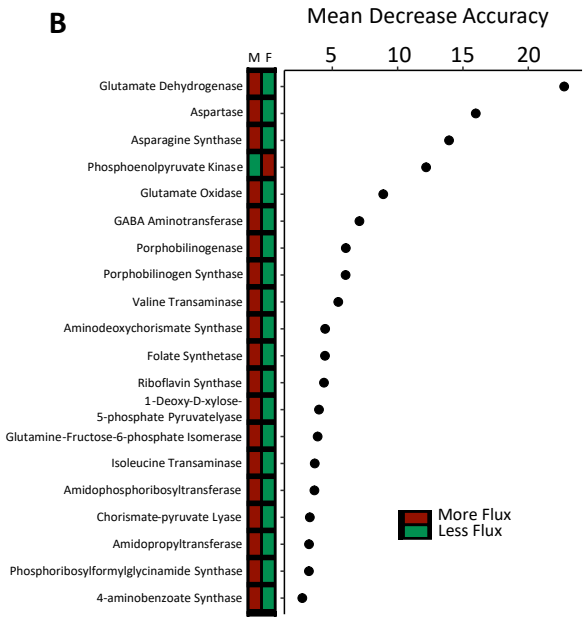
B
Mean Decrease Accuracy
M F
5
10
15
20
Glutamate Dehydrogenase
Aspartase
Asparagine Synthase
Phosphoenolpyruvate Kinase
Glutamate Oxidase
GABA Aminotransferase
Porphobilinogenase
Porphobilinogen Synthase
Valine Transaminase
Aminodeoxychorismate Synthase
Folate Synthetase
Riboflavin Synthase
1-Deoxy-D-xylose-
5-phosphate Pyruvatelyase
Glutamine-Fructose-6-phosphate Isomerase
Isoleucine Transaminase
Amidophosphoribosyltransferase
Chorismate-pyruvate Lyase
Amidopropyltransferase
Phosphoribosylformylglycinamide Synthase
4-aminobenzoate Synthase
More Flux
Less Flux

Figure 2.9. Contextualization of global gene expression reveals broad similarities and differences in metabolic state. RNAseq datasets (Nobori et al., 2018a) were integrated into iPst19 to constrain fluxes of reactions using the RIPTIDE integration algorithm. A. NMDS analysis of individual flux subsamples from within each ensemble member is presented, with blue circles representative of fluxes from mock constrained members and red from flg22 constrained members. Centroids for each condition are highlighted as a larger point within the plot. B. Random forest assessment of influential condition-determining reactions. Each point is representative of the decrease in accuracy (as a percent) of assigning the proper condition by which the members were constrained if the given reaction is removed from the forest. The colored bar indicates which condition carried more constrained flux (red) or less constrained flux (green) within each condition, as an average across all members.

Figure 2.10

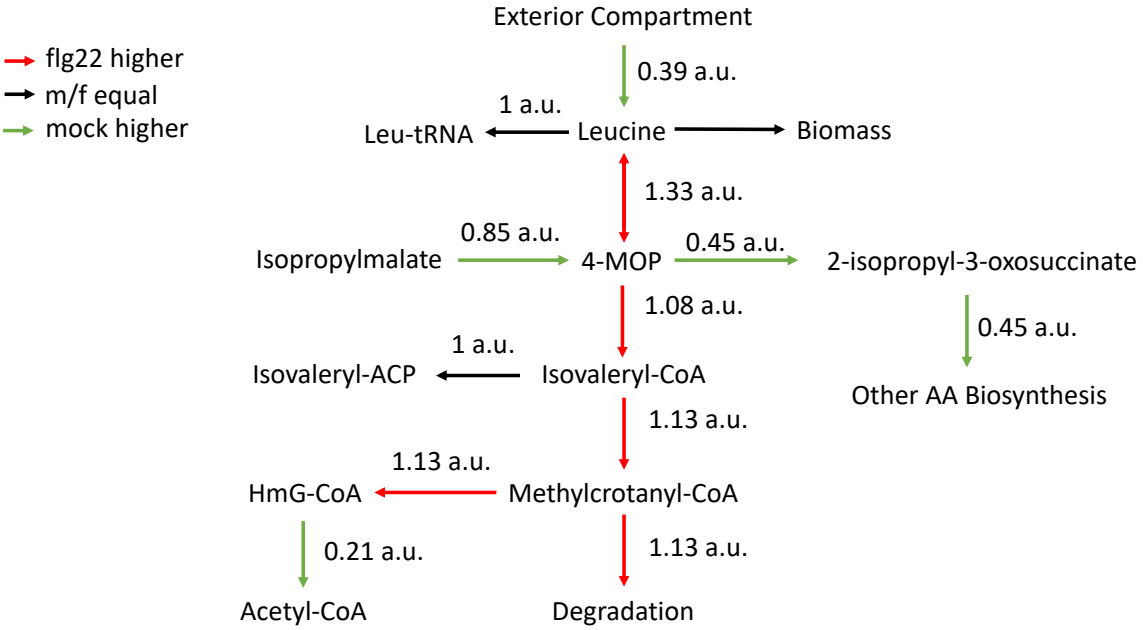
flg22 higher
m/f equal
mock higher
Exterior Compartment
0.39 a.u.
1 a.u.
Leu-tRNA
Leucine
Biomass
1.33 a.u.
0.85 a.u.
Isopropylmalate
4-MOP
0.45 a.u.
2-isopropyl-3-oxosuccinate
1.08 a.u.
0.45 a.u.
1 a.u.
Isovaleryl-ACP
Isovaleryl-CoA
Other AA Biosynthesis
1.13 a.u.
1.13 a.u.
HmG-CoA
Methylcrotanyl-CoA
0.21 a.u.
1.13 a.u.
Acetyl-CoA
Degradation

Figure 2.10. *Pst* gene expression-constrained iPst19 metabolic flux through the BCAA catabolic pathway and surrounding metabolism. RNAseq datasets (Nobori et al., 2018a) were integrated into iPst19 to constrain fluxes of reactions using the GIMME integration algorithm. The presented values next to each conversion step are a ratio of arbitrary units (a.u.) for flg22 constrained flux from 100 ensembles to mock constrained flux from 100 ensembles. Anything above a value of 1 shows more flux through flg22 constrained reactions (red), while less than 1 shows more flux between mock constrained reactions (green).

Figure 2.11

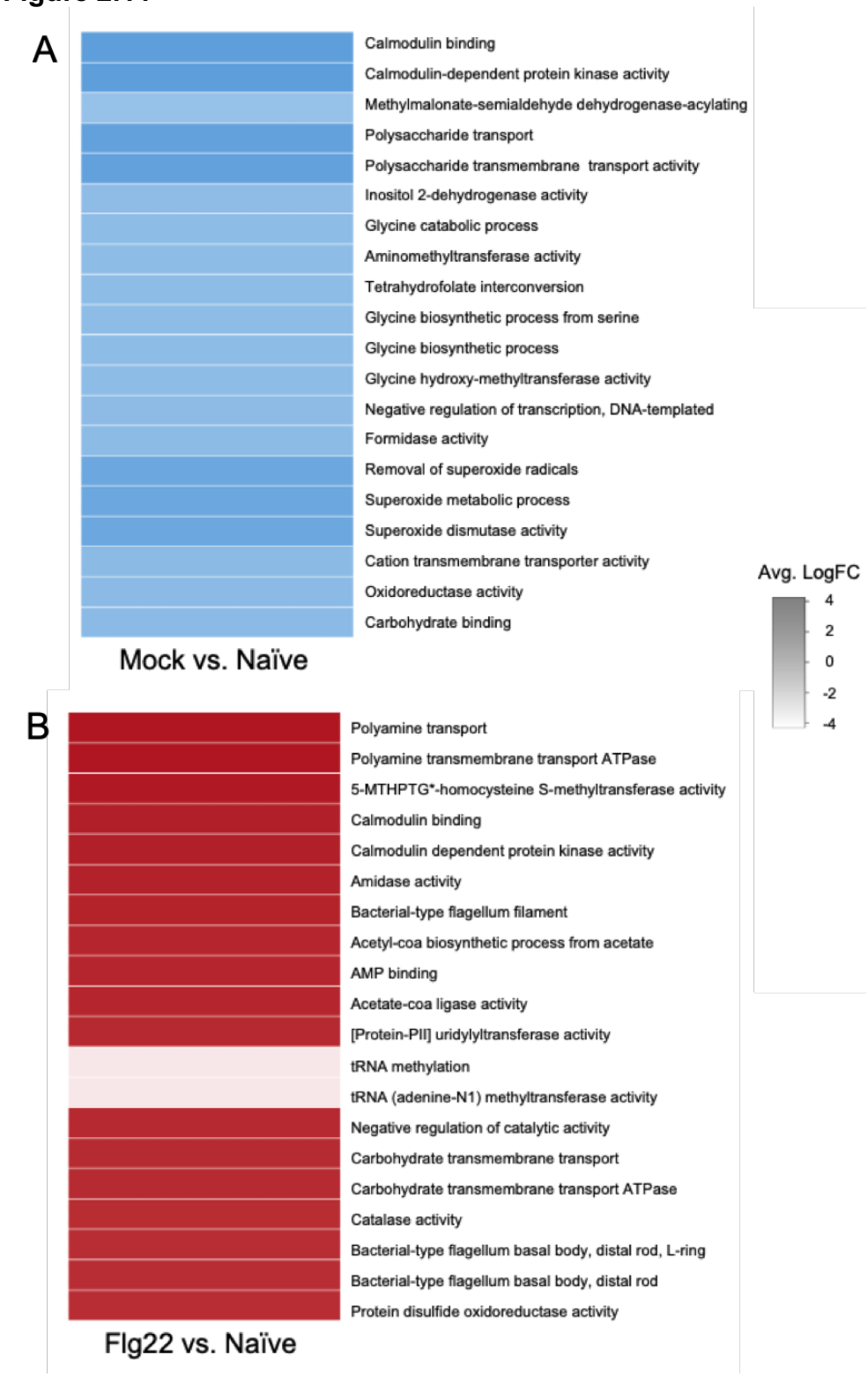
A
Calmodulin binding
Calmodulin-dependent protein kinase activity
Methylmalonate-semialdehyde dehydrogenase-acylating
Polysaccharide transport
Polysaccharide transmembrane transport activity
Inositol 2-dehydrogenase activity
Glycine catabolic process
Aminomethyltransferase activity
Tetrahydrofolate interconversion
Glycine biosynthetic process from serine
Glycine biosynthetic process
Glycine hydroxy-methyltransferase activity
Negative regulation of transcription, DNA-templated
Formidase activity
Removal of superoxide radicals
Superoxide metabolic process
Superoxide dismutase activity
Cation transmembrane transporter activity
Oxidoreductase activity
Carbohydrate binding
Mock vs. Naïve
Avg. LogFC
4
2
0
-2
-4
B
Polyamine transport
Polyamine transmembrane transport ATPase
5-MTHPTG*-homocysteine S-methyltransferase activity
Calmodulin binding
Calmodulin dependent protein kinase activity
Amidase activity
Bacterial-type flagellum filament
Acetyl-coa biosynthetic process from acetate
AMP binding
Acetate-coa ligase activity
[Protein-PII] uridylyltransferase activity
tRNA methylation
tRNA (adenine-N1) methyltransferase activity
Negative regulation of catalytic activity
Carbohydrate transmembrane transport
Carbohydrate transmembrane transport ATPase
Catalase activity
Bacterial-type flagellum basal body, distal rod, L-ring
Bacterial-type flagellum basal body, distal rod
Protein disulfide oxidoreductase activity
Flg22 vs. Naïve

Figure 2.11. Twenty GO terms with the most differentially expressed genes on average in Pst *in planta*. (A.) Mock and (B.) flg22 elicited plants were pretreated for 24 hours and infected with Pst for 5 hours before harvesting. Full RNAseq dataset can be found from Nobori and colleagues (Nobori et al., 2018a).

2.7 Tables

Table 1.1

	E. coli W Model[a,b]	*P. aeruginosa PAO1 Model*[c,d]	*Pst* iPto19[e]
Genome	5.0 Mbp	6.3 Mbp	6.5 Mbp
GC Content	50.6	66.2	58.4
Genes	4776	6125	5842
Reactions	2782	1493	1439
Metabolites	1973	1284	1224
GPRs	1372	1146	889

Table 1.1. Comparison of the size of well-curated models and the corresponding genomes. Genome information for Escherichia coli ([a]) Pseudomonas aeruginosa ([c]) and Pseudomonas syringae ([e]) were acquired from publicly available genome assemblies ([a] (Archer et al., 2011); [c] NCBI Tax ID 187; [e] (Buell et al., 2003)). ([b]) The *E. coli* W model was obtained from BiGG ((King et al., 2016); (Monk et al., 2013)). ([d]) The *P. aeruginosa* model was originally created by (Oberhardt, Puchałka, Fryer, Martins dos Santos, et al., 2008).

Chapter 3: BCAAs function as signaling molecules to suppress Pst virulence in vitro and in planta

3.1 Summary

Pathogens and non-pathogens use environmental queues to regulate growth and metabolisms. Pathogens specifically use similar queues to regulate virulence and pathogenesis. Pst has been shown to use culture density to regulate the timing of virulence onset, where the highest rate of production of virulence factors occurs at low culture densities. Different metabolites cause Pst to suppress or induce virulence factor synthesis, including organic acids and amino acids. Here, we demonstrate how BCAAs suppress virulence through downregulation of key genes both *in vitro* and *in planta*. The suppression is not due to compromised growth but does lead to compromised infectivity during long-term foliar infections.

3.2 Introduction

Bacteria are exceedingly proficient at recognizing metabolite abundance in their environment. The abundance of carbon for energy production and nitrogen for protein synthesis are key environmental components that act as signals to many bacteria. In liquid culture, the canonical growth curve of bacteria perfectly illustrates the sense and response habit of a population of cells: at the start, when both carbon and nitrogen are abundant, cells rapidly divide; as time elapses and the culture becomes saturated, nutrients become scarce, and cells division slows down.

Perception of nutrient abundance not only impacts the growth rate of cells but in the case of many pathogens, certain nutrients and molecules act as queues that the pathogen uses while invading a host. Enterohemorrhagic *E. coli* uses different sugars present in the gut as signals for transcription of the Locus of Enterocyte Effacement (LEE) pathogenicity island. Glucose scarcity increases the induction of LEE due to internal signaling mechanisms relating to glycolysis (Miranda et al., 2004). External levels of fucose regulate LEE expression through a two-component system, which directly associates with metabolites outside the cell and creates a signal cascade inside the cell for transcriptional reprogramming. In the absence of the two component system, *E. coli* is not able to respond to external levels of fucose and becomes hyper-virulent, suggesting direct control of virulence expression through metabolite sensing two component systems (Pacheco et al., 2012).

Several different carbon and nitrogen sources have been described as contributing to virulence regulation in Pst. Fructose has been shown to act as an inducer of the effector protein AvrPto, while GABA metabolism and transport has been reported to be necessary for full virulence by Pst in tomatoes(Anderson et al., 2014a; Park et al., 2010).

Many pathogens utilize quorum sensing to control the expression of virulence factors. Quorum sensing allows cell-to-cell communication and regulation through the production of diffusible factors: more cells produce more factors, which in turn increases local concentration and perception by surrounding cells(Miller & Bassler, 2001). Gram-positive bacteria produce small diffusible peptides while Gram-negative bacteria produce small molecules as signal factors. Both mechanisms cause signaling cascades in receptive cells and alter the transcriptional machinery to respond to density accordingly(Miller & Bassler, 2001). Interestingly, *P. syringae* virulence seems to follow a different regulation pattern than other pathogens. While many pathogenic bacteria only initiate virulence at higher densities, like *Pseudomonas aeruginosa* in biofilms, Pst initiates virulence early during the exponential growth phases (McCraw et al., 2016). The induction of the *cma* promoter peaks during exponential growth *in vitro* and then decreases with the transition to the stationary phase. Similarly, transcript abundances are highest for *cmaABT* during the earliest points of the growth stage (Weingart et al., 2004). *In planta*, the expression dynamics for virulence genes mimic those found *in vitro*. *P. syringae* pv. actinidiae, a pathogen of kiwifruits, shows large induction of T3SS-related genes from 3 hours to 24 HPI, when active colonization of the leaf is

occurring (McAtee et al., 2018). *P. syringae* mutants lacking the ability to produce the quorum sensing molecule alginate show a hypervirulent phenotype and can quickly colonize host leaves (Quiñones et al., 2005). Taken together, these studies suggest that the induction of virulence is critical during early growth phases and could be an evolutionary adaptation by *P. syringae* to ensure effective colonization in plants.

Here, we only focus on a subset of amino acids that impact the survival of Pst during foliar infections. Previous work in our lab has described the roles of glutamine, serine, and sugars impacting pathogen infectivity and virulence; however, due to the critical observations of BCAA metabolism carrying disproportionate flux in flg22 elicited plants, we sought to elucidate the impacts of BCAAs acting as nutritional queues for Pst *in vitro* and *in planta*.

An important consideration for this section is the use of high concentrations of amino acids when supplementing bacteria both *in planta* and *in vitro*. Previous studies have characterized the concentration of all amino acids combined within the apoplast at 10mM. The majority of these are glutamine and arginine, both of which appear in the highest concentrations in our studies as well. The combined BCAA concentration is roughly 100uM to 150uM (Lohaus et al., 1995). In these studies, we have used 10mM BCAAs. Importantly, the 90% of the apoplasmic space is air, with a limited amount of liquid in which amino acids can be in solution which must be accounted for per Lohaus and colleagues (Lohaus et al., 2001). Dilution factors for recovery of apoplasmic washing fluid (AWF) have been

predicted at 3-9 times for *A. thaliana* and other plants, based on modeling of the air space within the leaf (Lohaus et al., 2001).

Beyond dilution factors, there are several other aspects of the traditional vacuum infiltration and recovery method to obtain AWF that complicate the interpretation of the concentrations of metabolites obtained in the leaf AWF. For instance, osmolarity, pH of the recovery liquid, time of infiltration, and the pressure used to infiltrate leave, may affect the recovery of different metabolites. Importantly, there is more-limited solubility of BCAAs in highly polar recovery fluids when compared to polar amino acids. As such, there has been no established standard protocol to use for the enriched recovery of AA from AWF. These point to potential limitations in the recovery of AA, but other factors were considered for our use of 10 mM BCAA, including active transport by plant amino acid transports and phloem loading of supplemented AA.

For *in planta* studies, the whole pathosphere must be considered in designing experiments. *A. thaliana* is not agnostic of high amino acid concentrations and will import AAs down a concentration gradient from the apoplast to cytosol ultimately to the tonoplast. Previous studies exploring the inducing effects of fructose have used 50mM fructose supplementation while apoplastic concentrations of fructose in leaves have been described at 200 µM to 500 µM (Anderson et al., 2014a; Kang et al., 2007). A higher amount of supplementation for the metabolite of interest must be used during in planta infection assays due to the movement and sequestration of metabolites upon infiltration. Considering these factors, as well as the established supplementation protocols from Anderson and colleagues and

Kang and colleagues, where 100x concentration of metabolite was used to study inducing and repressing gene expression effects *in planta*, we similarly used 100x BCAA concentration (from 100-150uM to 10mM) to account for the rapid sequestration of metabolites across membranes.

3.3 Materials and methods

Bacterial Growth Conditions:

Pst grown in liquid King's B culture at shaking at 230 RPM and 28C. Bacteria for growth rate assessment and plant infection experiments were taken from fresh LB agar plates and grown overnight in the liquid media, followed by sub-culturing 10% until mid-exponential phase.

Plant growth conditions:

A. thaliana Columbia-0 (col0) plants were grown in peat pellets with a 12-hour photoperiod at 23C and 70% humidity. Plants were watered three times a week with Hoagland's solution or water, depending on age. At six weeks old, plants were used for infections and gene expression quantification.

RNA and cDNA preparation:

RNA was extracted with Trizol reagent (Ambien). For samples containing with plant alone or plant and bacterial tissue, flash-frozen samples were ground in 1 mL of Trizol with metal beads for at 25Hz until liquified. Samples with bacteria were then homogenized using 0.1mm silica beads at 8000rpm. Samples with only bacteria began at this step. Liquid phase separation with chloroform isolated RNA from protein, DNA and phenolics at 11,200 x g for 15 minutes at 4C. Supernatant was combined with equal parts isopropyl alcohol to precipitate RNA, at 13,300 x g for 15 minutes. Contaminating DNA was digested using DNase 1 from Promega for 30 minutes to an hour, followed by cDNA synthesis using m-

MLV and normalized inputs of DNA-free RNA, also from Promega using the supplied protocol and reaction conditions.

Transcript quantification:

Transcripts of genes were quantified via quantitative RT-PCR using an ABI7500 Fast thermocycler and CW Biosciences qRT-PCR ready mix. Primer sequences can be found in the primer addendum within the supplemental information. Reactions were prepared to the specifications of the ready mix. Transcripts were relatively quantified using the $\Delta\Delta$Ct normalization method, whereby the Ct values of the gene of interest are subtracted from the housekeeping gene within each sample (internal normalization) followed by subtracted these results between the experimental condition and the reference condition (external normalization). All bacteria transcripts were internally normalized to *recA* unless otherwise noted. All plant transcripts were internally normalized to *act2* unless otherwise noted. Primer names and sequences can be found in Chapter 4, Table 4.6. All statistical tests for gene expression were Student's T test against the externally normalizing condition, unless otherwise noted. * $p < 0.05$, ** $p < 0.01$, *** $p < 0.001$, **** $p < 0.0001$.

Pre-elicitation:

Prior to infiltration, plants were covered with plastic domes to increase localized humidity to near 100%, ensuring stomata are fully open. 4 leaves per plant (leaf pairs 5 and 6, according to order of emergence from the meristem) were elicited via blunt end syringe with either water (mock) or 1μM flg22 in water. Any remaining liquid on the exterior of the leaf was wiped off. Plants were elicited for 24 hours. Elicitation with BCAAs was done using 10mM BCAA in water or water alone for 24 hours, after which leaves were harvested for gene expression.

Long term infection quantification and gene expression:

4 leaves per plant (pairs 5 and 6) were infiltrated with 0.0002 OD Pst (or derivative strain). For naïve plants, infection duration was 72 hours. For elicited plants, infection duration

was 48 hours to prevent total leaf collapse. Leaves were harvested; normalized amounts of leaf tissue were taken using a 4mm cork borer. 8 leaf discs from one plant contributed to one CFU sample. Discs were pulverized with a metal bead for 5 minutes at 25Hz in 400µL sterile water. Samples were serially diluted 1:10, 5µL from each dilution was plated on solid LB agar with appropriate selection markers. 16-20 hours post plating, CFUs were quantified. For gene expression, remaining leaf tissue was flash frozen. RNA was extracted and transcripts quantified as previously described.

Short term infection and gene expression:

4 leaves per plant (pairs 5 and 6) were infiltrated with 0.02 OD Pst (or derivative strain). For all plants, infection duration was 3 hours. Leaves were harvested; normalized amounts of leaf tissue were taken using a 4mm cork borer. 8 leaf discs from one plant contributed to one CFU sample. Discs were pulverized with a metal bead for 5 minutes at 25Hz in 400µL sterile water. Samples were serially diluted 1:10, 5µL from each dilution was plated on solid LB agar with appropriate selection markers. 16-20 hours post plating, CFUs were quantified. Due to the limited bacteria present after 3 HPI, samples used for gene expression were infiltrated with 0.2 OD bacteria. Leaves were harvested and flash frozen and RNA was extracted as previously described.

Co-infiltration treatments:

Bacteria that were co-infiltrated with either water or amino acids were first resuspended in water at 10x OD concentration. Immediately before infiltration into a leaf, the bacteria were mixed with the appropriate dilution of either water or amino acids suspended in water. The amount of time bacteria were exposed to the co-infiltration treatment was minimized.

Plate preparation:

Bacterial growth curves were generated using a Spectramax i3x 96-well plate reader using the kinetic read feature with continuous agitation at 28C. Overnight bacterial cultures were

grown as previously described. Cultures were pelleted and washed three times with water before inoculation into assay media at the appropriate concentration.

Media formulations:

For growth curves in a rich media, bacteria were inoculated in King's B liquid media with the appropriate selection marker. For growth curves in virulence inducing media, HMM was used. For growth curves in minimal media, modified M9 media was used. In addition to salts from typical M9 media, sterile 100μM sucrose and 5mM $MgSO_4$, final concentrations, were added to facilitate Pst growth. Without these additions, growth is not observable within this system.

Doubling time calculations:

To calculate doubling time from a growth curve, each well within a 96 well plate was treated as an individual technical replicate. Averaging across technical replicates and proceeding with calculations is not advisable, as subtle differences in the results may be lost. 10 to 15 measurements within the exponential growth phase were used to produce an interpolating line; the line was optimized within the curve to have the best R^2 value and the highest exponent manually. Doubling time was calculated from taking the natural log of 2 divided by the exponent within the equation for the interpolated curve.

Grouped gene expression sets:

Heatmaps were generated from the expression values calculated from publicly available data from Brunner and Nürnberger on TAIR (ExpressionSet:1008080727). Genes were previously grouped by association with specific amino acids. These were then grouped by similar characteristics. Similarly, these gene-sets were grouped by GO term association. The average expression across all of the genes within a go term was presented.

3.4 Results

In planta virulence dynamics during PTI – A Timecourse

Appropriate expression of virulence markers is a key aspect of a successful infection by Pto. As previously shown, in a naïve plant, expression of the T3SS and coronatine synthesis genes increases during the initial phase of infection, after which expression falls off. Conversely, in defense-elicited plants, expression of these virulence markers is delayed, contributing in part to the resistance phenotype in the plant (Figure 3.1). It is clear that the delayed onset of virulence protocol leads to a less successful pathogen, yet inappropriate overexpression of virulence markers can also be detrimental to the pathogen during infection.

Previous studies have illustrated the importance of strict regulation between virulence and growth. However, current assessments of *in planta* virulence of Pts are limited towards immediate and short time course assays, often within the first six hours of infiltration with bacteria. We have extended the profiling of virulence over 48 hours post-inoculation (HPI) in naïve and PTI-elicited plants. At the six-hour timepoint, expression of *hrpA* and *cfl* remain consistent with what has previously been described: PTI suppresses the expression of virulence genes (Figure 3.2) (Lovelace et al., 2018; Nobori et al., 2018b). However, Pts exposed to PTI-elicited plants significantly increase the expression of both genes for the remainder of the time course, with the highest expression at 48 HPI (Figure 3.2A). While the expression of virulence-related genes increases, this does not lead to the successful long-term colonization of the leaf (Figure 3.1). These data suggest the importance of early induction of virulence during an infection is necessary to gain a foothold in the leaf. Failing to do so will lead to an unsuccessful infection.

In vitro gene expression

We have provided evidence that 10 mM BCAA, while a high concentration, is not toxic at these levels to Pst. The doubling time drastically decreases with supplementation of 10 mM BCAA in modified M9 media compared to non-supplemented M9 (Figure 3.3A), suggesting Pst can use this concentration of BCAA for growth. Further, there is no significant difference with using less BCAA, as presented in Figure 3.3A. While adding BCAAs does not support robust growth, it is evident that any supplementation produces faster growth and more growth than non-supplemented media (Figure 3.3B).

When the BCAAs are supplemented individually into MM, leucine supports growth, while both valine and isoleucine slow the doubling time significantly (Figure 3.4). Due to the growth support shown in the combination of BCAAs (Figure 3.3A), these data suggest leucine is able to compensate for any growth-suppressing effects *in vitro* of valine and isoleucine alone.

We were able to replicate *in vitro* the *liuA* (PSPTO_2739) and *liuD* (PSPTO_2736) similar to induction seen in Pst when infecting flg22-elicited plants in Nobori and colleagues' transcriptional profiling by supplementing minimal media with BCAAs, either individually or combined. We tested two minimal media formulations: HMM and modified M9 media, the first to replicate a virulence inducing environment and the second as a carbon-restricted growth producing environment. Individual supplementation of BCAAs into HMM significantly induced expression of both *liuD* and *liuA* when compared to the non-supplemented bacteria (Figure 3.5A).

Individual BCAA supplementation, as well as a combination of all three, has the same effect (Figure 3.5B). The induction does not appear to be concentration dependent *in vitro*, as supplementation between 100μM and 10mM all produce induction of these catabolic genes (Figure 3.5C). Interestingly, the expression of *lrp* (PSPTO_0100) does not change in response to the concentration of BCAAs, suggesting that the BCAA-sensing activity of Lrp occurs post transcriptionally and probably post-translationally (Figure 3.5C).

The expression patterns of *liuD* and *liuA* seems to be BCAA specific. Supplementation of 10mM Gln or 10mM Ser significantly suppress the expression of both genes in minimal media (Figure 3.6).

Supplementation of BCAAs *in vitro* also impacts the expression patterns of virulence markers *hrpL* and *cfl.* While there are several mechanisms by which Pst regulates virulence factor synthesis, regulation by BCAAs has not been previously described. In HMM, we expect the synthesis of virulence factors to be high. However, after supplementation with 10mM BCAA, the expression patterns of both *hrpL* and *cfl* were significantly suppressed. This effect was not present at concentrations lower than 10 mM BCAA (Figure 3.7).

Supplementation of AA suppresses virulence and reduces colonization

The accumulation of AA after elicitation of leaves with flg22 has been described in our previous studies (Zhang et al., 2023b). In adult leaves, the highest concentration of AA observed occurred 24 hours post-elicitation. Profiling of these amino acids revealed stark increases in glutamine, serine and valine (a BCAA)

when compared to mock-treated leaves. Both glutamine and serine, when co-infiltrated with Pto, suppressed virulence and led to less leaf colonization after 72 hours (Zhang et al., 2023b). This is not the result of amino acid toxicity, which is supported by the enhanced growth in minimal media supplemented with glutamine, serine, and a combination of both AA in a concentration-dependent manner (Figure 3.8). Further, within the first three hours of infiltration with both glutamine and serine, there is no significant bottleneck effect to suggest a die-off upon infiltration into the leaf (Figure 3.9).

Again, we sought to replicate the expression pattern seen in the flg-22 treated bacteria regarding *liuD* and *liuA,* though *in planta*. Similar to our results *in vitro,* the expression of *liuD* and *liuA* is significantly induced *in planta* when co-infiltrated with 10mM BCAAs for 3 hours (Figure 3.10). It was important to confirm the induction of *liuD* and *liuA in planta* due to the predicted gene essentialities presented in Chapter 2 (Figures 1.8 and 1.9) showing the alleviation of essentiality in a complex mixture of carbon sources.

Similar to Gln and Ser co-infiltration, 10 mM BCAAs did not immediately reduce the infecting titer of bacteria (Figure 3.11A). Because there is no apparent bottleneck effect with the pathogen, it is clear that the compromised leaf colonization we see at 72 HPI (Figure 3.11B) is due to a more complex effect that BCAAs are having on Pst or *A. thaliana.*

We were able to rule out plant-immune induction by BCAAs as a primary cause of reduced Pst infection. *A. thaliana* plants do not show any induction of either SA-mediated immunity (through expression of *Pathogenesis-related 1* (PR1)) or JA-

mediated immunity (through expression of *Vegetative Storage Protein 2* (VSP2)) (Figure 3.12). Importantly, these two pathways comprise the primary induced defense responses by biotrophic and necrotrophic pathogens. PR1 induction is exacerbated by SA, and has been shown to respond transcriptionally to pathogens and flg22 in as little as 12 hours rendering it a robust readout for SA-mediated immunity (Backer et al., 2019). Similarly, VSP2 responds transcriptionally to the presence of JA (Verhage et al., 2011). Because neither of these genes are induced at 24 HPE with BCAAs (Figure 3.12), it is reasonable to conclude that neither of these defense pathways is induced by high levels of BCAAs in the apoplast.

Similar to Gln and Ser supplementation *in planta* and BCAA supplementation *in vitro*, supplementation with 10 mM BCAAs significantly reduces *hrpL* and *cfl* induction *in planta* (Figure 3.13).

3.5 Discussion

Data presented here and in previous works in our lab (Zhang et al., 2022, 2023) suggest a critical part of flg22 elicitation is the modulation of AA transporters that lead to the increase of AA outside mesophyll cells, which in turn suppresses the virulence mechanisms of Pst at the early stages of leaf colonization. A similar, yet distinct, mechanism was previously described by Yamada and colleagues in 2016. They described how flg22 immunity was impacted by the increased abundance of the sugar transporters STP13 and STP1 on the PM of mesophyll cells, thus causing the withdrawal of hexoses from the leaf apoplast of elicited plants. When *stp1* and *stp13 A. thaliana* mutants were challenged with Pst, the plants were

significantly more susceptible to infection, suggesting that the abundance of sugars plays a role in the colonization of the leaf, likely through increased growth and energy production by Pst.

While the expression data regarding AA transporters provides a potential avenue for how *A. thaliana* shuttles the AA into the apoplast, the outstanding question of where the free AA originate remains unanswered. To aid in understanding this point, we used publicly available expression profile of *A. thaliana* gene expression in flg22 elicited plants at 1 and 4 HPE and compared the expression of genes within several known AA generating or consuming pathways, including glucosinolate biosynthesis, AA biosynthesis, proteolysis, autophagy, senescence, phenylpropanoid biosynthesis, and aminoacyl tRNA biosynthesis. Each gene was assigned to an AA group and presented as log2 (fold change) according to the available data from The Arabidopsis Information Resource (TAIR) (Figure 3.14). While there is no clear pattern to the expression of genes broken when grouped by biochemical characteristics, there does seem to be patterns of the same data when broken up by GO terms grouping. On average, genes related to amino acid sources show increased expression at 4 HPE, while genes related to the amino acid sinks show decreased expression at 4 HPE (Figure 3.15).

While there is a direct link between Gln and Ser abundance after flg22 treatment and suppression of virulence, the link between abundance of BCAA and virulence after flg22 treatment is less clear. First, of the BCAA, only valine is significantly more present in the apoplast after flg22 treatment. We have shown that valine is sufficient to induce *liuD (p-val 0.057)* and *liuA* in vitro (Figure 3.5A), but it is not

known if this induction is sufficient to induce *in planta*. However, given that all BCAAs together produces the same expression profile as each individual BCAA, it is likely that the expression profile would be similar *in planta*.

As previously discussed, induction of virulence factor early in infection is critical for Pst to set a foothold in foliar infections. Suppression of virulence gene expression by both Gln/Ser and BCAAs seems to critically alter the progression of infection at later time points, highlighting the importance of modulation of AA concentration as a primary defense mechanism of *A. thaliana,* similar to what was described by Yamada and colleagues regarding hexoses (Yamada et al., 2016). The impact of AAs on bacterial infection dynamics is specific to which AAs are present in the apoplast. As previously described by Anderson and colleagues, Asp is able to induce virulence in Pst *in planta* (Anderson et al., 2014b). Similarly, our lab has explored the role of a combination of Glu and Asp *in planta*; individually, as well as the combination of Glu and Asp, seem to equally induce virulence and promote long-term infection in *A. thaliana* (Khadka, manuscript in prep.).

Importantly, our data suggests Pst is not using these amino acids outright for energy production to sustain a robust infection. Rather, the increased abundance of AA in the apoplast inhibits infection by delaying the onset of virulence (Figure 3.2 and 2.12) (Zhang et al., 2023b). When considering the impacts of decreased hexose abundance and increase AA abundance, it is reasonable to appreciate how flg22 induction in leaves not only restricts access to fast-growth promoting nutrients while simultaneously suppressing critical mechanisms of bacterial infection during the early stages of colonization but could lead to considerable

inhibition of infection. It is important to note that these phenomena are not the only defense mechanisms induced in the leaf by flg22; there are substantial increases in SA and ROS that also impact the success of Pst infecting leaves. These features illustrate how plants inhibit the colonization of leaves from a broad range of microbial pathogens without the need for specific pathogen recognition during ETI and HR.

3.6: Figures

Figure 3.1

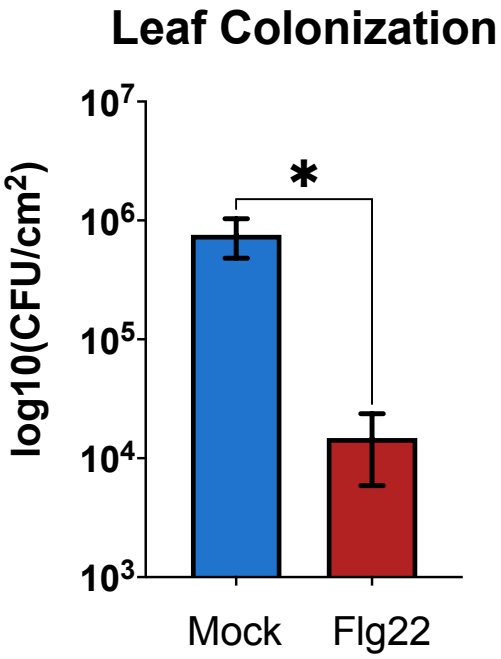

Figure 3.1. Infection of *A. thaliana* leaves by Pst. 24-hour elicitation of either water or flg22 followed by infection with Pst at 0.0002 IOD yielded CFUs per sq. cm of leaf tissue. Student's T test, * < 0.05. N = 6.

Figure 3.2

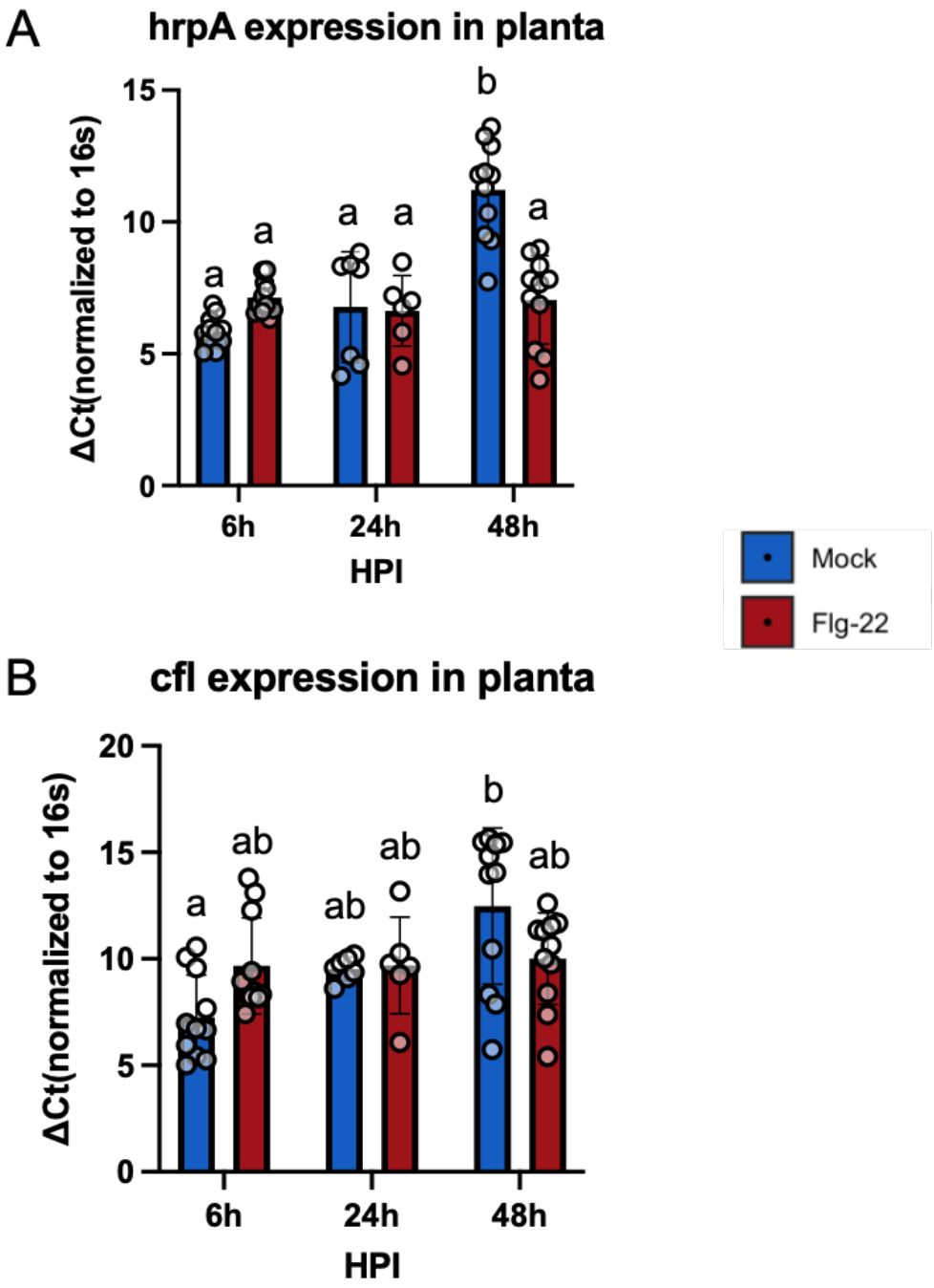
A
hrpA expression in planta
ΔCt(normalized to 16s)
15
10
5
0
a
a
a
a
b
a
6h
24h
48h
HPI
Mock
Flg-22
B
cfl expression in planta
ΔCt(normalized to 16s)
20
15
10
5
0
a
ab
ab
ab
b
ab
6h
24h
48h
HPI

Figure 3.2. Expression of *hrpA* and *cfl* by Pto *in planta* over time. Transcript abundances of virulence genes from Pto were quantified in reference to 16s transcript abundances in mock (blue) and flg22-elicited (red) plants. A. Transcript abundance of *hrpL*. B. Transcript abundances of *cfl.* ANOVA, n=6-12. Letters above each bar indicate whether the bars are significantly different from each other.

Figure 3.3

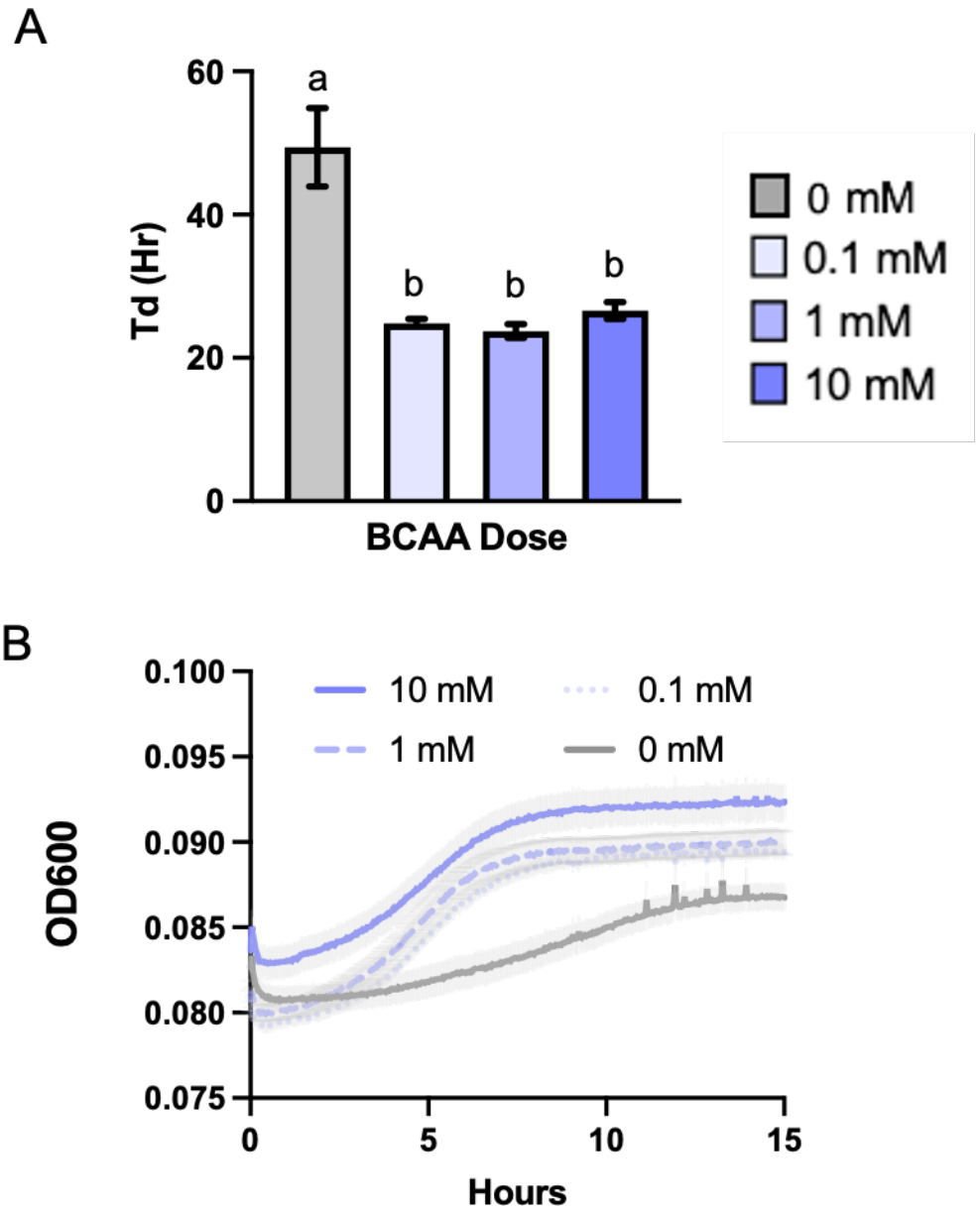
A
60
40
20
0
Td (Hr)
a
b
b
b
BCAA Dose
0 mM
0.1 mM
1 mM
10 mM
B
0.100
0.095
0.090
0.085
0.080
0.075
OD600
10 mM
0.1 mM
1 mM
0 mM
0
5
10
15
Hours

Figure 3.3. Supplementation of BCAAs in a minimal media supports growth. The addition of 100μM, 1mM, and 10mM each BCAA in combination was supplemented into mM9 media (grey). Pst was inoculated in the media at IOD (initial optical density) 0.01. A. Doubling time was calculated from individual growth curves per well presented in B and averaged, N = 16. B. Average growth curves presented as OD600 across all 16 wells within a given treatment over 15 hours. Grey shadows represent the SD for each curve, N = 16.

Figure 3.4

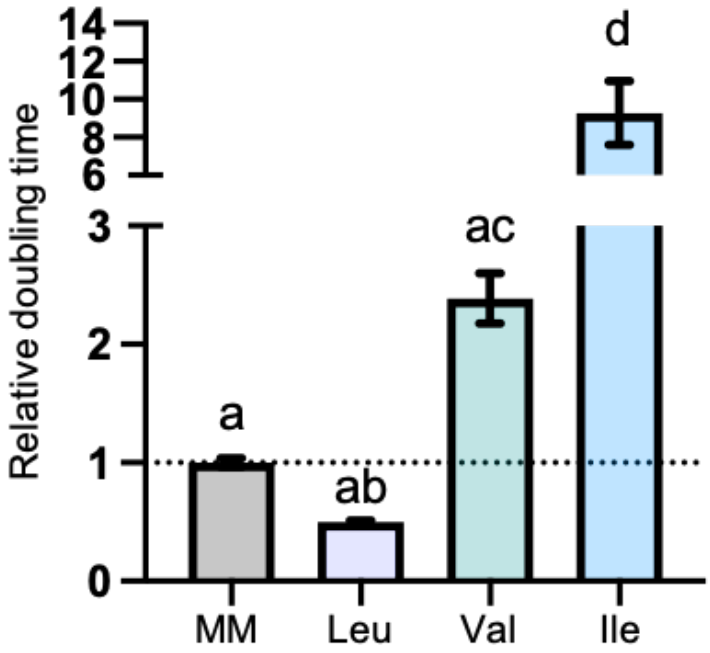

Figure 3.4. Individual BCAAs have different effects on Pst doubling times. 10mM each BCAA individually was supplemented into mM9 media (grey). Pst was inoculated in the media at IOD 0.01. Doubling time was calculated from individual growth curves per well and averaged. Doubling times are informed normalized to the non-supplemented media, N = 9-16.

Figure 3.5

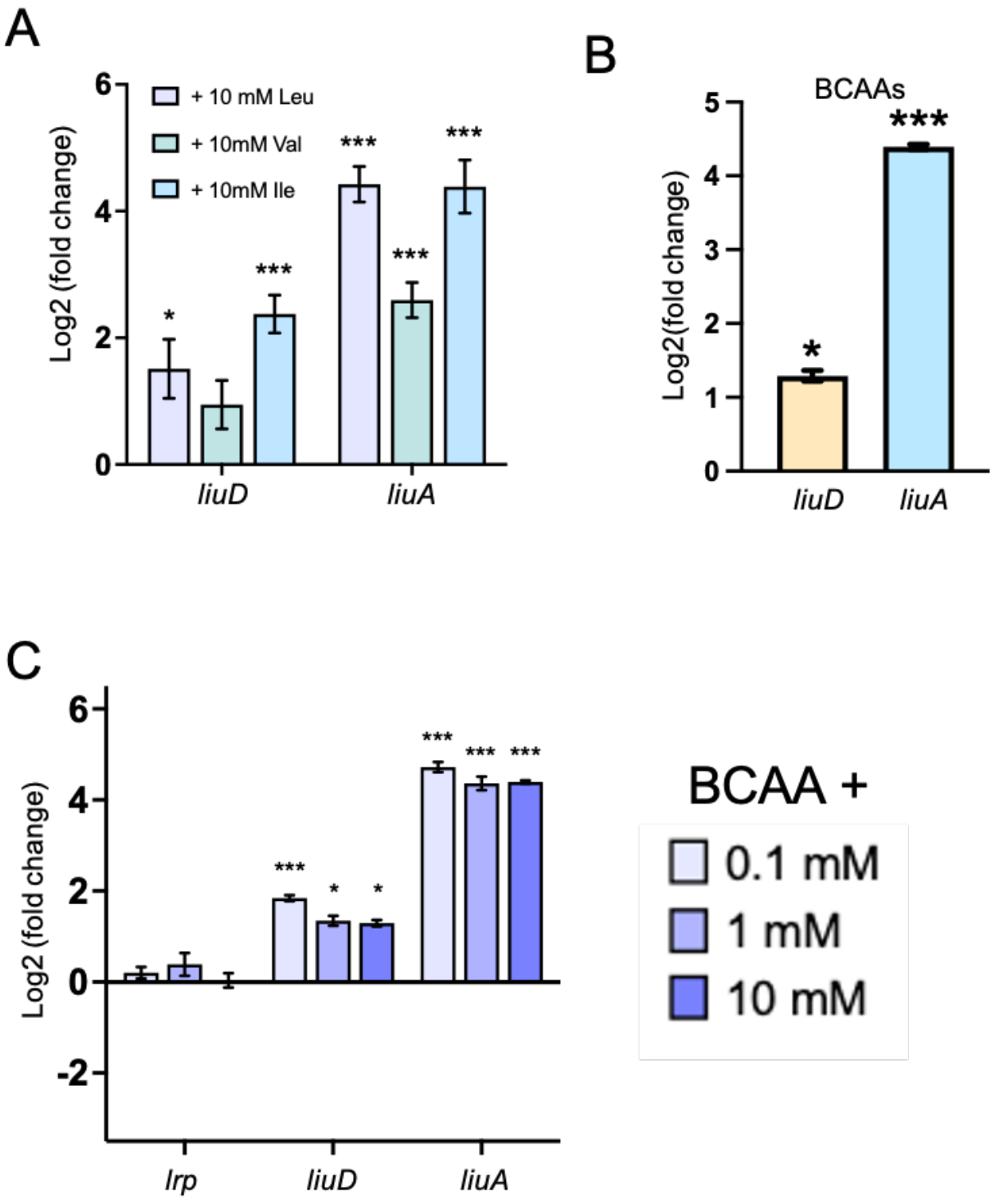
A
+ 10 mM Leu
+ 10mM Val
+ 10mM Ile
Log2 (fold change)
liuD
liuA
B
BCAAs
Log2(fold change)
liuD
liuA
C
Log2 (fold change)
lrp
liuD
liuA
BCAA +
0.1 mM
1 mM
10 mM

Figure 3.5. The addition of BCAAs induces expression of BCAA catabolic genes, but not a regulatory gene. All transcript levels are internally normalized to *recA.* A. Transcript levels of *liuD* and *liuA* in Pst exposed to mM9 in 10mM individual BCAA supplemented media normalized to Pst exposed to mM9 alone. B. Transcript abundances of *liuD* and *liuA* in Pst exposed to mM9 containing each BCAA at 10mM, normalized to Pst exposed to mM9 alone. C. Transcript abundances of *lrp*, *liuD,* and *liuA* in Pst exposed to 100μM, 1mM, and 10mM each BCAA in HMM, normalized to transcript abundances in Pst exposed to HMM alone. Student's T test, * < 0.05, ** < 0.01, *** < 0.001.

Figure 3.6

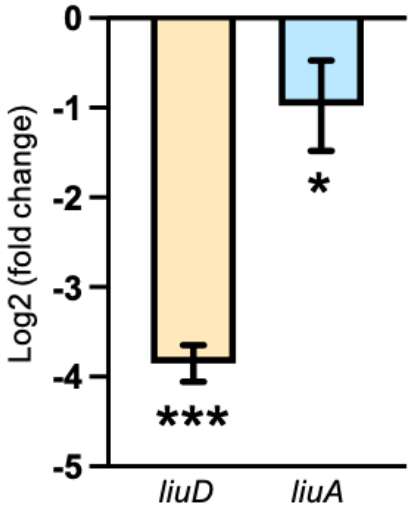

Figure 3.6. BCAA catabolic gene expression in response to high levels of glutamine and serine. Transcript abundance of *liuD* and *liuA*, internally normalized to *recA*, in Pst exposed to 10 mM Gln and Ser in minimal media normalized to non-supplemented minimal media (N = 6). Student's T test, * < 0.05, *** < 0.001.

Figure 3.7

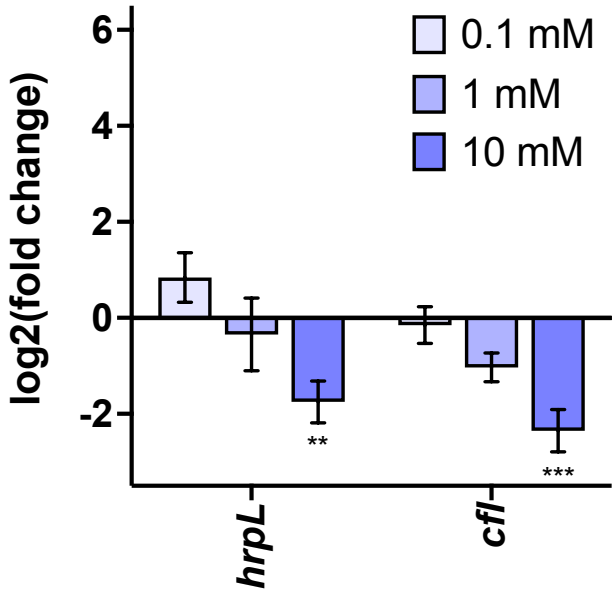

Figure 3.7. Virulence factor gene expression responds to concentration changes in BCAAs. Transcript abundance of *hrpL* and *cfl*, internally normalized to *recA*, in Pst exposed to 100μM, 1mM, and 10mM combined BCAAs in HMM normalized to non-supplemented HMM. Student's T test, ** < 0.01, *** < 0.001.

Figure 3.8

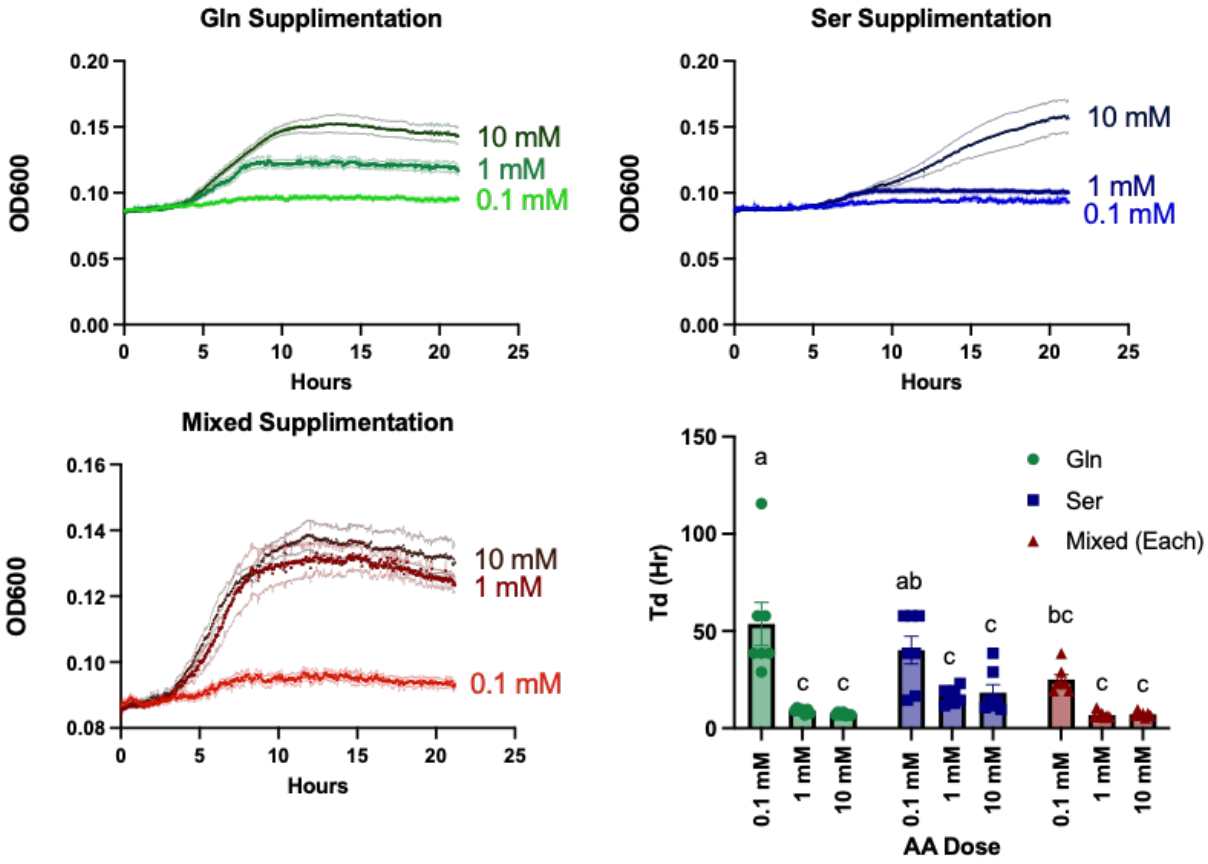
Gln Supplimentation
OD600
Hours
10 mM
1 mM
0.1 mM
Ser Supplimentation
OD600
Hours
10 mM
1 mM
0.1 mM
Mixed Supplimentation
OD600
Hours
10 mM
1 mM
0.1 mM
Td (Hr)
Gln
Ser
Mixed (Each)
a
c
c
ab
c
c
bc
c
c
0.1 mM
1 mM
10 mM
AA Dose

Figure 3.8. Supplementation of increasing concentrations of Gln or Ser in minimal media changes the growth capacity of a culture. A-C. Average growth curves of Pto growing in mM9 media supplemented with either 100μM, 1mM, 10mM glutamine, serine, or both. Each solid line is an average of n=7 cultures, with the translucent flanking lines representing SEM. D. Average doubling times of Pto from the curves in A-C, SEM. ANOVA, multiple comparisons.

Figure 3.9

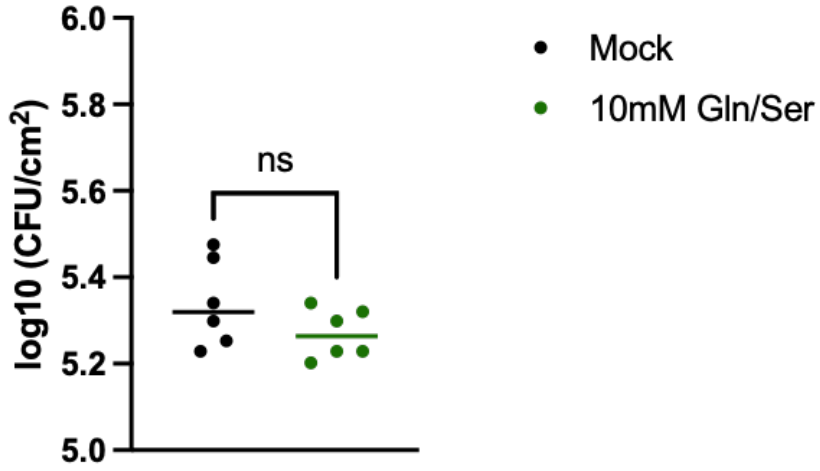

Figure 3.9. Gln and Ser do not create an immediate bottleneck *in planta*. CFUs/ sq cm infected leaf tissue, 3HPI with Pst, IOD 0.02, co-infiltrated with both 10mM Gln and Ser or MES alone. Student's T test.

Figure 3.10

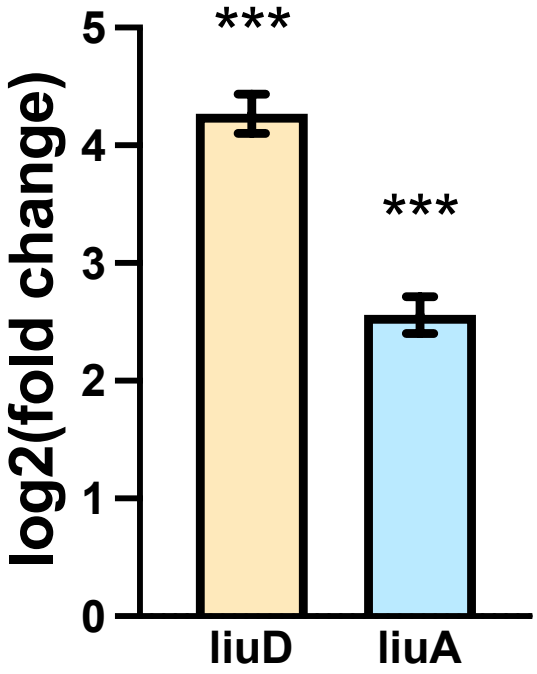

Figure 3.10. BCAAs induce BCAA catabolic genes in the apoplast. Pst co-infiltrated at IOD 0.2 with 10mM BCAAs show increased transcript abundances 3 HPI in *A. thaliana* leaves when compared to MES alone. Student's T test. *** < 0.001.

Figure 3.11

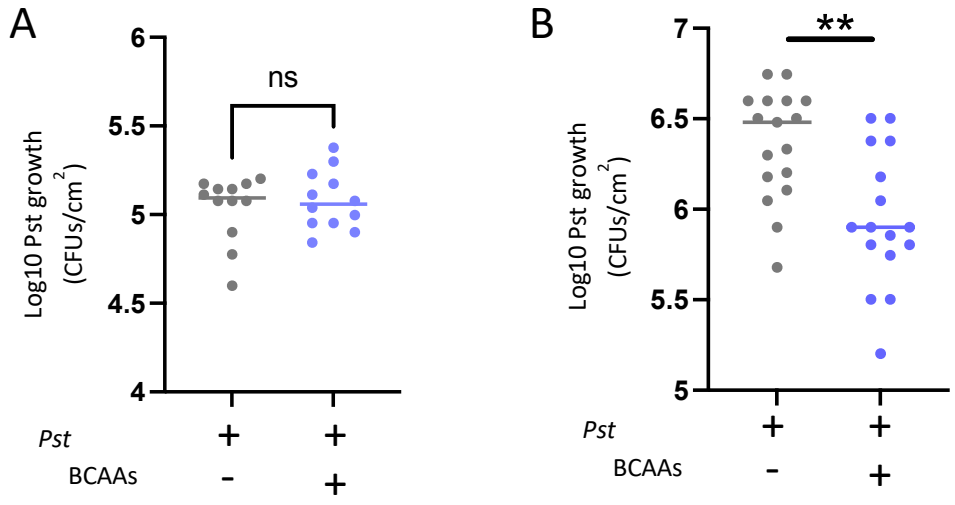
A
Log10 Pst growth (CFUs/cm2)
6
5.5
5
4.5
4
ns
Pst
BCAAs
+
-
+
+
B
Log10 Pst growth (CFUs/cm2)
7
6.5
6
5.5
5
**
Pst
BCAAs
+
-
+
+

Figure 3.11. BCAAs do not create an immediate bottleneck *in planta* but reduce long term colonization. A. CFUs/ sq cm infected leaf tissue, 3HPI with Pst, IOD 0.02, co-infiltrated with both 10mM BCAAs or MES alone. B. CFUs/ sq cm infected leaf tissue, 72HPI with Pst, IOD 0.0002, co-infiltrated with both 10mM BCAAs or MES alone. Student's T test. ** < 0.01.

Figure 3.12

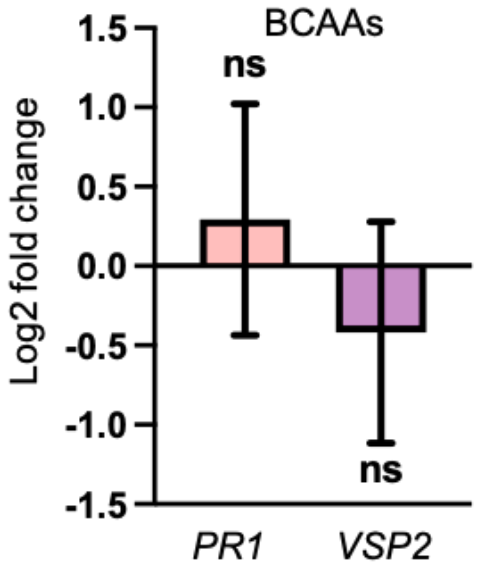

Figure 3.12. Plant defense pathways are not induced by BCAAs. Gene expression of plant defense markers genes *PR1* and *VSP2* 24 internally normalized to *act2* HPE of leaves with 10mM each BCAA and normalized to MES infiltrated leaves (N=3, SD). Student's T test.

Figure 3.13

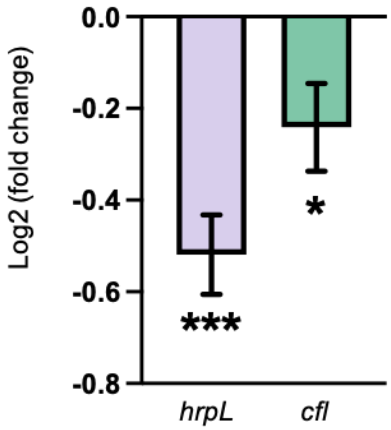

Figure 3.13. BCAAs reduce virulence factor transcript abundances *in planta*. *hrpL* and *cfl* expression, internally normalized to *recA,* from Pst co-infiltrated for 3 hours with 10mM each BCAA and normalized to Pst infiltrated with 5mM MES alone. N = 6. * < 0.05, *** < 0.001. Student's T test.

Figure 3.14

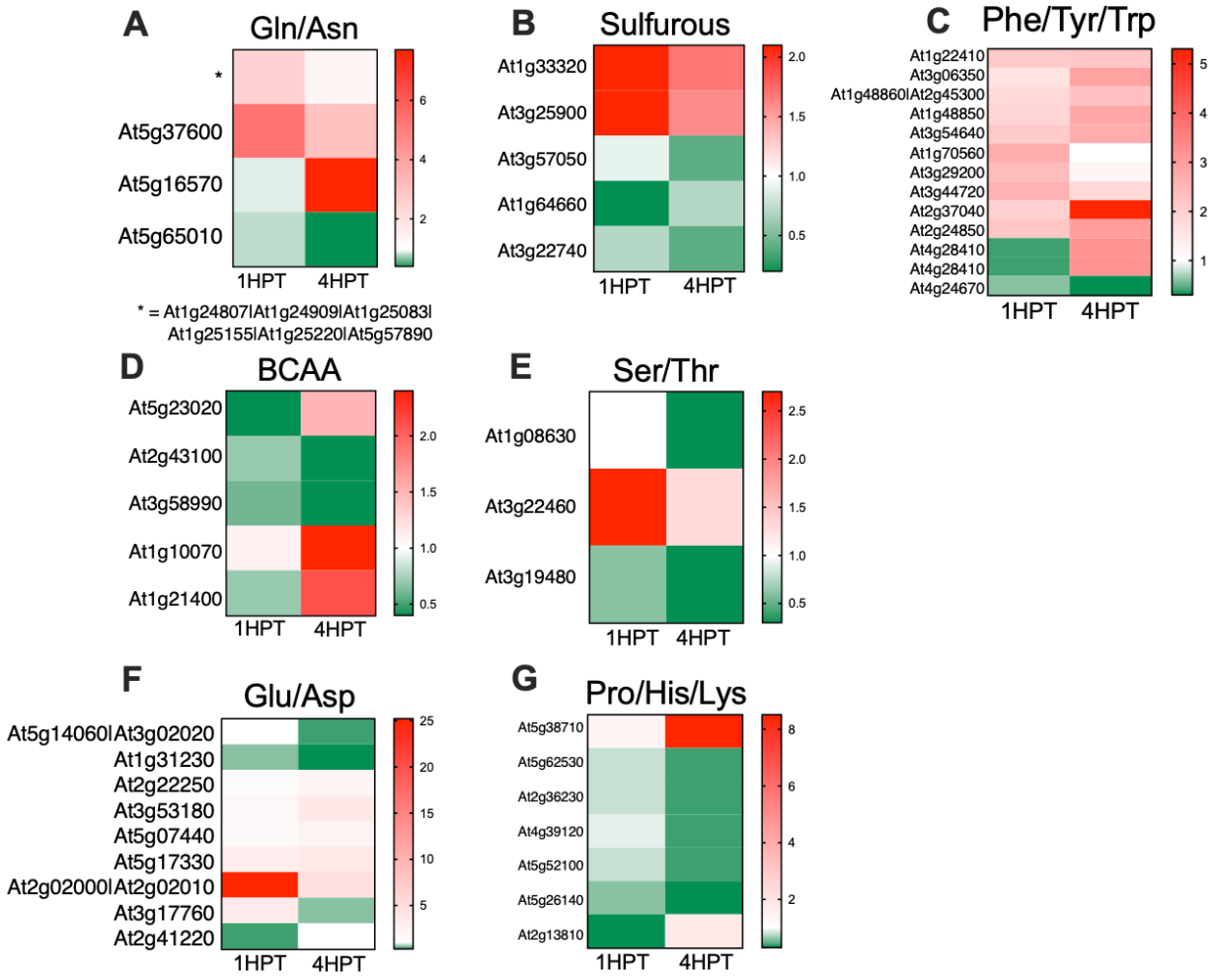
A
Gln/Asn
*
At5g37600
At5g16570
At5g65010
1HPT
4HPT
6
4
2
* = At1g24807|At1g24909|At1g25083|
At1g25155|At1g25220|At5g57890
B
Sulfurous
At1g33320
At3g25900
At3g57050
At1g64660
At3g22740
1HPT
4HPT
2.0
1.5
1.0
0.5
C
Phe/Tyr/Trp
At1g22410
At3g06350
At1g48860|At2g45300
At1g48850
At3g54640
At1g70560
At3g29200
At3g44720
At2g37040
At2g24850
At4g28410
At4g28410
At4g24670
1HPT
4HPT
5
4
3
2
1
D
BCAA
At5g23020
At2g43100
At3g58990
At1g10070
At1g21400
1HPT
4HPT
2.0
1.5
1.0
0.5
E
Ser/Thr
At1g08630
At3g22460
At3g19480
1HPT
4HPT
2.5
2.0
1.5
1.0
0.5
F
Glu/Asp
At5g14060|At3g02020
At1g31230
At2g22250
At3g53180
At5g07440
At5g17330
At2g02000|At2g02010
At3g17760
At2g41220
1HPT
4HPT
25
20
15
10
5
G
Pro/His/Lys
At5g38710
At5g62530
At2g36230
At4g39120
At5g52100
At5g26140
At2g13810
1HPT
4HPT
8
6
4
2

Figure 3.14. Expression of AA-consuming/generating-related genes in *A. thaliana* flg22 elicited plants. Amino acids are grouped by similar properties. A. Nitrogenous AA glutamine and asparagine. B. Sulfur containing AA cysteine and methionine. C. Aromatic amino acids phenylalanine, tyrosine, and tryptophan. D. BCAAs leucine, valine, and isoleucine. E. Hydroxyl containing AA threonine and serine. F. Acidic residues glutamic acid and aspartic acid. G. Large, charged AA proline, histidine, and lysine. For all scales, green is representative of less expression, white is no change between mock and flg22 elicitation, and red is increased expression.

Figure 3.15

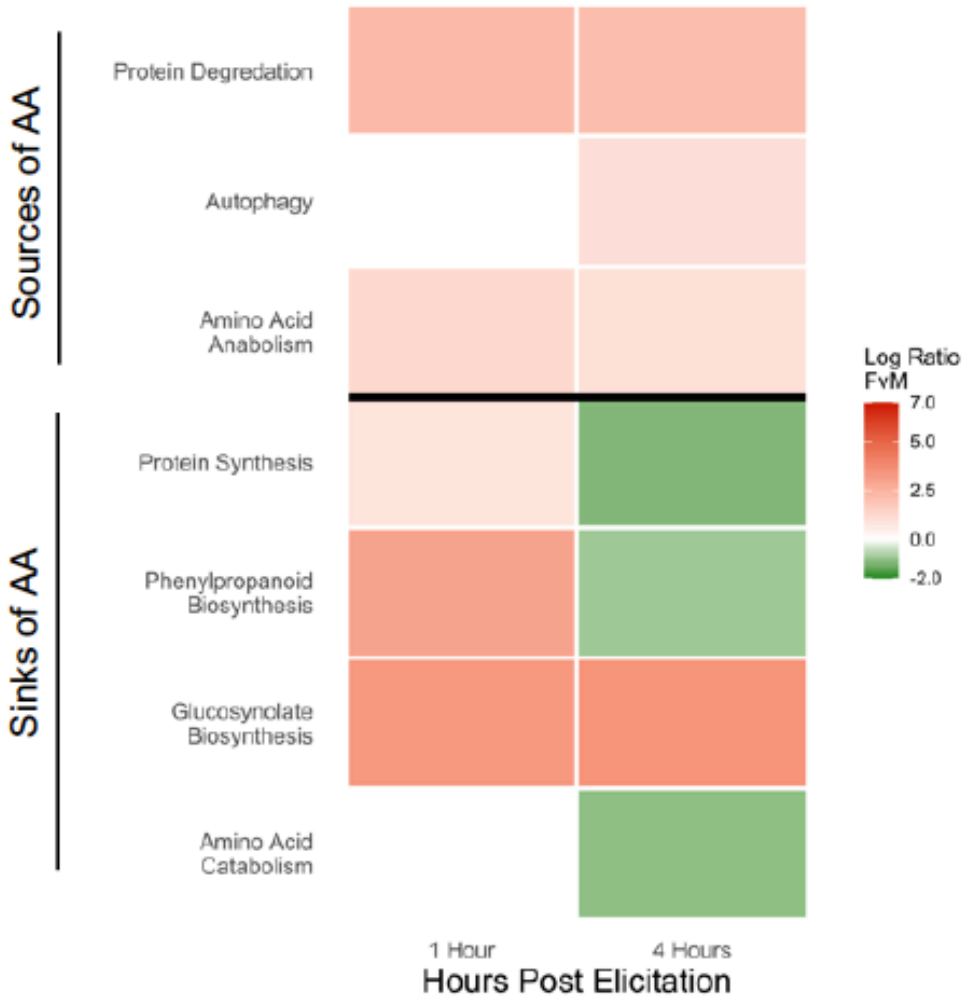
Sources of AA
Sinks of AA
Protein Degredation
Autophagy
Amino Acid Anabolism
Protein Synthesis
Phenylpropanoid Biosynthesis
Glucosynolate Biosynthesis
Amino Acid Catabolism
1 Hour
4 Hours
Hours Post Elicitation
Log Ratio FvM
7.0
5.0
2.5
0.0
-2.0

Figure 3.15. Average log2(fold change) of genes related to AA metabolic functions in flg22 elicited *A. thaliana* plants. The genes are grouped by GO terms Protein degradation (proteolysis), autophagy, AA anabolism (biosynthesis) which comprise sources of AA, as well as protein biosynthesis, phenylpropanoid biosynthesis, glucosynolate biosynthesis, and AA catabolism which comprise sinks of AA. Green is representative of less expression on average in flg22 elicited plants, white is no change between mock and flg22 elicitation, and red is increased average expression.

Chapter 4: Modulation of BCAA metabolic and regulatory genes in Pst alters infectivity in A. thaliana

4.1 Summary

Pathogens are in a constant contest with their hosts to sequester growth-promoting nutrients and prevent the onset of defense mechanisms. In previous chapters, connections between BCAAs and pathogenesis have been described; here, we assess the impacts of genetic modulation of BCAA catabolic genes and a BCAA-responsive regulatory gene *in vitro* and *in planta*. Overexpression of catabolic genes leads to growth dysregulation under normally permissive conditions as well as compromises the infectivity of the pathogen. Modulation of the BCAA-responsive regulatory gene *lrp* lead to dysregulation of growth and virulence, resulting in decreased leaf colonization during foliar infections. These findings implicate direct ties between metabolism of Pst and virulence induction, necessitating further study on potential avenues of pathogen control leveraging these mechanisms.

4.2 Introduction

Amino acids are critical to bacteria not only for peptide synthesis but also because they can be used as primary metabolites for biomass production. Thus, AA metabolism is tightly regulated. Pst is able to use many amino acids as single carbon sources (Figure 2.5). However, Pst lacks the *bkd* (*b*ranched chain *k*eto-acid *d*ehydrogenase) operon, which is responsible for the first step in BCAA catabolism (Figure 4.1). This limits the utility of BCAAs as a single carbon source. In these experiments, as well as previous studies, Pst has been shown to produce growth on leucine, though not to the extent of other organisms. Further, isoleucine and valine are reported to produce little to no growth, all as a function of lacking the *bkd* operon.

The bkd *operon*

Due to the growth produced by leucine, there must be alternative pathways or enzymes to catalyze the first steps of BCAA metabolism in Pst. We have predicted based on homology what these enzymes could be that convey the ability to use BCAAs by Pst (Figure 4.1). The most closely homologous Pst genes to members of the bkd operon in Pae are illustrated in Table 3.1. The multienzyme complex of *bkd* falls into the oxo-acid dehydrogenase complexes (OADHC) protein family, of which the homologous pyruvate dehydrogenase and succinate dehydrogenase complexes are a part. In *Thermoplasma acidophilum,* the constituents of the OADHC most closely related to pyruvate dehydrogenase also show 4-methyl-2-oxopentanoate-producing capabilities. This suggests OADHCs could be fairly

permissive in their substrate usage (Heath et al, 2004). Because Pst contains two paralogous OADHCs, there is likely substrate utilization that allows for modest growth on leucine as the single carbon source.

In *P. putida*, the *bkd* operon contributes a set of reactions that produce substrates for the *liu* operon (Figure 4.1). Notwithstanding that this operon is missing in Pst, leucine still produces modest growth when supplied as a sole carbon source (Figure 2.5). In addition, and as suggested previously (Rico & Preston, 2008) the DNA re-arrangements present at the *liu* operon would suggest that Pst could not catabolize leucine. Again, contrasting this assumption, *in vitro* growth data presented in our study (Figure 2.5, Figure 3.4A) shows that leucine, or a combination of the three BCAAs, supports Pst growth, suggesting that other enzymes compensate for the loss of 2-oxoacid dehydrogenases encoded by the *bdk* operon. In *P. aeruginosa* and *P. putida*, the pyruvate dehydrogenase complex (PDC) and the succinate dehydrogenase complex (SDHC), share significant homology with the 2-oxoacid dehydrogenases (Burns et al., 1988; Hester et al., 1995). In Pst, PSPTO_3860, PSPTO_5005, PSPTO_5006, and PSPTO_2201 encode the PDC enzymes, while PSPTO_2199, PSPTO_2200, and PSPTO_2201, encode the SDHC enzymes. Importantly, enzymes in these two complexes show a degree of promiscuity in substrate utilization, suggesting that they could also initiate BCAAs catabolism in the absence of the *bkd* operon (Heath et al., 2004). Indeed, SDH enzymes encoded by PstDC300 showed the highest identity to those encoded by the bkd operon in *P. putida* (Figure 4.1, Table 3.2). It is likely through these related enzymes that *Pst* is still able to use leucine as a

single carbon source. Importantly, Pst synthesizes BCAAs likely via enzymes encoded by the *ilv* and *leu* operons, both present in its genome (Buell et al., 2003).

Two types of expression modulation

For the purposes of these experiments involving direct modulation of metabolic and regulatory genes, we have constructed several plasmids that use the neomycin phosphotransferase II (NPTII) promoter to drive gene expression. We have constructed two types of expression plasmids: sense overexpression and antisense overexpression. Due to the properties of Gateway cloning, it is relatively easy to create interchangeable gene cassettes for one plasmid backbone. A full illustration of the cloning scheme is presented in Figure 4.3.

For sense expression constructs, we cloned the sense strand of the GOI to overexpress the gene. These constructs were straightforward and allowed us to test excess expression of our GOIs. Conversely, the antisense expression constructs overexpress the antisense strand of the GOI to create what is functionally a knock-down of the gene. We used this approach as opposed to deletion knockouts to control for the metabolic draw overexpression itself creates, and because metabolic genes are more likely to be essential for the survival of an organism. Antisense-mediated gene down-regulation has been previously used on essential genes in E. coli with success, as it creates viable strains to test the function of essential genes (Chan et al, 2010). Further, several instances of antisense regulation has been described across several species of bacteria,

suggesting it could be a broad spectrum tool for knockdown generation (Chan et al., 2010; Georg & Hess, 2011; Gillaspie et al., 2009).

Targets of Modulation

The two studies (Lovelace et al., 2018; Nobori et al., 2018) looking at Pst global gene expression during infection in flg22-treated plants show increasing expression of *liuA* and *liuD* over time, while *lrp* expression is decreased in flg22-treated plants. Both predictions from iPst19 and transcript abundance from unconstrained global gene expression (non-contextualized data) point to the catabolism of BCAAs as a feature of infection in defense-elicited plants. Catabolism of amino acids is part of a feedback loop in many bacterial species; regulation of expression and function of anabolic and catabolic operons is linked to the concentration of starting, intermediary and terminal products. Leucine catabolism has been shown in *E. coli* to be under partial control of the leucine-responsive regulatory protein (Lrp). Lrp has been shown in *E. coli* to alter the expression of >30% of the genome; the full spectrum of regulation reinforced by Lrp are not fully understood, yet it is clear that amino acids, particularly BCAAs, influence which genetic targets are regulated by Lrp (Cho et al., 2008; Kroner et al., 2019). The homolog for Lrp in Pst (PSPTO_0100) shares significant similarity to Lrp in E. coli, with roughly 61% identity at the amino acid level using BLAST (Table 3.3). It is not known which genes Lrp in Pst regulates; however, in *Salmonella* and *E. coli*, Lrp regulates virulence, transition into stationary phase, and amino acid metabolism, among many other processes (Baek et al., 2009; Cho

et al., 2008). Considering this, we included the leucine-responsive regulatory protein (Lrp; PSPTO_0100) in our studies for the purpose of understanding BCAA involvement at the regulatory level. By including Lrp in the scope of our studies, we sought to understand if the catabolism of BCAAs, present in the transcriptional profiles of previous studies and highlighted by iPst19, directly influenced the outcome of infection by this upregulation alone, or if catabolism of BCAAs existed as a compensatory mechanism to influence regulation by the Lrp-BCAA relationship. As previously illustrated in Chapter 1, the regulatory mechanisms by Lrp in relation to concentrations of BCAA levels can be thought of as a ratio; when one aspect of the ratio is modulated, be it BCAA levels or Lrp levels, this can create an excess of non-BCAA bound Lrp, thus altering its transcriptional targets.

Importantly, Pseudomonads have been shown to tightly regulate intracellular levels of BCAAs that could impact this ratio of Lrp to BCAA. In iron replete conditions, Pae has been shown to greatly increase transcript levels of BCAA catabolic genes and suppress BCAA synthetic genes; regardless of the external levels of BCAA (Nelson et al., 2019b). This suggests tight regulation of internal levels of BCAA is necessary, likely because of their regulatory impact on Lrp or other BCAA sensors. Further, these previous studies could explain why, despite significantly increased transcription of *liuD* and *liuA* in Pst exposed to flg22 plants, there is no appreciable increase in BCAAs aside from valine in flg22 plants. The decoupling of external BCAA levels and internal levels could be an important homeostatic regulatory mechanism.

In this chapter, we sought to understand how changing the levels of Lrp and liuD/liuA could impact this ratio between Lrp and BCAAs, and thus the transcriptional targets. We have already illustrated how high levels of BCAAs suppress the virulence markers *hrpL* and *cfl* both *in vitro* and *in planta*. Within our working model of Lrp in Figure 1.1, increasing the levels of Lrp causes more Lrp to act outside the presence of BCAAs. Conversely, decreasing the levels of Lrp should have the opposite effect, where the is less Lrp, so there is a lower functional concentration of BCAA necessary to bind with the available Lrp. The creates a situation where most of the Lrp molecules are bound with BCAA and share a transcriptional profile similar to a high BCAA concentration.

Lrp shares significant homology with 8 other loci in Pst. All ORFs belong to a family of transcriptional regulators called feast-famine regulatory proteins (FFRPs). Lrp belongs to a subclass of global regulators, while asnC type proteins belong in a subclass that regulates specific targets. Pst has 9 FFRPs annotated within its genome, whereas *E. coli* has 3, *Bacillus subtilis* has 7 and *Pseudomonas putida* has 13 (Table 3.4). The expansion of FFRPs in gammaproteobacteria does not seem to be related to lifestyle, as both pathogens and non-pathogens within *Pseudomonads* contain several FFRPs.

4.3 Materials and methods

Plasmid construction:

All bacterial strains and plasmid specifications can be found in Chapter 4, Table 4.5.

pBBR5pemIKpKan was purchased from Addgene and prepared via Qiagen miniprep spin kit according to kit specifications. The complete *lrp, liuD* and *liuA* sense and anti-sense

transcripts sequences from Pto were PCR amplified with Gateway attB sites integrated at each end, oriented in the sense direction. PCR products were gel purified and first integrated into pDONR221 (Invitrogen) via BP recombination, followed by LR recombination into pBBR5pemIKpKan to yield overexpressing or antisense expressing plasmids. pENTR-uidA(Gateway cloning kit) was recombined with pBBR5pemIKpKan to yield puidAOX. E coli DH5a were transformed with the final plasmid constructs selected on gentamicin 25µg/mL supplemented media. Plasmids were transformed into *Pto* via triparental mating with helper strain *E. coli* : pRK2013.

Triparental Mating:

To transfer the plasmid of interesting into Pst, triparental mating was needed. The donor strain, the recipient strain (Pst), and the helper strain (E. coli containing pERK2013) were grown overnight in rich culture with appropriate selection marker, separately. Cultures were pelleted and washed five times to eliminate any contaminating antibiotics. Pellets were resuspended in water at an OD >1.0. The tree strains were combined in a ratio of 10 (Recipient) : 1 (Helper) : 1 (Donor) by OD and plated in compact puddles on non-selective LB agar plates. Puddles were allowed to sit overnight at 28C, face up. Puddles were scraped off the surface the following day and resuspended in water. Cells were then plated on selective media containing markers for both Pst and the plasmid of interest. Colonies typically formed within 48 hours of selection. Colonies were screened for resistances and the genes of interest via qRT-PCR.

RNA and cDNA preparation:

RNA was extracted with Trizol reagent (Ambien). For samples containing with plant alone or plant and bacterial tissue, flash-frozen samples were ground in 1 mL of Trizol with metal beads for at 25Hz until liquified. Samples with bacteria were then homogenized using 0.1mm silica beads at 8000rpm. Samples with only bacteria began at this step. Liquid phase separation with chloroform isolated RNA from protein, DNA and phenolics at 11,200

x g for 15 minutes at 4C. Supernatant was combined with equal parts isopropyl alcohol to precipitate RNA, at 13,300 x g for 15 minutes. Contaminating DNA was digested using DNase 1 from Promega for 30 minutes to an hour, followed by cDNA synthesis using m-MLV and normalized inputs of DNA-free RNA, also from Promega using the supplied protocol and reaction conditions.

Transcript quantification:

Transcripts of genes were quantified via quantitative RT-PCR using an ABI7500 Fast thermocycler and CW Biosciences qRT-PCR ready mix. Primer sequences can be found in the primer addendum within the supplemental information. Reactions were prepared to the specifications of the ready mix. Transcripts were relatively quantified using the ΔΔCt normalization method. All bacteria transcripts were internally normalized to *recA* unless otherwise noted. All plant transcripts were internally normalized to *act2* unless otherwise noted. Primer names and sequences can be found in Chapter 4, Table 4.6. All statistical tests for gene expression were Student's T test against the externally normalizing condition, unless otherwise noted. * $p < 0.05$, ** $p < 0.01$, *** $p < 0.001$, **** p

Short term bacterial culturing for gene expression:

For short term transcript quantification, bacteria were grown overnight as previously described. Cultures were washed and resuspended to a final OD of 0.2 to 0.3 in the assay media. 3 HPI, samples were taken for gene expression and RNA was isolated as previously described.

Pre-elicitation:

Prior to infiltration, plants were covered with plastic domes to increase localized humidity to near 100%, ensuring stomata are fully open. 4 leaves per plant (pairs 5 and 6) were elicited via blunt end syringe with either water (mock) or 1μM flg22 in water. Any remaining liquid on the exterior of the leaf was wiped off. Plants were elicited for 24 hours. Elicitation

with BCAAs was done using 10mM BCAA in water or water alone for 24 hours, after which leaves were harvested for gene expression.

Long term infection quantification and gene expression:

4 leaves per plant (pairs 5 and 6) were infiltrated with 0.0002 OD Pst (or derivative strain). For naïve plants, infection duration was 72 hours. For elicited plants, infection duration was 48 hours to prevent total leaf collapse. Leaves were harvested; normalized amounts of leaf tissue were taken using a 4mm cork borer. 8 leaf discs from one plant contributed to one CFU sample. Discs were pulverized with a metal bead for 5 minutes at 25Hz in 400µL sterile water. Samples were serially diluted 1:10, 5µL from each dilution was plated on solid LB agar with appropriate selection markers. 16-20 hours post plating, CFUs were quantified. For gene expression, remaining leaf tissue was flash frozen. RNA was extracted and transcripts quantified as previously described.

Short term infection and gene expression:

4 leaves per plant (pairs 5 and 6) were infiltrated with 0.02 OD Pst (or derivative strain). For all plants, infection duration was 3 hours. Leaves were harvested; normalized amounts of leaf tissue were taken using a 4mm cork borer. 8 leaf discs from one plant contributed to one CFU sample. Discs were pulverized with a metal bead for 5 minutes at 25Hz in 400µL sterile water. Samples were serially diluted 1:10, 5µL from each dilution was plated on solid LB agar with appropriate selection markers. 16-20 hours post plating, CFUs were quantified. Due to the limited bacteria present after 3 HPI, samples used for gene expression were infiltrated with 0.2 OD bacteria. Leaves were harvested and flash frozen and RNA was extracted as previously described.

Media formulations:

For growth curves in a rich media, bacteria were inoculated in King's B liquid media with the appropriate selection marker. For growth curves in virulence inducing media, HMM was used. For growth curves in minimal media, modified M9 media was used. In addition

to salts from typical M9 media, sterile 100μM sucrose and 5mM $MgSO_4$, final concentrations, were added to facilitate Pst growth. Without these additions, growth is not observable within this system.

Doubling time calculations:

To calculate doubling time from a growth curve, each well within a 96 well plate was treated as an individual technical replicate. Averaging across technical replicates and proceeding with calculations is not advisable, as subtle differences in the results may be lost. 10 to 15 measurements within the exponential growth phase were used to produce an interpolating line; the line was optimized within the curve to have the best R^2 value and the highest exponent. Doubling time was calculate from taking the natural log of 2 divided by the exponent within the equation for the interpolated curve.

Western blot analysis:

To quantify the extent of Lrp overexpression and knockdown influenced by transcript modulation, we used traditional western blotting and fluoro-immunochemistry. Soluble proteins were extracted from Pst or E. coli grown overnight via sonication in PBS-SDS buffer. Samples were sonicated at 25% power for 3 seconds on 10 seconds off a total of 8 times. Samples were centrifuged for 5 minutes at 13,000g. Soluble proteins were quantified from the supernatant using Bradford's reagent quantification. Samples were added to 3x Laemmli's buffer and heated for 5 minutes at 85C, after which they were centrifuged again at 13,000g for 5 minutes. 15μg total protein was loaded and separated into a 8-16% gradient denaturing PAGE Tris-Glycine gel, transferred to a nitrocellulose membrane; total protein was visualized using Ponceau's stain. Anti-Lrp (*E. coli* origin) was added for overnight incubation at 4C post-blocking, followed by anti-Mouse secondary antibody conjugated to LiCor fluorophore for 1 hour.

4.4 Results

Construction of Plasmids and Validation of Overexpression

We cloned the ORFs for PSPTO_0100(*lrp*), PSPTO_2736(*liuD*), and PSPTO_2739(*liuA*) into the broad host range vector pBBR5pemIKpKan, placed under the control of the NPTII promoter to increase transcript abundance and transformed them into Pst (Figure 4.3). For functional knockdowns, we cloned the ORFs in antisense orientation into the same plasmid backbone. Transcript abundance was confirmed via q-RTPCR (Figure 4.5). *lrp* was significantly overexpressed in both the sense and the antisense orientation, while both *liuA* and *liuD* were each moderately overexpressed by comparison. The *liuA* antisense construct did not show significantly overexpression of the AS-transcript. AS construction was confirmed using RT-PCR specifically using internal primers as a control and the attB1 primer, which sits specifically upstream of “start” codon within the AS transcript (Figure 4.5C). The overexpression of *lrp* did not change expression levels of *liuD* or *liuA,* nor did the overexpression of the catabolic genes impact the expression of *lrp,* all relative to expression in the *uidA* overexpressor (uidA-OX) (Figure 4.5). This is also true for the antisense contracts: there is no significant suppression or induction of the tested GOIs other than the specific GOI in the construct.

To test if there was a specific transcript disruption caused by AS expression, we designed primers to amplify only endogenous mRNAs for Lrp. Neither lrp-OX or lrp-AS showed any significant modulation of the endogenous *lrp* transcript when

compared to *uidA*-OX (Figure 4.6A). This suggests the AS modulation likely does not happen at the level of the mRNA transcript.

Because we could not confirm AS knockdown via qRT-PCR, we used western blotting of total soluble protein lysates. To visualize Lrp in the total protein gradient, we used an antibody developed by Kroner and colleagues (Kroner et al., 2019) that was developed against a highly-conserved epitope of Lrp (personal correspondence, actual epitope was not described). Using WT *E. coli* and *E. coli*Δ*lrp,* we were able to confirm the specificity of the antibody. However, in *E. coli*Δ*lrp* complimented with Pst *Lrp,* there was no apparent cross-hybridization of the anti-Lrp antibody (Figure 4.6B). Further, there was no cross-hybridization in any of the Pst samples, suggesting this method would not allow us to draw conclusions about the extent of knockdown from AS expression.

Impacts of Plasmids on in vitro Growth

The overexpression of *lrp* and *liuD* showed dramatic growth inhibition in rich media. Both construct carriers showed longer lag phases than the uidA-OX control (Figure 4.7AB). At the fastest growth rate, the doubling time for both liuD-OX and lrp-OX was significantly higher than both WT Pst and uidA-OX. The overexpression of *liuA* showed moderate growth inhibition compared to WT Pst and no significant difference to uidA-OX in rich media.

We included the uidA-OX as a control for the potential metabolic draw produced by constitutively expressing a gene from a plasmid. Interestingly, there is no

significant difference between WT Pst and uidA-OX, suggesting that the metabolic sink is not as dramatic as we originally thought (Figure 4.7D).

The overexpression of all antisense GOIs did not show growth inhibition in rich media when compared to uidA-OX (Figure 4.7). However, the same construct carriers show significantly different doubling times from WT Pst (Figure 4.7D).

Impacts of Plasmids on Infection Dynamics

The overexpression of sense catabolic genes and *lrp* resulted in lower colonization of the leaf than uidA-OX in naïve plants over 72 hours (Figure 4.8A). The growth of uidA-OX was similar to WT levels in previous experiments under the same conditions, suggesting the differences we see are not the result of hyper infectivity of uidA-OX.

Interestingly, infectivity of lrp-OX, liuD-OX and liuA-OX did not deviate from uidA-OX in pre-treated plants; neither mock nor flg22 elicitation highlights the differences in infectivity seen in naive plants. Likely, this is a result of the different experimental designs, where treated plants begin to develop leaf collapse past 48 HPI, thus rendering 72 HPI similar to the naive infection leaf harvest difficult. Flg22 pretreatment still resulted in dramatically less colonization in all genotypes, where on average, there is a difference of two logs of growth between mock and flg22 pretreatment (Figure 4.8B). There did not seem to be any qualitative differences in the symptom development on the leaves between carriers in both naive and pretreated conditions. For the remainder of the studies, we only used the modulation constructs for Lrp. While it is clear that *liuD* and *liuA* warrant further

study, our choice to continue only with *lrp* is a direct result of the potential impacts it has as a global transcriptional regulator. Further characterization of *liuD/A* modulated expressors is necessary.

Impacts of Lrp modulation on virulence targets

Overexpression of the sense transcript of Lrp showed increased transcript abundance of both *hrpL* (A) and *cfl* (C) compared to uidA-OX when incubated in a KB medium (Figure 4.9). Interestingly, the overexpression of virulence targets is medium dependent, as expression of *hrpL* and *cfl* appears as expected in the virulence-inducing HMM (Figure 4.9BD). This suggests that the overexpression of virulence in *lrp* sense expresser strain does not constitutively add to the physiological expression levels of virulence markers; rather, there is a maximum transcriptional output that is achieved in HMM that cannot be surpassed by *lrp* modulation (Figure 4.9AB).

Overexpression of the antisense *lrp* transcript shows a contrasting pattern. For both *hrpL* (A) and *cfl* (B) in KB medium, the transcript abundance is significantly reduced, both compared to the uidA-OX control and to the lrp-OX strain. The pattern is extended to a reduction of *hrpL* (C) transcripts in HMM, but not *cfl* (D) transcripts in HMM, suggesting virulence is partially modulated in virulence-inducing media (Figure 4.9).

The modulation of *lrp* lead to a decreased colonization during naïve foliar infections in both overexpression and antisense expression of *lrp* (Figure 4.10). For Lrp-OX, this is unsurprising, as it has a metabolic growth phenotype even in KB medium.

Further, lrp-OX constitutively activates virulence gene transcription (Figure 4.9), which has been shown in other species to decrease growth and colonization due to the large metabolic cost of dysregulation of virulence (Sturm et al., 2011). Conversely, the decreased colonization of lrp-AS is likely not due to metabolic restriction of growth, as there was no growth phenotype present in liquid culture (Figure 4.7D). Again, we propose a contributing factor to this decreased colonization is dysregulation of virulence in the opposite direction of lrp-OX. Due to the apparent constitutive downregulation we see in both inducing and suppressing media, it appears lrp-AS cannot induce virulence, which will have drastic impacts on its ability to proliferate in a host during infection (Deng et al., 1998).

Impacts of *Lrp* modulation on other potential targets

Modulation of *lrp* transcripts also causes differential expression of the high-affinity BCAA transporter *braD*. In KB media (high in BCAA), the overexpression of the both the sense and antisense *lrp* lead to an increase in the expression of *braD* (Figure 4.11). While the regulation of *braD* by *lrp* has not been previously described, if the regulatory relationship exists, it is likely that *lrp* regulates the expression of *braD* indirectly due to the shared overexpression in both strains.

Due to the dissimilarity of lrp homologous sequences with other FFRPs at the nucleotide level, it is unlikely that expression of an antisense Lrp would have any impact on transcriptional levels of these FFRPs.

4.5 Discussion

Branched-chain amino acids serve a central role in integrating extracellular and intracellular cues to maximize bacterial growth and survival (Kaiser & Heinrichs, 2018; Tani et al., 2002). BCAAs exert their regulatory role through the modulation of transcriptional regulators that control the expression of metabolic and virulence genes in pathogenic bacteria (Kaiser & Heinrichs, 2018). Recent studies have provided evidence that BCAAs and the sensor proteins that integrate gene expression also play an important role in the pathogenesis of plant bacterial pathogens. In *Xanthomonas citri* pv. citri, leucine degradation takes place via the acyl-CoA carboxylase complex (ACC) encoded by the *acc* locus. Open reading frames in the *acc* locus show an organization similar to that of the *liu* operon in *P. aeruginosa*. In addition, *AccC* and *AccD* show 53% and 70% identity with *liuD* (PSPTO_2736) and *liuB* (PSPTO_2738), respectively, strongly suggesting that both the *X. citri acc* operon and the *Pst liu* operon are functionally equivalent and both contribute to leucine catabolism. Mutant strains in *accC* and *accD* showed attenuated growth on citrus plants, suggesting that leucine catabolism in *X. citri* is important for virulence expression *in planta* (Tomassetti et al., 2018).

The BCAA responsive transcriptional regulator *Lrp* belongs to a large and conserved family of proteins that bind DNA and regulate gene expression in response to changing levels of intracellular BCAAs (Thaw et al., 2006). The modulation of virulence gene expression exerted by BCAAs on *Lrp* is both ways, positive on certain genes and negative on others (Calvo & Matthews, 1994). In *Erwinia amylovora, Lrp* is necessary to express virulence genes that control

motility and synthesis of exopolysaccharides when BCAA levels are low (Schachterle & Sundin, 2019). The evidence contributed by Tomassetti et al. (Tomassetti et al., 2018), Schachterle and Sundin (Schachterle & Sundin, 2019), and the data presented in this study, strongly suggest that leucine degradation, and more broadly, BCAAs degradation, plays a positive role in virulence modulation. The molecular mechanisms by which BCAAs degradation translates into *Lrp*-mediated expression of virulence in these plant pathogens are still unclear. However, our data suggest that a complex balance between *Lrp* protein levels and intracellular levels of BCAAs drives *Lrp* transcriptional activity towards virulence genes expression when *Lrp* is not associated with BCAAs. For instance, the overexpression of *Lrp* induces virulence gene expression in a rich medium where virulence genes are usually suppressed **(Figure 4.8AC**). On the other hand, the *lrp* down-regulation strain (*lrpAS*) shows *hrpL* expression levels below control levels in a minimal medium where *Pst* expresses high levels of *hrpL* (**Figure 4.8BD**). These data suggest that *Lrp* plays either a direct or indirect role in modulating Pst virulence. Since high BCAAs levels suppress *Pst* virulence gene expression (**Figure 3.5**) and induce *liuA* and *liuD*, the increased flux in leucine degradation detected in Pst that have been inoculated in MAMP-treated plants (**Figure 2.10**) suggests that lowering BCAAs levels could contribute to re-direct *Lrp* activity towards the expression of virulence genes to counter the overall virulence suppression exerted by MAMP-elicited plants.

4.6: Figures

Figure 4.1

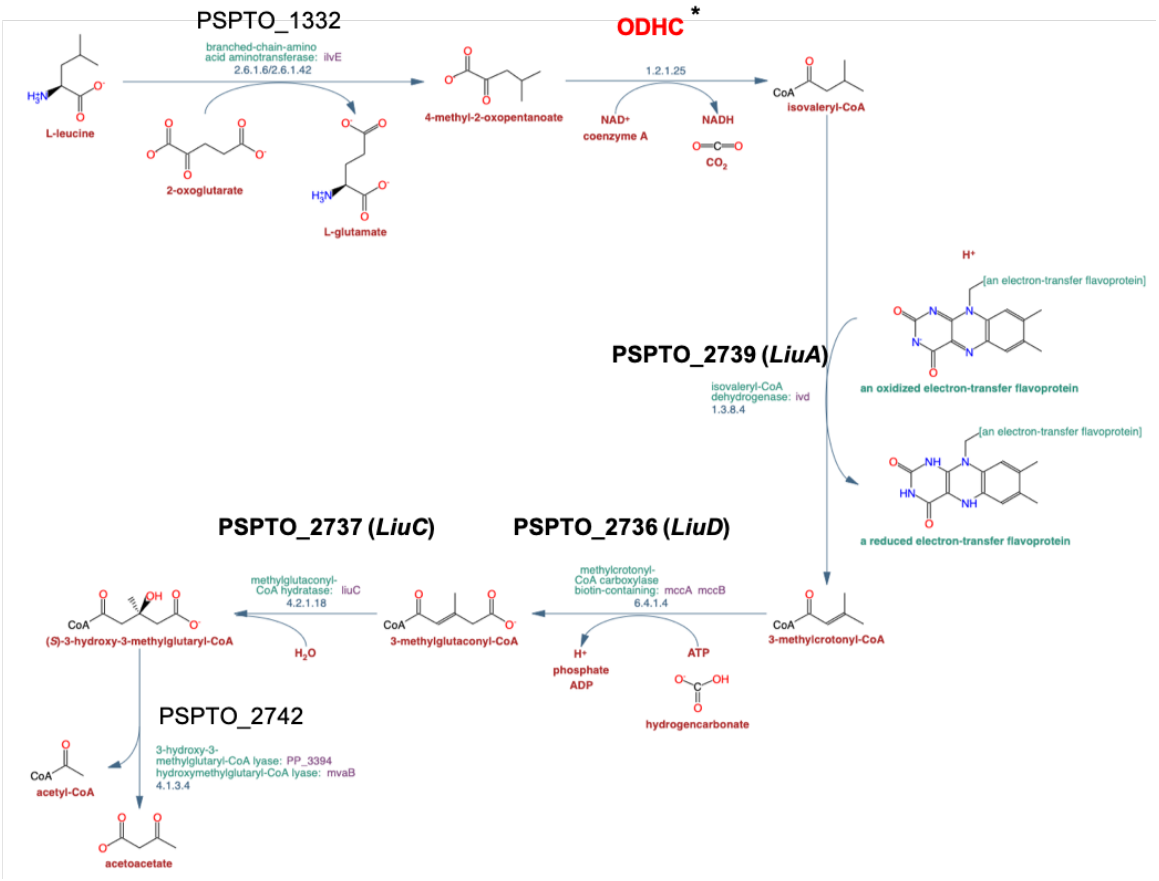

Figure 4.1. *Pst* tentative leucine catabolic pathway. Genes of the *liu* operon are shown in bold. In red is shown the metabolic step tentatively contributed by the *Pst* ODHC enzymes. (*) *Pst* genes encoding enzymes with significant identity to the BCKDC enzymes encoded by *P. putida bkd* operon: 2-oxoglutarate dehydrogenase-E1 component encoded by PSPTO_2199; 2-oxoglutarate dehydrogenase-E2 component encoded by PSPTO_2200 or PSPTO_5006; 2-oxoglutarate dehydrogenase-E3 component encoded by PSPTO_2201. Modified from MetaCyc (https://metacyc.org/).

Figure 4.2

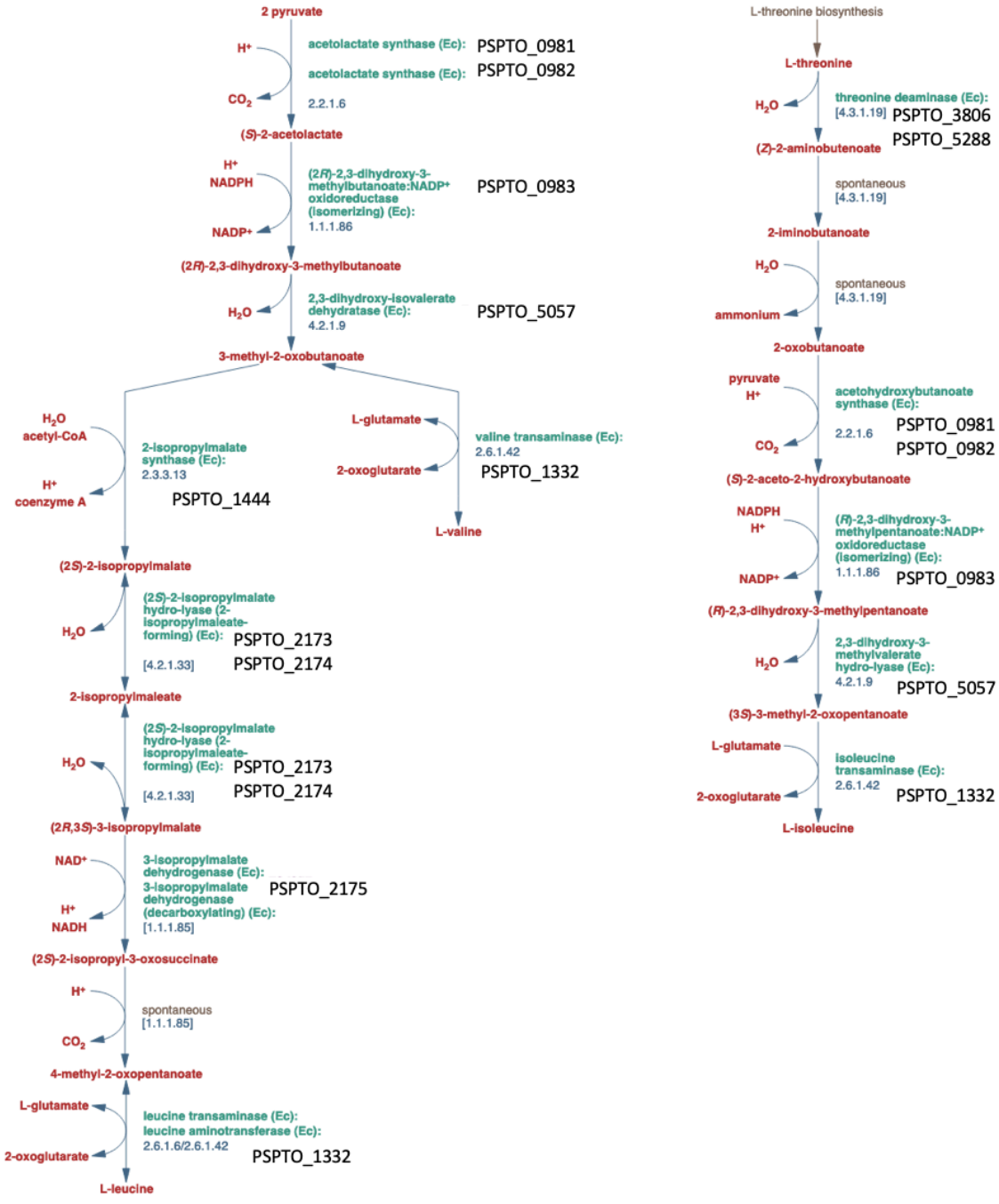
2 pyruvate
H+
CO2
acetolactate synthase (Ec): PSPTO_0981
acetolactate synthase (Ec): PSPTO_0982
2.2.1.6
(S)-2-acetolactate
H+
NADPH
NADP+
(2R)-2,3-dihydroxy-3-methylbutanoate oxidoreductase (isomerizing) (Ec): 1.1.1.86 PSPTO_0983
(2R)-2,3-dihydroxy-3-methylbutanoate
H2O
2,3-dihydroxy-isovalerate dehydratase (Ec): 4.2.1.9 PSPTO_5057
3-methyl-2-oxobutanoate
H2O
acetyl-CoA
H+
coenzyme A
2-isopropylmalate synthase (Ec): 2.3.3.13 PSPTO_1444
L-glutamate
2-oxoglutarate
valine transaminase (Ec): 2.6.1.42 PSPTO_1332
L-valine
(2S)-2-isopropylmalate
H2O
(2S)-2-isopropylmalate hydro-lyase (2-isopropylmaleate-forming) (Ec): [4.2.1.33] PSPTO_2173 PSPTO_2174
2-isopropylmaleate
H2O
(2S)-2-isopropylmalate hydro-lyase (2-isopropylmaleate-forming) (Ec): [4.2.1.33] PSPTO_2173 PSPTO_2174
(2R,3S)-3-isopropylmalate
NAD+
H+
NADH
3-isopropylmalate dehydrogenase (Ec): 3-isopropylmalate dehydrogenase (decarboxylating) (Ec): [1.1.1.85] PSPTO_2175
(2S)-2-isopropyl-3-oxosuccinate
H+
CO2
spontaneous [1.1.1.85]
4-methyl-2-oxopentanoate
L-glutamate
2-oxoglutarate
leucine transaminase (Ec): leucine aminotransferase (Ec): 2.6.1.6/2.6.1.42 PSPTO_1332
L-leucine
L-threonine biosynthesis
L-threonine
H2O
threonine deaminase (Ec): [4.3.1.19] PSPTO_3806 PSPTO_5288
(Z)-2-aminobutenoate
spontaneous [4.3.1.19]
2-iminobutanoate
H2O
ammonium
spontaneous [4.3.1.19]
2-oxobutanoate
pyruvate
H+
CO2
acetohydroxybutanoate synthase (Ec): 2.2.1.6 PSPTO_0981 PSPTO_0982
(S)-2-aceto-2-hydroxybutanoate
NADPH
H+
NADP+
(R)-2,3-dihydroxy-3-methylpentanoate oxidoreductase (isomerizing) (Ec): 1.1.1.86 PSPTO_0983
(R)-2,3-dihydroxy-3-methylpentanoate
H2O
2,3-dihydroxy-3-methylvalerate hydro-lyase (Ec): 4.2.1.9 PSPTO_5057
(3S)-3-methyl-2-oxopentanoate
L-glutamate
2-oxoglutarate
isoleucine transaminase (Ec): 2.6.1.42 PSPTO_1332
L-isoleucine

Figure 4.2. BCAA anabolic pathway in Pst. The anabolic pathway is present and fully intact in Pst, suggesting synthesis of BCAAs responds to regulatory components and Pst is not auxotrophic to BCAAs. Modified from MetaCyc (https://metacyc.org/).

Figure 4.3

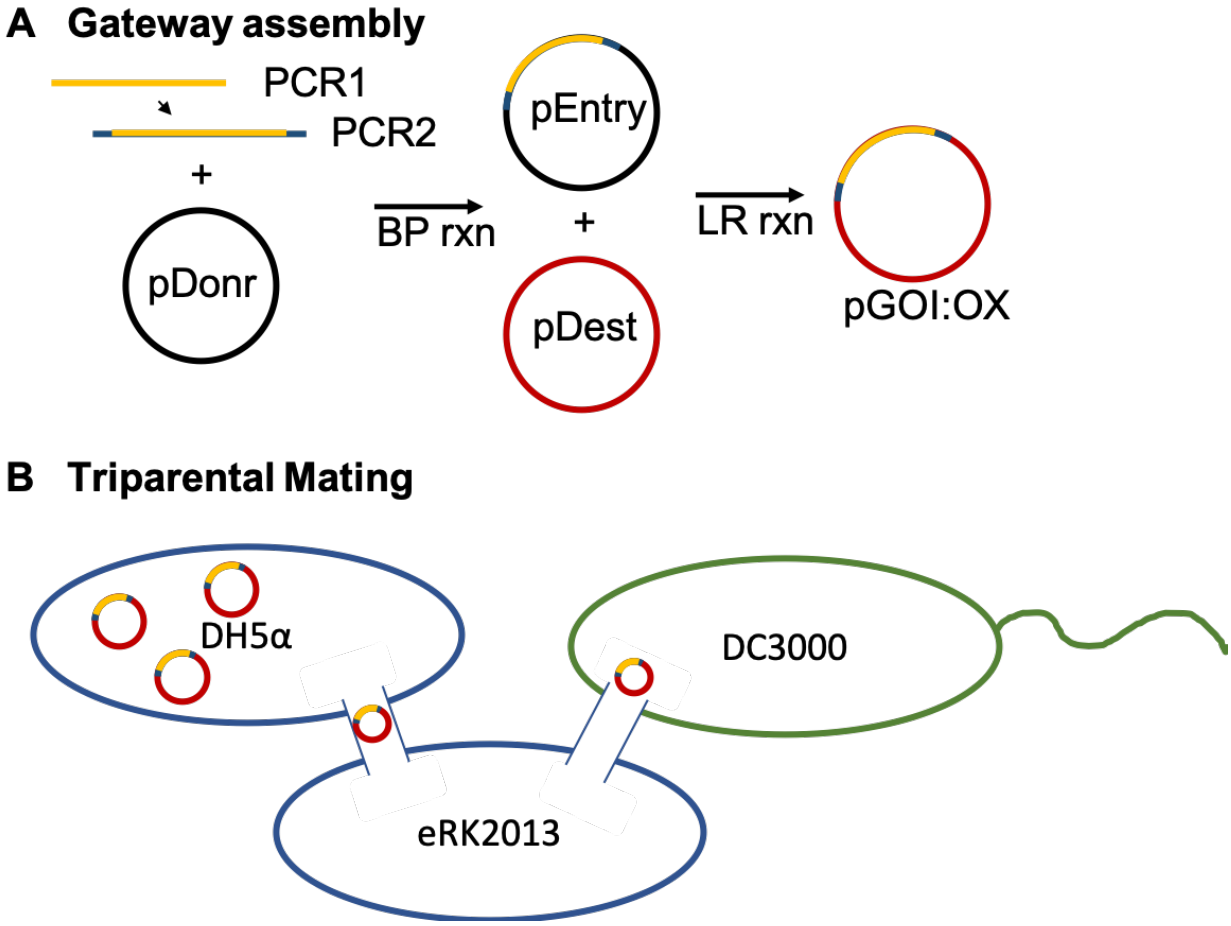
A Gateway assembly
PCR1
PCR2
+
pDonr
BP rxn
pEntry
+
pDest
LR rxn
pGOI:OX
B Triparental Mating
DH5α
DC3000
eRK2013

Figure 4.3. Schematic of the cloning strategy used for modulating metabolic and regulatory gene expression. A. Two-step gateway cloning was used to first amplify the gene of interest (GOI), followed by the addition of Gateway attB sites. The PCR amplicon was conjugated via BP reaction with a pDONR221 vector, and transformed into DH5a cells as the pEntry vector. pEntry was harvested and included in a LR reaction with the destination vector pBBR5pemIKpKan resulting in pGOI:OX. The final plasmid was again transformed into DH5a cells. B. The resultant DH5a cells were used with *E. coli* carrying the pERK2013 helper plasmid, allowing the pGOI:OX to be transformed into Pst, where the GOI was transcriptionally under the control of the strong NPTII promoter. *For functional knockdowns, the AS GOI was cloned using this same scheme.

Figure 4.5

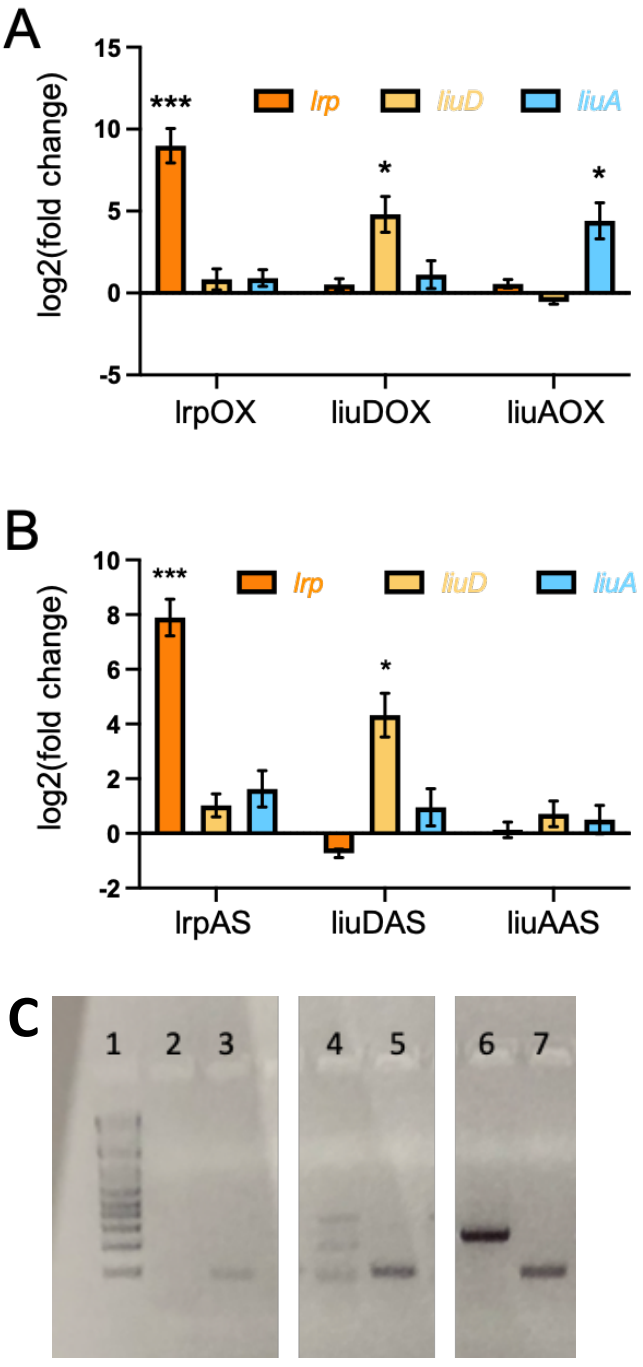
A
log2(fold change)
15
10
5
0
-5
***
*
*
lrp
liuD
liuA
lrpOX
liuDOX
liuAOX
B
log2(fold change)
10
8
6
4
2
0
-2
***
*
lrp
liuD
liuA
lrpAS
liuDAS
liuAAS
C
1
2
3
4
5
6
7

Figure 4.5. Confirmation of overexpressing plasmids in Pst. *lrp, liuD,* and *liuA* expression in *Pst* strains harboring either *lrp*OX*, liuD*OX*,* and *liuA*OX internally normalized to *recA* transcript abundance when compared to uidAOX. B. Antisense transcripts of *lrp, liuD,* and *liuA* expression in *Pst* strains harboring either *lrp*AS*, liuD*AS*,* and *liuA*AS internally normalized to *recA* transcript abundance when compared to uidAOX. Student's T test, * $p < 0.05$, *** $p < 0.001$. C. Confirmation of antisense construction of lrp-AS. 1: KB+ ladder, 2: uidA-OX (attB1-LrpF), 3: uidA-OX (LrpR-LrpF), 4: lrp-OX (attB1-LrpF), 5: lrp-OX (LrpR-LrpF), 6: lrp-AS (attB1-LrpF), 7: lrp-AS (LrpR-LrpF)

Figure 4.6

A

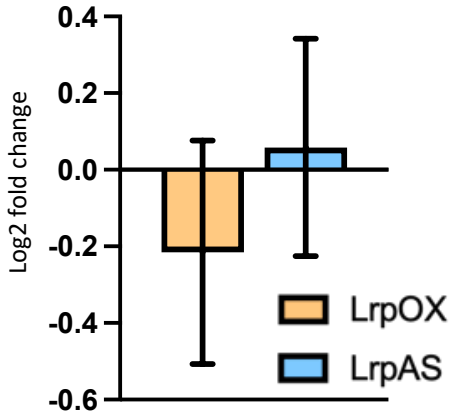
0.4
0.2
0.0
-0.2
-0.4
-0.6
Log2 fold change
LrpOX
LrpAS

B

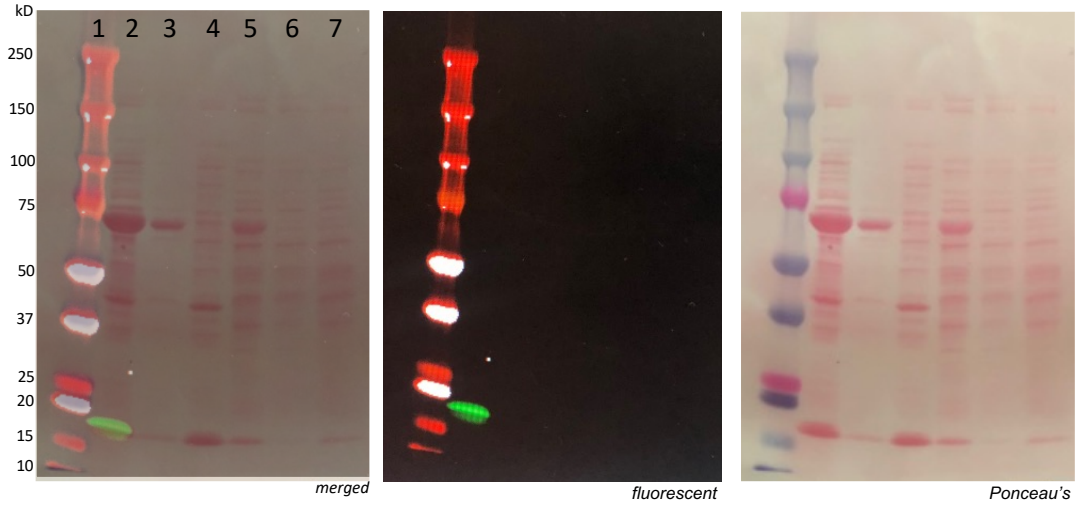
kD
1 2 3 4 5 6 7
250
150
100
75
50
37
25
20
15
10
merged
fluorescent
Ponceau's

Figure 4.6. Determination of modulation of Lrp by lrp-AS. A. Transcript abundance measured using primers that only anneal to the endogenous mRNA internally normalized to *recA* transcript abundance when compared to uidAOX. N = 4 independent cultures. B. Western blot analysis of total protein lysates. 15ug (10ug for lane 3) total protein was loaded in each lane of a gradient 8-16% SDS-PAGE. Anti-Lrp, designed to bind *E. coli* Lrp, does not cross hybridize with Pst Lrp. 1. BioRad Precision Plus Ladder, 2. *E. coli uidA*OX, 3. *E. coli* ∆*lrp uidA*OX, 4. *E. coli* ∆*lrp* (Pst)*lrp*OX, 5. Pst *uidA*OX, 6. Pst *lrp*OX, 7. Pst *lrp*AS

Figure 4.7

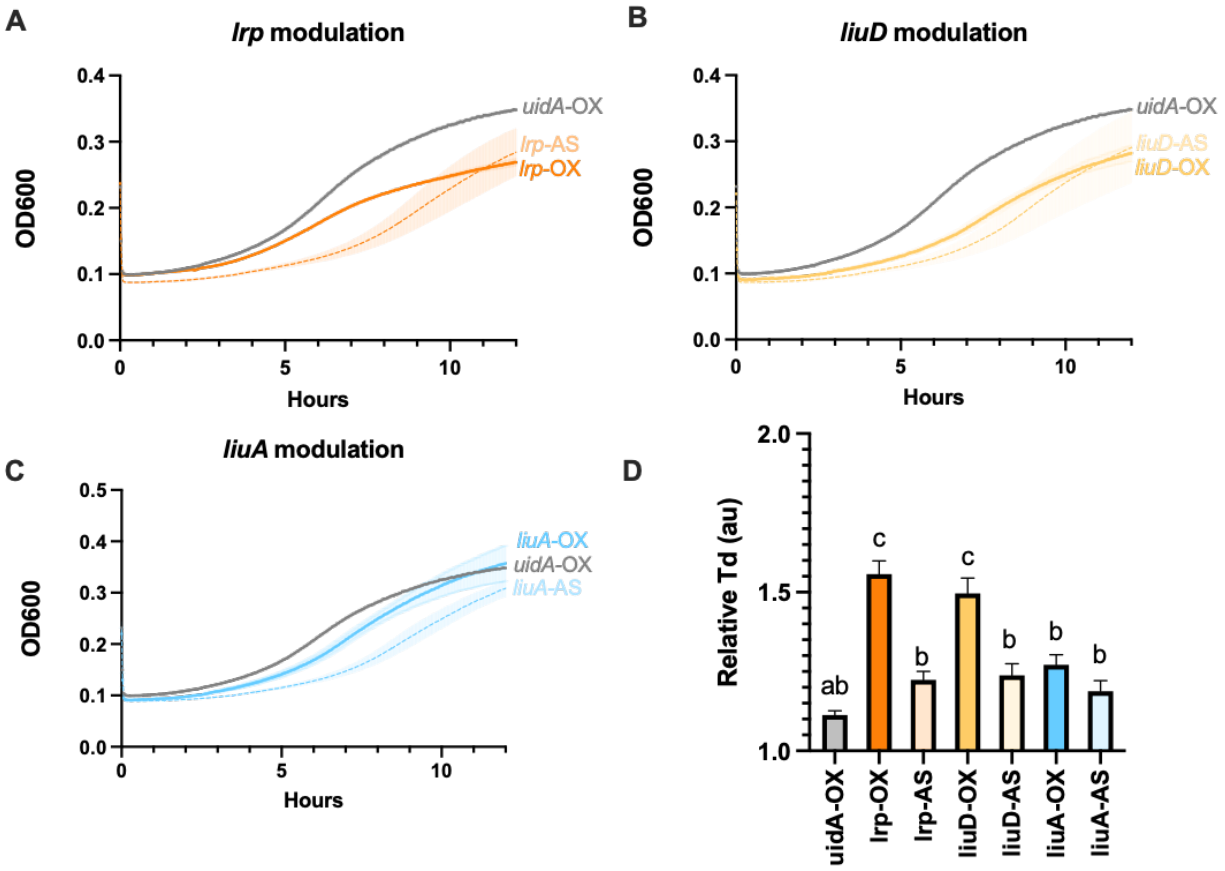
A
lrp modulation
OD600
Hours
uidA-OX
lrp-AS
lrp-OX
B
liuD modulation
OD600
Hours
uidA-OX
liuD-AS
liuD-OX
C
liuA modulation
OD600
Hours
liuA-OX
uidA-OX
liuA-AS
D
Relative Td (au)
ab
c
b
c
b
b
b
uidA-OX
lrp-OX
lrp-AS
liuD-OX
liuD-AS
liuA-OX
liuA-AS

Figure 4.7. Overexpression of sense and antisense GOIs impact normal growth dynamics in rich media. A. Average growth curves for Pst overexpressing *uidA* (gray), lrp (dark orange), and *AS lrp* (lighter orange). B. Average growth curves for Pst overexpressing *uidA* (gray), *liuD* (dark yellow), and *AS liuD* (lighter yellow). C. Average growth curves for Pst overexpressing *uidA* (gray), *liuA* (dark blue), and *AS liuA* (lighter blue). For A-C center lines represent the average of n = 8 individual replicates, with SE represented as the surrounding shaded region of each line. D. The relative doubling times for each constructed carrier normalized to Pst growth in rich media N = 14-21 individual cultures. Error bars represent SE. One-way ANOVA.

Figure 4.8

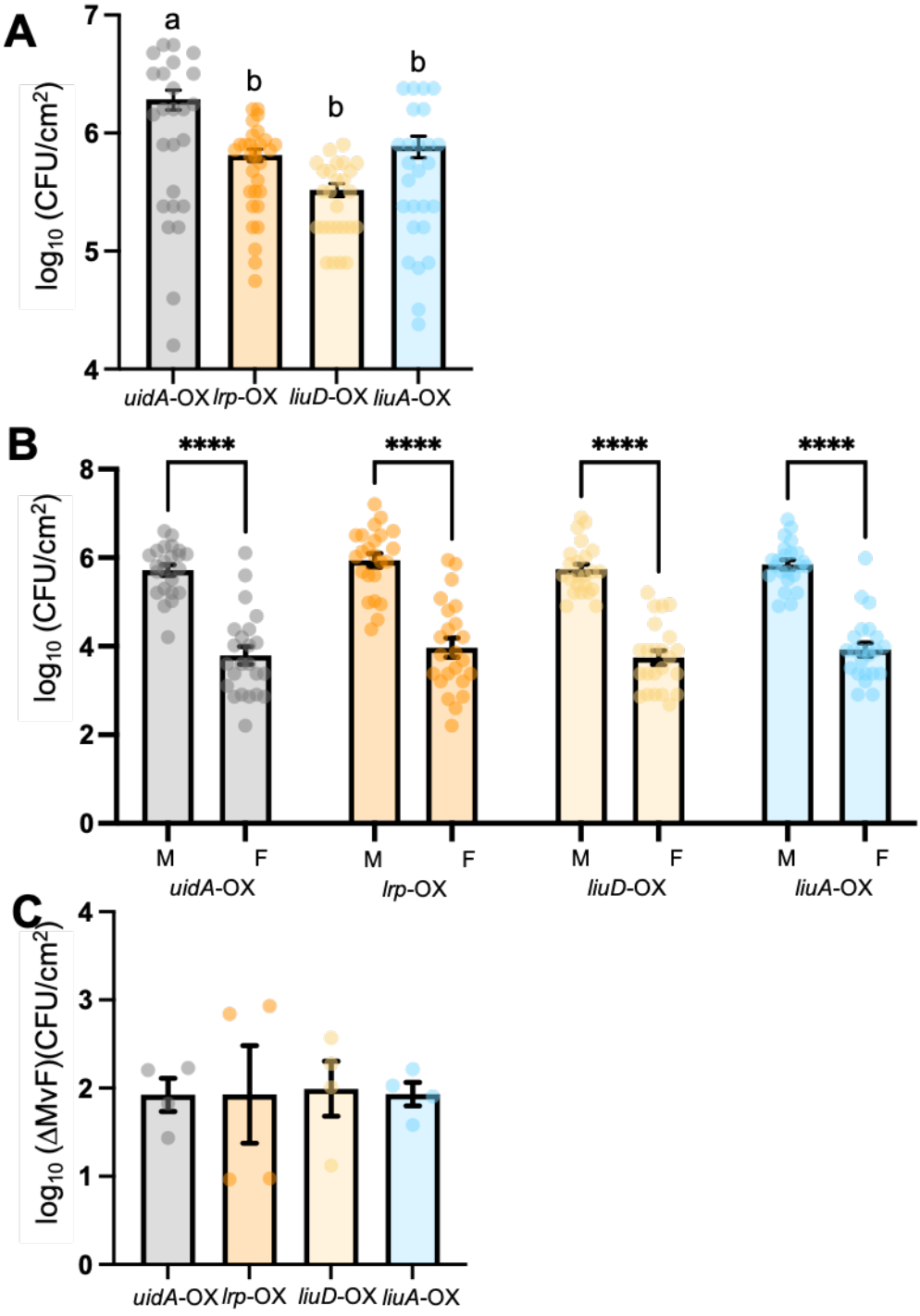
A
a
b
b
b
log10 (CFU/cm2)
uidA-OX lrp-OX liuD-OX liuA-OX
B
****
****
****
****
log10 (CFU/cm2)
M F M F M F M F
uidA-OX lrp-OX liuD-OX liuA-OX
C
log10 (ΔMvF)(CFU/cm2)
uidA-OX lrp-OX liuD-OX liuA-OX

Figure 4.8. BCAA catabolic and regulatory gene overexpression leads to decreased leaf colonization in naïve plants, but not pre-elicited plants. A. CFUs from 72 HPI of naive *A. thaliana* leaves after infection with plasmid carriers for OX of GOIs, IOD 0.0002. N = 25-30 plants per treatment. B. CFUs from 48 HPI, 72 HPE of pre-elicited *A. thaliana* leaves after infection with plasmid carriers for OX of GOIs, IOD 0.0002. N = 23 plants per treatment. C. The calculated differences of CFUs between mock and flg-22 elicited and infected leaves in B. One-way ANOVA, multiple T-tests. * $p < 0.05$, *** $p < 0.001$, **** $p < 0.0001$.

Figure 4.9.

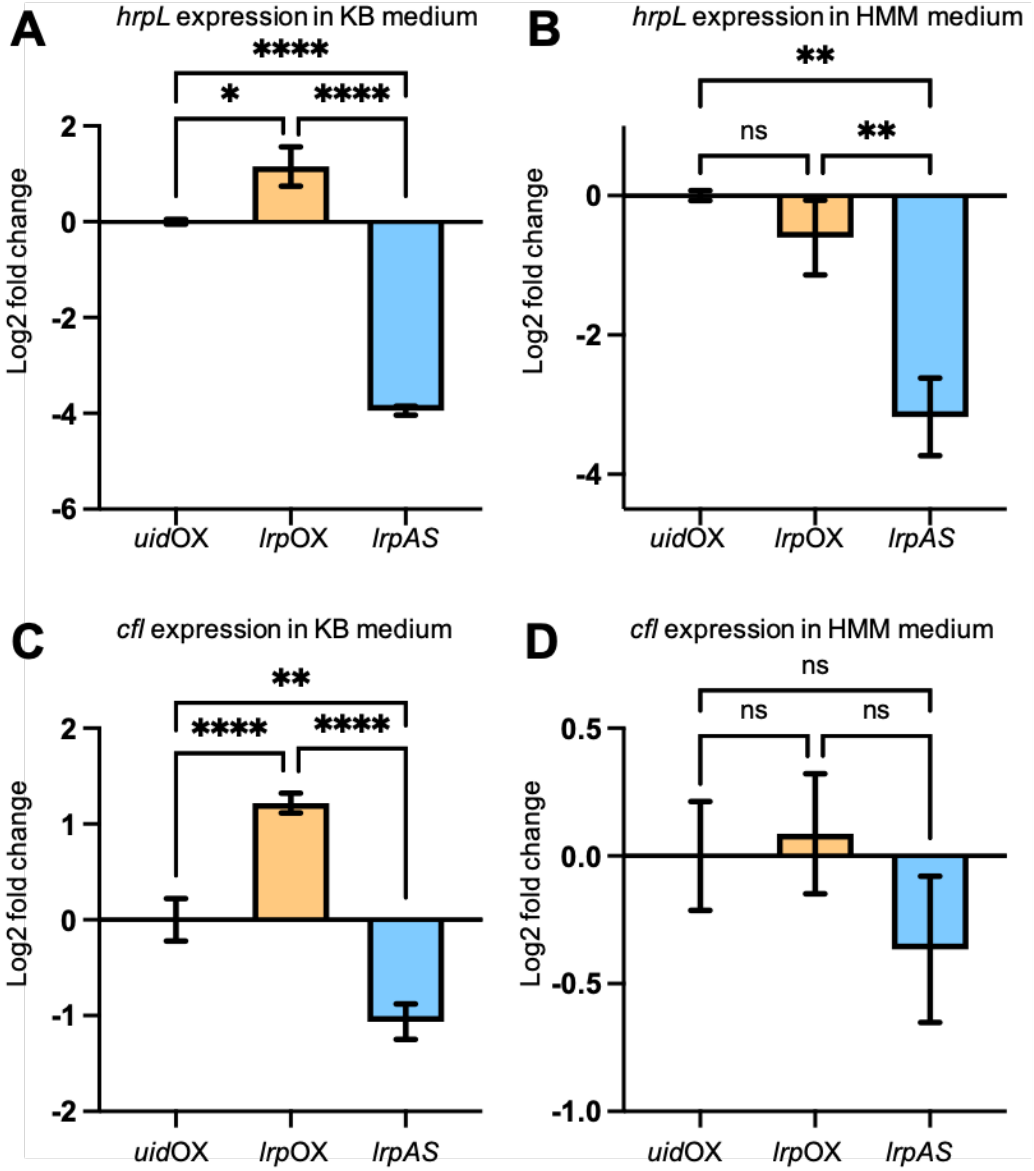
A
hrpL expression in KB medium
****
*
****
Log2 fold change
2
0
-2
-4
-6
uidOX
lrpOX
lrpAS
B
hrpL expression in HMM medium
**
ns
**
Log2 fold change
0
-2
-4
uidOX
lrpOX
lrpAS
C
cfl expression in KB medium
**
****
****
Log2 fold change
2
1
0
-1
-2
uidOX
lrpOX
lrpAS
D
cfl expression in HMM medium
ns
ns
ns
Log2 fold change
0.5
0.0
-0.5
-1.0
uidOX
lrpOX
lrpAS

Figure 4.9. Constitutive Lrp overexpression or down-regulation leads to virulence dysregulation. *hrpL* expression in lrpOX and lrpAS in KB medium (A) or HMM (B) at the mid-exponential growth phase normalized to *hrpL* expression in uidOX grown in identical conditions. *cfl* expression in lrpOX and lrpAS in KB medium (C) or HMM (D) at the mid-exponential growth phase normalized to *cfl* expression in uidOX grown in identical conditions. Mean □ SEM (N = 7-13 independent cultures). A, B, C, D One-way ANOVA with multiple comparisons, * = < 0.05, ** p < 0.01, **** p < 0.0001.

Figure 4.10

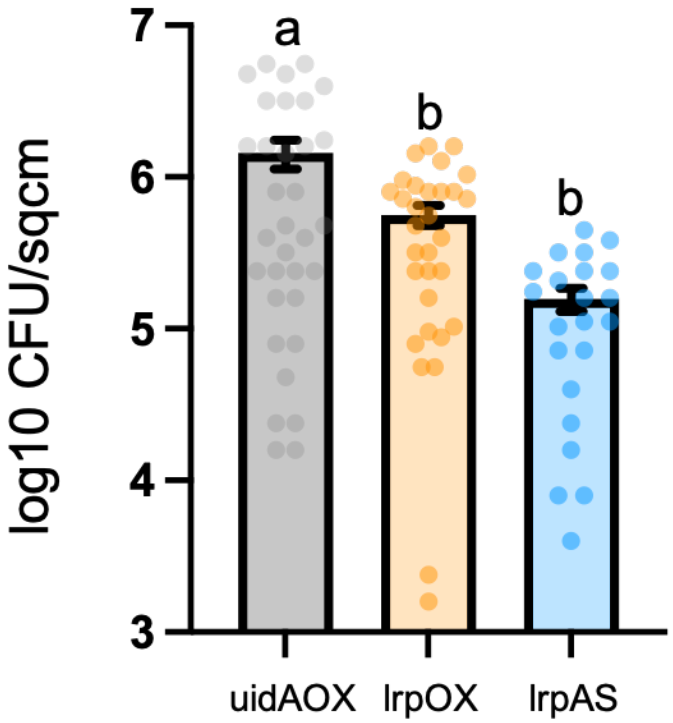

Figure 4.10. Modulation of Lrp transcript levels leads to decrease colonization of the leaf. A. CFUs from 72 HPI of naive *A. thaliana* leaves after infection with uidAOX, lrpOX, or lrpAS. lOD 0.0002. N=22-33 plants. One way ANOVA.

Figure 4.11

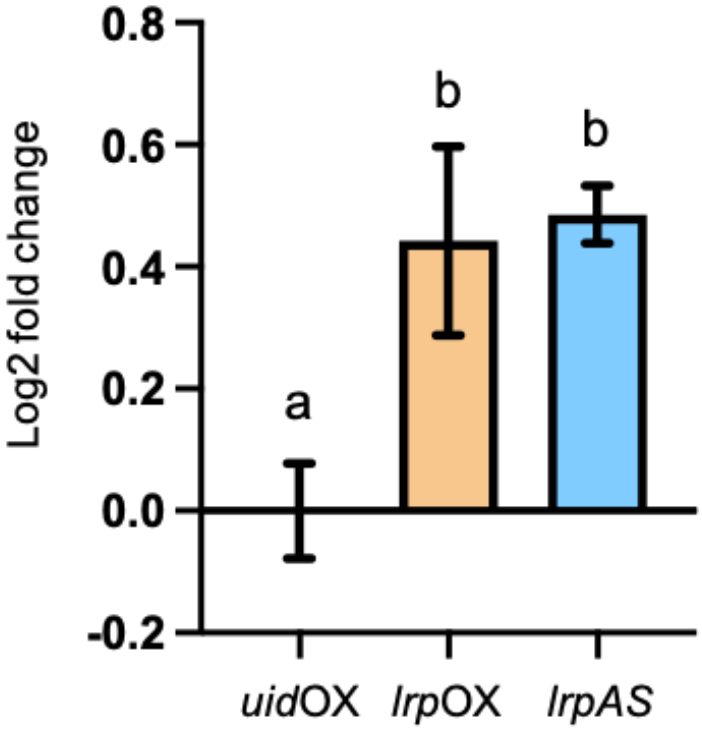

Figure 4.11. Constitutive Lrp down-regulation leads to high affinity transporter modulation. The high affinity BCAA transporter *braD* expression normalized internally to recA and externally to expression in *uidA-OX.* On way ANOVA with multiple comparisons.

Figure 4.12

A

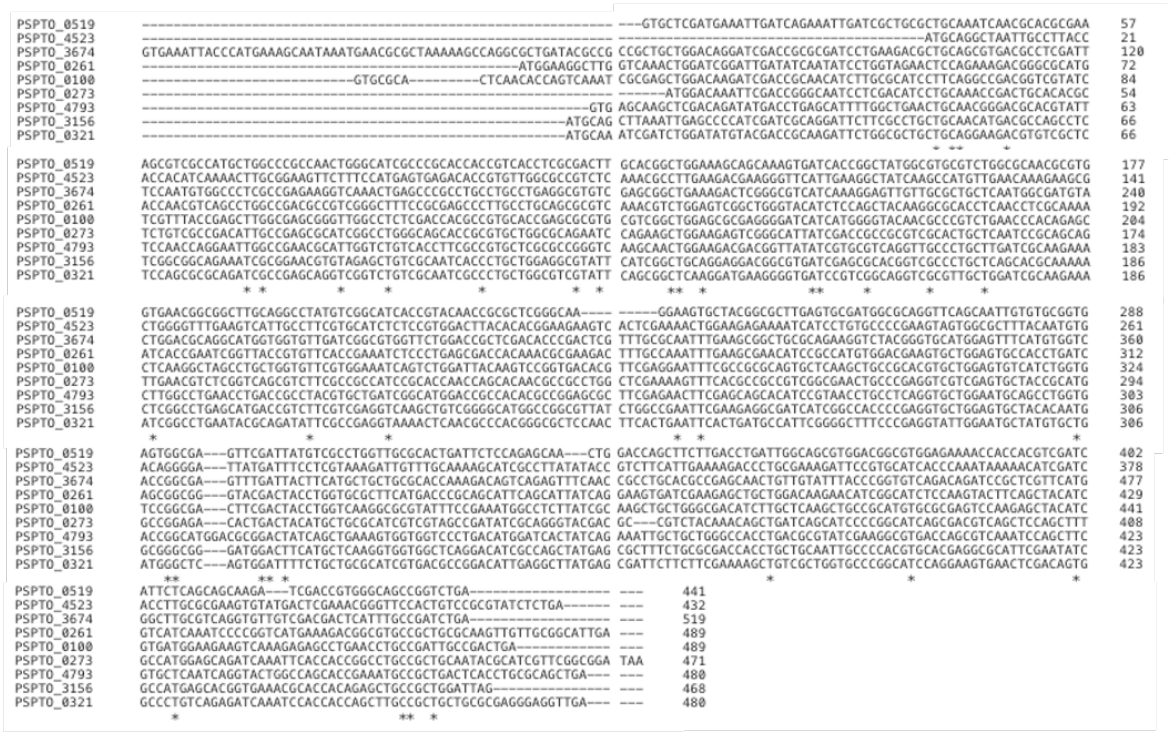

B

Figure 4.12. Sequence alignments of all asnC-family homologs in Pst. A. Nucleotide sequence alignment. B. Amino acid sequence alignment, where color indicates amino acids with similar characteristics.

Table 4.1

P. aeruginosa locus tag (query)*	PstDC3000 locus tag (hits) *	Identity %	E Value	Proposed enzyme activity
PA2250	PSPTO_2201	39.24	0.0	ODHC-E3 component
PA2249	PSPTO_2200	30.14	0.0	ODHC-E2 component
PA2248	PSPTO_0698	18.43	2e-93	ODHC-E1 component
PA2247 + PA2248	PSPTO_2199	15.88	3e-39	ODHC-E1 component

Table 4.1. Putative Pst homologs of the bkd operon in *P. aeruginosa*. *(*) P. aeruginosa protein sequences were used as query against the P. syringae pv. tomato DC3000 strain using the DELTA-BLASTp algorithm at NCBI (https://blast.ncbi.nlm.nih.gov/).*

Table 4.2

P. putida locus tag (query)*	*Pst* DC3000 locus tag (hits)*	Identity %	E Value	Proposed enzyme activity
PP_4404	PSPTO_2201	39.65	1.70E-102	ODHC-E3 component
PP_4403	PSPTO_2200	32.71	6.00E-65	ODHC-E2 component
PP_4402	PSPTO_2199	19.08	2.00E-22	ODHC-E1 component

Table 4.2. Putative Pst homologs of the bkd operon in *P. putida*. *(*) P. putida protein sequences were used as query against the P. syringae pv. tomato DC3000 strain using the DELTA-BLASTp algorithm at NCBI (https://blast.ncbi.nlm.nih.gov/).*

Table 4.3

PstDC3000 Locus	Preotein ID	Protein Name	Query Cover	E value	% ident
PSPTO_0100	AAO53654.1	leucine-responsive regulatory protein	96%	3.00E-69	60.76
PSPTO_3674	AAO57143.1	AsnC family transcriptional regulator	95%	2.00E-47	45
PSPTO_0261	AAO53807.1	AsnC family transcriptional regulator	85%	4.00E-41	42.86
PSPTO_4793	AAO58223.1	AsnC family transcriptional regulator	90%	1.00E-40	44.97
PSPTO_0273	AAO53819.1	AsnC family transcriptional regulator	90%	3.00E-35	36.49
PSPTO_0321	AAO53866.1	AsnC family transcriptional regulator	90%	4.00E-34	34.23
PSPTO_3156	AAO56642.1	AsnC family transcriptional regulator	90%	5.00E-33	35.81
PSPTO_4523	AAO57971.1	AsnC family transcriptional regulator	83%	3.00E-24	27.74
PSPTO_0519	AAO54062.1	AsnC family transcriptional regulator	85%	2.00E-15	27.46

Table 4.3. Homologs of *E. coli lrp* in Pst. *E. coli* protein sequence for *lrp* (eco:b0889) was used as query against the P. syringae pv. tomato DC3000 strain using the DELTA-BLASTp algorithm at NCBI (https://blast.ncbi.nlm.nih.gov/).

Table 4.4

Species	Lrp-like	AsnC-Like	Total
Escherichia coli K-12 (eco)	1	2	3
Bacillus subtalis (bsu)	3	4	7
Pseudomonas putida (ppu)	2	11	13
Pseudomonas aeruginosa (pae)	1	7	8
Pseudomonas syringae B228 (psb)	1 (unannotated)	9	10
Pseudomonas syringae tomato (pst)	1	8	9
Salmonella enterica typhi (sty)	1	4	5
Salmonella enterica typherium (stm)	1	3	4
Xanthomonas oryzae pv oryzae (xom)	1	2	3
Vibrio cholerae	1	3	4
Legionella pneumophila (lpn)	0	2	2

Table 4.4. Number of Lrp-like and AsnC like proteins in various bacterial species. Numbers were counted either from direct annotations or homology sequence alignments in KEGG.

Table 4.5.

Pst DC3000 locus tag	Query Cover	E-value	Identity %
PSPTO_3156	-	NS	-
PSPTO_0273	-	NS	-
PSPTO_3674	-	NS	-
PSPTO_0261	8%	4e-07	79.55%
PSPTO_4793	-	NS	-
PSPTO_0321	-	NS	-
PSPTO_4523	-	NS	-
PSPTO_0519	2%	0.026	100%

Table 4.5 Sequence similarities of *lrp* homologs within Pst. PSPTO_0100 nucleotide sequence for was used as query against the P. syringae pv. tomato DC3000 strain using the BLASTn algorithm at NCBI (https://blast.ncbi.nlm.nih.gov/).

Table 4.6. Bacterial Strains and plasmids

Name	Purpose	Source
pBBR5pemIKpKan	Gateway destination vector, GmR with NPTII promoter	Addgene
Escherichia coli Helper pERK2013	Helper strain for triparental conjugation using pERK2013, kanR	Addgene
Escherichia coli DH5α	Cloning transformation and plasmid preperation	NEB
Pst (Pseudomonas syringae DC3000)	Wild-type P. syringae strain for this study, rifR	Cuppels, 1986
pLrpOX	Derivative of pBBR5pemIKpKan, containing Pst lrp (PSPTO_0100) sense strand under the control of the pNPTII promotor, gmR	This study
pLiuDOX	Derivative of pBBR5pemIKpKan, containing Pst liuD (PSPTO_2736) sense strand under the control of the pNPTII promotor, gmR	This study
pLiuAOX	Derivative of pBBR5pemIKpKan, containing Pst liuA (PSPTO_2739) sense strand under the control of the pNPTII promotor, gmR	This study
pLrpAS	Derivative of pBBR5pemIKpKan, containing Pst lrp (PSPTO_0100) antisense strand under the control of the pNPTII promotor, gmR	This study
pLiuDAS	Derivative of pBBR5pemIKpKan, containing Pst liuD (PSPTO_2736) antisense strand under the control of the pNPTII promotor, gmR	This study
pLiuAAS	Derivative of pBBR5pemIKpKan, containing Pst liuA (PSPTO_2739) antisense strand under the control of the pNPTII promotor, gmR	This study
pUidAOX	Derivative of pBBR5pemIKpKan, containing Arabidopsis thaliana uidA (AT5G07830) under the control of the pNPTII promotor, gmR	This study

Table 4.7. Primers:

Name	Sequence	Purpose
attB1 adapter	GGGGACAAGTTTGTACAAAAAAGCAGGCT	2 step Gateway cloning
attB2 adapter	GGGGACCACTTTGTACAAGAAAGCTGGGT	2 step Gateway cloning
attB1 Lrp	AAAAAGCAGGCTGTGCGCACTCAACACCAGTCAA	2 step Gateway cloning
attB2 Lrp	AGAAAGCTGGGTTCAGTCGGCAATCGGCAG	2 step Gateway cloning
attB1 AS Lrp	AAAAAGCAGGCTTCAGTCGGCAATCGGCAG	2 step Gateway cloning
attB2 AS Lrp	AGAAAGCTGGGTGTGCGCACTCAACACCAGTC	2 step Gateway cloning
attB1 liuD	AAAAAGCAGGCTATGAACACGCCTGAACTGAC	2 step Gateway cloning
attB2 liuD	AGAAAGCTGGGTTCAACCCATCTCCACCAGCA	2 step Gateway cloning
attB1 liuD AS	AAAAAGCAGGCTTCAACCCATCTCCACCAGCA	2 step Gateway cloning
attB2 liuD AS	AGAAAGCTGGGTTCATGAACACGCCTGAACTGAC	2 step Gateway cloning
attB1 liuA	AAAAAGCAGGCTATGAGTTACCCCAGCCTGAACT	2 step Gateway cloning
attB2 liuA	AGAAAGCTGGGTTCAACGGGTTTCGTTGAACAGTTC	2 step Gateway cloning
attB1 liuA AS	AAAAAGCAGGCTTCAACGGGTTTCGTTGAACAGTTC	2 step Gateway cloning
attB2 liuA AS	AGAAAGCTGGGTATGAGTTACCCCAGCCTGAACT	2 step Gateway cloning
Lrp F	ACGTGCTGGAGTGTCATCTG	qRTPCR
Lrp R	TTGCGATAAGAGGCCATTTC	qRTPCR
Endogenous Lrp F	CGCTTTGCTAGAGGGGAAATTACCC	qRTPCR
Endogenous Lrp R	CTCGCCAAGCTCGGTAAAC	qRTPCR
recA F	TAGAACTTCAGCGCGTTACC	qRTPCR
recA R	GCCAACTGCCTGGTTATCT	qRTPCR
act2 F	GTACGGTAACATTGTGCTCAGT	qRTPCR
act2 R	GAGATCCACATCTGCTGGAATGT	qRTPCR
pr1 F	TTCTTCCCTCGAAAGCTCAA	qRTPCR
pr1 R	AAGGCCCACCAGAGTGTATG	qRTPCR
vsp2 F	ATGCCAAAGGACTTGCCCTA	qRTPCR
vsp2 R	GTCTTCTCTGTTCCGTAT	qRTPCR
hrpL F	TCAGGAAAGCTGGGAAGACGAAGT	qRTPCR
hrpL R	ATGTTCGACGGCAGGCAATCAATG	qRTPCR
cfl F	TGCTCGTCTCGTCGCCAA	qRTPCR
cfl R	CGATACCCTTAGTTAGTCCTGTGG	qRTPCR
liuD F	GGCTGAGCGGATCGACTTTA	qRTPCR
liuD R	CGCTTGCTGGATAACGATGC	qRTPCR
liuA F	GACGATGTCCAAGTGCCTGA	qRTPCR
liuA R	GAATGTAGGGGACCACCACG	qRTPCR
uidA F	TGCTGTGCCTGAACCGTTAT	qRTPCR
uidA R	GCTAACGTATCCACGCCGTA	qRTPCR

Chapter 5: Conclusions and Future Directions

While plant innate immunity relies on a complex combination of mechanisms, it has become increasingly clear that one aspect of defense against pathogens is modulation of nutrient availability. Previous studies have explored the impacts of hexoses and sucrose, showing that these are restricted from the site of infection, thus restricting the growth capabilities of the pathogen (Yamada et al., 2016). Other studies have explored the impact of organic acids and fructose as virulence inducers; when they are not available to the pathogen, infections are less severe(Anderson et al., 2014). Finally, previous work in our lab has highlighted the importance of plant-exuded glutamine and serine in suppressing bacterial virulence in the early stages of infection (Zhang et al., 2022, 2023).

In this thesis, we present another important facet of the interaction between *A. thaliana* and Pst. We have shown that BCAAs suppress the synthesis of virulence related genes, and that this could be associated with transcriptional control through global nutrient signaling factors such as Lrp. We have also demonstrated the usefulness of genome scale metabolic reconstructions at predicting novel pathways that contribute to a pathogen's fitness during infection.

Understanding disease state and pathogenicity

While we have characterized pathogenesis of Pst in *A. thaliana*, several other strains of *Pseudomonas syringae* impact important crop species. Using iPst19 as a framework, several more models can be adapted to specific strains of *P. syringae* to increase the speed of curation and simulation. Importantly, these could lead to

the understanding of pathogenesis beyond specific host-pathogen pairs. As we have previously discussed in this thesis, PTI is the predominant mechanism by which plants defend themselves. By using iPst19, we have uncovered another facet of PTI defenses that includes modulation of specific AA and sugars within the pathosphere. Creating strains specific metabolic reconstructions and constraining models with appropriate *in planta* omics data could reveal even more facets of PTI or plant defense generally that have remained obscured thus far. Critically, this has the potential to connect crop development and intraspecies pathogenesis; using these data could allow development of broad resistance to previously devastating pathogens.

Another development that would greatly benefit predictive power of iPst19 is assembling a suite of datasets of regulatory protein modifications. In this thesis, we have presented an Lrp overexpressor and functional Lrp antisense expressor. Assessing global gene expression for both of these stains could begin to provide insights into the regulatory targets of Lrp in Pst, which remain unexplored. Further, by understating these regulatory targets, we could refine iPst19 to make more conditional predictions over the course of a growth curve.

Interactions between coronatine biosynthesis and BCAAs

As previously stated, one aspect of the metabolic reconstruction we ensured was present was coronatine biosynthesis. We have described how BCAAs decrease the abundance of *cfl* transcripts in several situations (Figure 3.7, Figure 3.13, Figure 4.8BD). Because isoleucine is reported to be a precursor to coronatine, the

relationship between coronatine biosynthesis and regulation by BCAAs should be further explored.

There are several coronatine biosynthesis knockouts, each of which cannot synthesize a specific moiety within the pathway. Interestingly, we have generated some preliminary data to suggesting that COR- strains are insensitive to growth rate inhibition seen in wild type Pst in either valine or isoleucine supplemented minimal medium. This could suggest an alternative regulatory function of the COR biosynthesis pathway, such as acting as a metabolic sink to reduce free BCAAs intracellularly, thus preventing them from interacting with Lrp or another transcriptional regulator.

Confirmation of a potential bkd operon in Pst

It is clear that Pst can convert leucine into other metabolites used to produce biomass. We have proposed a set of OADHC similar to the *bkd* operon in P. putida could be responsible for leucine utilization. To address this hypothesis, functional analysis of these genes (PSPTO_2199, PSPTO_2200, and PSPTO_2201) should be conducted. If these gene products carry *bkd*-like functions, a knockout mutant should not be able to produce biomass on leucine as the single carbon source. These strains should be made with a note of caution, however, because these genes are considered to be the succinate dehydrogenase complex of Pst; they may be essential for growth to begin with, rendering a knockout impossible but a knockdown possible.

Further Curation of iPst19

Any metabolic model cannot be assumed to be perfect from the first iteration of curation and drafting. Models typically undergo continuous curation, reaction additions, pruning, and GPR updates as new evidence and literature arises. For the further curation of iPst19, one of the first steps should be increasing the stringency of the protein alignments in the homologous semi-autonomous curation step of model building. First, both of the P. aeruginosa models have undergone further curation since the initial homologous comparison, and thus may have new GPR-reaction associations that could be including in the next iteration of iPst. Second, the e-value threshold used in this study, while purposely relaxed for the initial reconstruction, could be tightened to ensure any spurious reaction included in the first iteration is pruned for the following curation steps. If the confirmation of the potential *bkd* operon is completed, these GPRs could also be updated within iPst and could be consequential in further metabolic modeling on single carbon sources.

Metabolic modeling of beneficial Pseudomonas bacteria

An aspect of plant microbe interactions not discussed at length in this thesis are the relationships with beneficial, growth promoting bacteria. Typically, these mutualisms occur in the roots of plants, where bacteria fix nutrients such as nitrogen in exchange for sugars and other plant made metabolites. A close relative of Pst, *Pseudomonas simiae* (Pss), engages in plant growth promoting bacteria (PGPB) like behavior with *A. thaliana.*

Previous findings in our lab suggest exogenous application of some plant made metabolites, such as glutamine, causes this relationship to deteriorate. Plants that are exposed to glutamine sated bacteria appear symptomatic and stunted, while plants grown in the presence of non-supplemented bacteria do not appear sickly. Interestingly, symptomatic observations only occur in the presence of both glutamine and Pss. This suggests Pss is converting glutamine into another metabolite that is causing distress in the plant.

To better understand the complexities of this exchange, which closely mimics a relationship of pathogen to host, a similar type of metabolic modeling as demonstrated in this thesis can be employed. Due to the high species relatedness, many of the GPRs and pathway architectures will likely be homologous, easing the initial burden of reconstruction and curation. An added advantage of using metabolic modeling in a root-PGPB system is the ease of sample preparation. Compared to bacteria infiltrated in a leaf, there is relatively less work involved in stripping roots of biofilm-ed bacteria for gene expression profiling or any other omics assay.

While it is mostly likely that we will be working on the interactions between PGPB and *A. thaliana* specifically, this system translates nicely into agriculturally relevant crops, as Pss has been shown to act as PGPB for tomatoes and other species. Importantly, this work could reveal why certain bacteria act as PGPB and others as pathogens, despite the close relatedness and similar mechanisms used to interact with the host species. Understanding these facets could lead to the development of better PGPB strains and novel crop enhancements.

Broadly, the integration of computational modeling and plant development has the potential to make impactful discoveries and developments leading to a more resistant food system. Already, this type of metabolic modeling has proposed novel antibacterial targets for multi-drug resistant bacterial strains and drug targets for genetic diseases. In this thesis, we have presented the first computational metabolic model for a foliar pathogen that has highlighted the importance of BCAAs during the course of disease; by leveraging these techniques within the agricultural sphere, these small discoveries can lead to major innovation in crop yield and resistance.

References

Anderson, J. C., Wan, Y., Kim, Y. M., Pasa-Tolic, L., Metz, T. O., & Peck, S. C. (2014a). Decreased abundance of type III secretion systeminducing signals in Arabidopsis mkp1 enhances resistance against Pseudomonas syringae. *Proceedings of the National Academy of Sciences of the United States of America*, *111*(18), 6846–6851. https://doi.org/10.1073/pnas.1403248111

Anderson, J. C., Wan, Y., Kim, Y. M., Pasa-Tolic, L., Metz, T. O., & Peck, S. C. (2014b). Decreased abundance of type III secretion systeminducing signals in Arabidopsis mkp1 enhances resistance against Pseudomonas syringae. *Proceedings of the National Academy of Sciences of the United States of America*, *111*(18), 6846–6851. https://doi.org/10.1073/pnas.1403248111

Archer, C. T., Kim, J. F., Jeong, H., Park, J. H., Vickers, C. E., Lee, S. Y., & Nielsen, L. K. (2011). The genome sequence of E. coli W (ATCC 9637): Comparative genome analysis and an improved genome-scale reconstruction of E. coli. *BMC Genomics*, *12*(Atcc 9637). https://doi.org/10.1186/1471-2164-12-9

Aziz, R. K., Bartels, D., Best, A., DeJongh, M., Disz, T., Edwards, R. A., Formsma, K., Gerdes, S., Glass, E. M., Kubal, M., Meyer, F., Olsen, G. J., Olson, R., Osterman, A. L., Overbeek, R. A., McNeil, L. K., Paarmann, D., Paczian, T., Parrello, B., … Zagnitko, O. (2008). The RAST Server: Rapid annotations using subsystems technology. *BMC Genomics*, *9*, 1–15. https://doi.org/10.1186/1471-2164-9-75

Backer, R., Naidoo, S., & van den Berg, N. (2019). The NONEXPRESSOR OF PATHOGENESIS-RELATED GENES 1 (NPR1) and related family: Mechanistic insights in plant disease resistance. *Frontiers in Plant Science*, *10*(February), 1–21. https://doi.org/10.3389/fpls.2019.00102

Badel, J. L., Nomura, K., Bandyopadhyay, S., Shimizu, R., Collmer, A., & He, S. Y. (2003). Pseudomonas syringae pv. tomato DC3000 HopPtoM (CEL ORF3) is important for lesion formation but not growth in tomato and is secreted and translocated by the Hrp type III secretion system in a chaperone-dependent manner. *Molecular Microbiology*, *49*(5), 1239–1251. https://doi.org/10.1046/j.1365-2958.2003.03647.x

Baek, C. H., Wang, S., Roland, K. L., & Curtiss, R. (2009). Leucine-responsive regulatory protein (Lrp) acts as a virulence repressor in Salmonella enterica serovar typhimurium. *Journal of Bacteriology*, *191*(4), 1278–1292. https://doi.org/10.1128/JB.01142-08

Bartell, J. A., Blazier, A. S., Yen, P., Thøgersen, J. C., Jelsbak, L., Goldberg, J. B., & Papin, J. A. (2017). Reconstruction of the metabolic network of Pseudomonas aeruginosa to interrogate virulence factor synthesis. *Nature Communications*, *8*. https://doi.org/10.1038/ncomms14631

Bender, C. L., Alarcón-Chaidez, F., & Gross, D. C. (1999). Pseudomonas syringae Phytotoxins: Mode of Action, Regulation, and Biosynthesis by Peptide and Polyketide Synthetases . *Microbiology and Molecular Biology Reviews*, *63*(2), 266–292. https://doi.org/10.1128/mmbr.63.2.266-292.1999

Blazier, A. S., & Papin, J. A. (2012). Integration of expression data in genome-

scale metabolic network reconstructions. *Frontiers in Physiology*, *3 AUG*(August). https://doi.org/10.3389/fphys.2012.00299

Bodey, G. P., Bolivar, R., Fainstein, V., & Jadeja, L. (1983). Infections caused by Pseudomonas aeruginosa. In *Reviews of infectious diseases* (Vol. 5, Issue 2, pp. 279–313). Oxford Academic. https://doi.org/10.1093/clinids/5.2.279

Brinkman, A. B., Ettema, T. J. G., Vos, W. M. De, & Oost, J. Van Der. (2003). *MicroReview The Lrp family of transcriptional regulators*. *48*, 287–294.

Buchfink, B., Xie, C., & Huson, D. H. (2014). Fast and sensitive protein alignment using DIAMOND. *Nature Methods*, *12*(1), 59–60. https://doi.org/10.1038/nmeth.3176

Buell, C. R., Joardar, V., Lindeberg, M., Selengut, J., Paulsen, I. T., Gwinn, M. L., Dodson, R. J., Deboy, R. T., Durkin, A. S., Kolonay, J. F., Madupu, R., Daugherty, S., Brinkac, L., Beanan, M. J., Haft, D. H., Nelson, W. C., Davidsen, T., Zafar, N., Zhou, L., … Collmer, A. (2003). The complete genome sequence of the Arabidopsis and tomato pathogen Pseudomonas syringae pv. tomato DC3000. *Proceedings of the National Academy of Sciences of the United States of America*, *100*(18), 10181–10186. https://doi.org/10.1073/pnas.1731982100

Burns, G., Brown, T., Hatter, K., Idriss, J., & Sokatch, J. R. (1988). *Similarity of the E l subunits of branched-chain-oxoacid dehydrogenase from*. *317*, 311–317.

Büttner, D., & Bonas, U. (2010). Regulation and secretion of Xanthomonas virulence factors. *FEMS Microbiology Reviews*, *34 2*, 107–133. https://doi.org/10.1111/j.1574-6976.2009.00192.x

Calvo, J. M., & Matthews, R. G. (1994). The leucine-responsive regulatory protein, a global regulator of metabolism in Escherichia coli. *Microbiological Reviews*, *58*(3), 466–490. https://doi.org/10.1128/mmbr.58.3.466-490.1994

Chan, E., Kuang, L., Lau, A., & Wang, J. (2010). Antisense mRNA Method as an Alternative to Generate a Catalase Double Knockout Phenotype in a Escherichia coli katG Mutant. *Journal of Experimental Microbiolgy and Immunology*, *14*(April), 127–134.

Chen, S., Rosner, M. H., & Calvo, J. M. (2001). Leucine-regulated self-association of leucine-responsive regulatory protein (Lrp) from Escherichia coli 1 1Edited by M. F. Moody. *Journal of Molecular Biology*, *312*(4), 625–635. https://doi.org/10.1006/jmbi.2001.4955

Chinchilla, D., Zipfel, C., Robatzek, S., Kemmerling, B., Nürnberger, T., Jones, J. D. G., Felix, G., & Boller, T. (2007). A flagellin-induced complex of the receptor FLS2 and BAK1 initiates plant defence. *Nature*, *448*(7152), 497–500. https://doi.org/10.1038/nature05999

Cho, B. K., Barrett, C. L., Knight, E. M., Park, Y. S., & Palsson, B. (2008). Genome-scale reconstruction of the Lrp regulatory network in Escherichia coli. *Proceedings of the National Academy of Sciences of the United States of America*, *105*(49), 19462–19467. https://doi.org/10.1073/pnas.0807227105

Choi, H. W., & Klessig, D. F. (2016). DAMPs, MAMPs, and NAMPs in plant innate immunity. *BMC Plant Biology*, *16*(1), 1–10.

https://doi.org/10.1186/s12870-016-0921-2
Collmer, A., Badel, J. L., Charkowski, A. O., Deng, W. L., Fouts, D. E., Ramos, A. R., Rehm, A. H., Anderson, D. M., Schneewind, O., Van Dijk, K., & Alfano, J. R. (2000). Pseudomonas syringae Hrp type III secretion system and effector proteins. *Proceedings of the National Academy of Sciences of the United States of America*, *97*(16), 8770–8777. https://doi.org/10.1073/pnas.97.16.8770
Cornelis, G. R., & Van Gijsegem, F. (2000). Assembly and Function of Type III Secretory Systems. *Annual Review of Microbiology*, *54*(1), 735–774. https://doi.org/10.1146/annurev.micro.54.1.735
Cowles, K. N., Cowles, C. E., Richards, G. R., Martens, E. C., & Goodrich-blair, H. (2007). The global regulator Lrp contributes to mutualism, pathogenesis and phenotypic variation in the bacterium Xenorhabdus nematophila. *Cellular Microbiology*, *9*(5), 1311–1323. https://doi.org/10.1111/j.1462-5822.2006.00873.x
Cui, H., Tsuda, K., & Parker, J. E. (2015). Effector-triggered immunity: From pathogen perception to robust defense. *Annual Review of Plant Biology*, *66*, 487–511. https://doi.org/10.1146/annurev-arplant-050213-040012
Daudi, A., Cheng, Z., O'Brien, J. A., Mammarella, N., Khan, S., Ausubel, F. M., & Paul Bolwell, G. (2012). The apoplastic oxidative burst peroxidase in Arabidopsis is a major component of pattern-triggered immunity. *Plant Cell*, *24*(1), 275–287. https://doi.org/10.1105/tpc.111.093039
Deng, W. L., Preston, G., Collmer, A., Chang, C. J., & Huang, H. C. (1998). Characterization of the *hrpC* and *hrpRS* operons of Pseudomonas syringae pathovars syringae, tomato, and glycinea and analysis of the ability of *hrpF*, *hrpG*, *hrcC*, *hrpT*, and *hrpV* mutants to elicit the hypersen. *Journal of Bacteriology*, *180*(17), 4523–4531.
Diard, M., Garcia, V., Maier, L., Remus-Emsermann, M. N. P., Regoes, R. R., Ackermann, M., & Hardt, W. D. (2013). Stabilization of cooperative virulence by the expression of an avirulent phenotype. *Nature*, *494*(7437), 353–356. https://doi.org/10.1038/nature11913
Dillon, M. M., Almeida, R. N. D., Laflamme, B., Martel, A., Weir, B. S., Desveaux, D., & Guttman, D. S. (2019). Molecular evolution of Pseudomonas syringae type iii secreted effector proteins. *Frontiers in Plant Science*, *10*(April), 1–18. https://doi.org/10.3389/fpls.2019.00418
Djonović, S., Urbach, J. M., Drenkard, E., Bush, J., Feinbaum, R., Ausubel, J. L., Traficante, D., Risech, M., Kocks, C., Fischbach, M. A., Priebe, G. P., & Ausubel, F. M. (2013). Trehalose Biosynthesis Promotes Pseudomonas aeruginosa Pathogenicity in Plants. *PLoS Pathogens*, *9*(3), e1003217. https://doi.org/10.1371/journal.ppat.1003217
Dunphy, L. J., Yen, P., & Papin, J. A. (2019). Integrated Experimental and Computational Analyses Reveal Differential Metabolic Functionality in Antibiotic-Resistant Pseudomonas aeruginosa. *Cell Systems*, *8*(1), 3-14.e3. https://doi.org/10.1016/j.cels.2018.12.002
Ebel J., & Mithöfer A. (1998). Early events in the elicitation of plant defence. *Planta*, *206*, 335–348.

Georg, J., & Hess, W. R. (2011). cis -Antisense RNA, Another Level of Gene Regulation in Bacteria . *Microbiology and Molecular Biology Reviews*, *75*(2), 286–300. https://doi.org/10.1128/mmbr.00032-10

Gillaspie, D., Perkins, I., Larsen, K., McCord, A., Pangonis, S., Sweger, D., Seleem, M. N., Sriranganathan, N., & Anderson, B. E. (2009). Plasmid-based system for high-level gene expression and antisense gene knockdown in Bartonella henselae. *Applied and Environmental Microbiology*, *75*(16), 5434–5436. https://doi.org/10.1128/AEM.00949-09

Gough, C. L., Genin, S., Zischek, C., & Boucher, C. A. (1992). hrp genes of Pseudomonas solanacearum are homologous to pathogenicity determinants of animal pathogenic bacteria and are conserved among plant pathogenic bacteria. In *Molecular plant-microbe interactions : MPMI* (Vol. 5, Issue 5, pp. 384–389). https://doi.org/10.1094/MPMI-5-384

Guo, W., Cui, Y., Li, Y., Che, Y.-Z., Yuan, L., Zou, L., Zou, H., & Chen, G. (2012). Identification of seven Xanthomonas oryzae pv. oryzicola genes potentially involved in pathogenesis in rice. *Microbiology*, *158 Pt 2*, 505–518. https://doi.org/10.1099/mic.0.050419-0

Heath, C., Jeffries, A. C., Hough, D. W., & Danson, M. J. (2004). Discovery of the catalytic function of a putative 2-oxoacid dehydrogenase multienzyme complex in the thermophilic archaeon Thermoplasma acidophilum. *FEBS Letters*, *577*(3), 523–527. https://doi.org/10.1016/j.febslet.2004.10.058

Helmann, T. C., Deutschbauer, A. M., & Lindow, S. E. (2019). Genome-wide identification of Pseudomonas syringae genes required for fitness during colonization of the leaf surface and apoplast. *Proceedings of the National Academy of Sciences of the United States of America*, *116*(38), 18900–18910. https://doi.org/10.1073/pnas.1908858116

Hendrickson, E. L., Guevera, P., Peñaloza-Vàzquez, A., Shao, J., Bender, C., & Ausubel, F. M. (2000). Virulence of the phytopathogen Pseudomonas syringae pv. maculicola is rpoN dependent. *Journal of Bacteriology*, *182*(12), 3498–3507. https://doi.org/10.1128/JB.182.12.3498-3507.2000

Hester, K., Luo, J., Burns, G., Braswell, E. H., & Sokatch, J. R. (1995). *Purification of active E1a2P2 of Pseudornonas putida branched-chain-oxoacid dehydrogenase*. *836*, 828–836.

Kaiser, J. C., & Heinrichs, D. E. (2018). Branching Out: Alterations in Bacterial Physiology and Virulence Due to Branched-Chain Amino Acid Deprivation. *MBio*, *9*(5). https://doi.org/10.1128/mBio.01188-18

Kang, Y., Outlaw, W. H., Andersen, P. C., & Fiore, G. B. (2007). Guard-cell apoplastic sucrose concentration - A link between leaf photosynthesis and stomatal aperture size in the apoplastic phloem loader Vicia faba L. *Plant, Cell and Environment*, *30*(5), 551–558. https://doi.org/10.1111/j.1365-3040.2007.01635.x

Kim, M., Zhang, Z., Okano, H., Yan, D., Groisman, A., & Hwa, T. (2012). Need-based activation of ammonium uptake in Escherichia coli. *Molecular Systems Biology*, *8*(616), 1–10. https://doi.org/10.1038/msb.2012.46

King, Z. A., Lu, J., Dräger, A., Miller, P., Federowicz, S., Lerman, J. A., Ebrahim, A., Palsson, B. O., & Lewis, N. E. (2016). BiGG Models: A platform for

integrating, standardizing and sharing genome-scale models. *Nucleic Acids Research*, *44*(D1), D515–D522. https://doi.org/10.1093/nar/gkv1049

Kroner, G. M., Wolfe, M. B., & Freddolino, P. L. (2019). Escherichia coli Lrp Regulates One-Third of the Genome via Direct, Cooperative, and Indirect Routes. *Journal of Bacteriology*, *201*(3). https://doi.org/10.1128/JB.00411-18

Landgraf, J. R., Jingcai, W. U., & Calvo, J. M. (1996). Effects of nutrition and growth rate on Lrp levels in Escherichia coli. *Journal of Bacteriology*, *178*(23), 6930–6936. https://doi.org/10.1128/jb.178.23.6930-6936.1996

Lin, W., Kovacikova, G., & Skorupski, K. (2007). The quorum sensing regulator HapR downregulates the expression of the virulence gene transcription factor AphA in Vibrio cholerae by antagonizing Lrp- and VpsR-mediated activation. *Molecular Microbiology*, *64*(4), 953–967. https://doi.org/10.1111/j.1365-2958.2007.05693.x

Lohaus, G., Pennewiss, K., Sattelmacher, B., Hussmann, M., & Muehling, K. H. (2001). Is the infiltration-centrifugation technique appropriate for the isolation of apoplastic fluid? A critical evaluation with different plant species. *Physiologia Plantarum*, *111*(4), 457–465. https://doi.org/10.1034/j.1399-3054.2001.1110405.x

Lohaus, G., Winter, H., Riens, B., & Heldt, H. W. (1995). Further Studies of the Phloem Loading Process in Leaves of Barley and Spinach. The Comparison of Metabolite Concentrations in the Apoplastic Compartment with those in the Cytosolic Compartment and in the Sieve Tubes. *Botanica Acta*, *108*(3), 270–275. https://doi.org/10.1111/j.1438-8677.1995.tb00860.x

Lovelace, A. H., Smith, A., & Kvitko, B. H. (2018). Pattern-Triggered Immunity Alters the Transcriptional Regulation of Virulence-Associated Genes and Induces the Sulfur Starvation Response in Pseudomonas syringae pv. tomato DC3000. *Molecular Plant-Microbe Interactions®*, *31*(7), 750–765. https://doi.org/10.1094/MPMI-01-18-0008-R

Lu, D., Wu, S., Gao, X., Zhang, Y., Shan, L., & He, P. (2010). A receptor-like cytoplasmic kinase, BIK1, associates with a flagellin receptor complex to initiate plant innate immunity. *Proceedings of the National Academy of Sciences of the United States of America*, *107*(1), 496–501. https://doi.org/10.1073/pnas.0909705107

Massey, L. K., Sokatch, J. R., & Conrad, R. S. (1976). Branched-Chain Amino Acid Catabolism in Bacteria. In *BACTERIOLOGICAL REVIEWS*.

McAtee, P. A., Brian, L., Curran, B., Van Der Linden, O., Nieuwenhuizen, N. J., Chen, X., Henry-Kirk, R. A., Stroud, E. A., Nardozza, S., Jayaraman, J., Rikkerink, E. H. A., Print, C. G., Allan, A. C., & Templeton, M. D. (2018). Re-programming of Pseudomonas syringae pv. actinidiae gene expression during early stages of infection of kiwifruit. *BMC Genomics*, *19*(1), 1–15. https://doi.org/10.1186/s12864-018-5197-5

McCraw, S. L., Park, D. H., Jones, R., Bentley, M. A., Rico, A., Ratcliffe, R. G., Kruger, N. J., Collmer, A., & Preston, G. M. (2016). GABA (γ-Aminobutyric Acid) uptake via the GABA permease GabP represses virulence gene expression in pseudomonas syringae pv. Tomato DC3000. *Molecular Plant-Microbe Interactions*, *29*(12), 938–949. https://doi.org/10.1094/MPMI-08-16-

0172-R
Medlock, G. L., & Papin, J. A. (2020). Guiding the Refinement of Biochemical Knowledgebases with Ensembles of Metabolic Networks and Machine Learning. *Cell Systems*, *10*(1), 109-119.e3. https://doi.org/10.1016/j.cels.2019.11.006
Miller, M. B., & Bassler, B. L. (2001). Quorum sensing in bacteria. *Annual Review of Microbiology*, *55*, 165–199. https://doi.org/10.1146/annurev.micro.55.1.165
Miranda, R. L., Conway, T., Leatham, M. P., Chang, D. E., Norris, W. E., Allen, J. H., Stevenson, S. J., Laux, D. C., & Cohen, P. S. (2004). Glycolytic and Gluconeogenic Growth of Escherichia coli O157:H7 (EDL933) and E. coli K-12 (MG1655) in the Mouse Intestine. *Infection and Immunity*, *72*(3), 1666–1676. https://doi.org/10.1128/IAI.72.3.1666-1676.2004
Mitchell, R. E., Young, S. A., & Bender, C. L. (1994). Coronamic acid, an intermediate in coronatine biosynthesis by Pseudomonas syringae. *Phytochemistry*, *35*(2), 343–348. https://doi.org/10.1016/S0031-9422(00)94761-7
Monk, J. M., Charusanti, P., Aziz, R. K., Lerman, J. A., Premyodhin, N., Orth, J. D., Feist, A. M., & Palsson, B. (2013). Genome-scale metabolic reconstructions of multiple Escherichia coli strains highlight strain-specific adaptations to nutritional environments. *Proceedings of the National Academy of Sciences of the United States of America*, *110*(50), 20338–20343. https://doi.org/10.1073/pnas.1307797110
Morel, J. B., & Dangl, J. L. (1997). The hypersensitive response and the induction of cell death in plants. *Cell Death and Differentiation*, *4*(8), 671–683. https://doi.org/10.1038/sj.cdd.4400309
Nelson, C. E., Huang, W., Brewer, L. K., Nguyen, A. T., Kane, M. A., Wilks, A., & Oglesby-Sherrouse, A. G. (2019a). Proteomic Analysis of the Pseudomonas aeruginosa Iron Starvation Response Reveals PrrF Small Regulatory RNA-Dependent Iron Regulation of Twitching Motility, Amino Acid Metabolism, and Zinc Homeostasis Proteins. *Journal of Bacteriology*, *201*(12). https://doi.org/10.1128/JB.00754-18
Nelson, C. E., Huang, W., Brewer, L. K., Nguyen, A. T., Kane, M. A., Wilks, A., & Oglesby-Sherrouse, A. G. (2019b). Proteomic Analysis of the Pseudomonas aeruginosa Iron Starvation Response Reveals PrrF Small Regulatory RNA-Dependent Iron Regulation of Twitching Motility, Amino Acid Metabolism, and Zinc Homeostasis Proteins. *Journal of Bacteriology*, *201*(12), 1–23. https://doi.org/10.1128/JB.00754-18
Nobori, T., Velásquez, A. C., Wu, J., Kvitko, B. H., Kremer, J. M., Wang, Y., He, S. Y., & Tsuda, K. (2018a). Transcriptome landscape of a bacterial pathogen under plant immunity. *Proceedings of the National Academy of Sciences of the United States of America*, *115*(13), E3055–E3064. https://doi.org/10.1073/pnas.1800529115
Nobori, T., Velásquez, A. C., Wu, J., Kvitko, B. H., Kremer, J. M., Wang, Y., He, S. Y., & Tsuda, K. (2018b). Transcriptome landscape of a bacterial pathogen under plant immunity. *Proceedings of the National Academy of Sciences of*

the United States of America, *115*(13), E3055–E3064. https://doi.org/10.1073/pnas.1800529115

Oberhardt, M. A., Puchałka, J., Fryer, K. E., Martins dos Santos, V. A. P., & Papin, J. A. (2008). Genome-scale metabolic network analysis of the opportunistic pathogen Pseudomonas aeruginosa PAO1. *Journal of Bacteriology*, *190*(8), 2790–2803. https://doi.org/10.1128/JB.01583-07

Oberhardt, M. A., Puchałka, J., Fryer, K. E., Martins Dos Santos, V. A. P., & Papin, J. A. (2008). Genome-scale metabolic network analysis of the opportunistic pathogen Pseudomonas aeruginosa PAO1. *Journal of Bacteriology*, *190*(8), 2790–2803. https://doi.org/10.1128/JB.01583-07

Pacheco, A. R., Munera, D., Waldor, M. K., Sperandio, V., & Ritchie, J. M. (2012). Fucose sensing regulates bacterial intestinal colonization. *Nature*, *492*(7427), 113–117. https://doi.org/10.1038/nature11623

Palmer, D. A., & Bender, C. L. (1993). Effects of environmental and nutritional factors on production of the polyketide phytotoxin coronatine by Pseudomonas syringae pv. glycinea. *Applied and Environmental Microbiology*, *59*(5), 1619–1626. https://doi.org/10.1128/aem.59.5.1619-1626.1993

Panchal, S., Roy, D., Chitrakar, R., Price, L., Breitbach, Z. S., Armstrong, D. W., & Melotto, M. (2016). Coronatine facilitates pseudomonas syringae infection of arabidopsis leaves at night. *Frontiers in Plant Science*, *7*(JUNE2016), 1–11. https://doi.org/10.3389/fpls.2016.00880

Park, D. H., Mirabella, R., Bronstein, P. A., Preston, G. M., Haring, M. A., Lim, C. K., Collmer, A., & Schuurink, R. C. (2010). Mutations in γ-aminobutyric acid (GABA) transaminase genes in plants or Pseudomonas syringae reduce bacterial virulence. *Plant Journal*, *64*(2), 318–330. https://doi.org/10.1111/j.1365-313X.2010.04327.x

Parry, R. J., Mhaskar, S. V, Lin, M.-T., Walker, A. E., & Mafoti, R. (1994). Investigations of the biosynthesis of the phytotoxin coronatine. *Canadian Journal of Chemistry*, *72*(1), 86–99. https://doi.org/10.1139/v94-014

Preston, G., Deng, W. L., Huang, H. C., & Collmer, A. (1998). Negative regulation of hrp genes in Pseudomonas syringae by hrpV. *Journal of Bacteriology*, *180*(17), 4532–4537. https://doi.org/10.1128/jb.180.17.4532-4537.1998

Quiñones, B., Dulla, G., & Lindow, S. E. (2005). Quorum sensing regulates exopolysaccharide production, motility, and virulence in Pseudomonas syringae. *Molecular Plant-Microbe Interactions*, *18*(7), 682–693. https://doi.org/10.1094/MPMI-18-0682

Richelle, A., Joshi, C., & Lewis, N. E. (2019). Assessing key decisions for transcriptomic data integration in biochemical networks. *PLoS Computational Biology*, *15*(7), 1–18. https://doi.org/10.1371/journal.pcbi.1007185

Rico, A., & Preston, G. M. (2008). Pseudomonas syringae pv. tomato DC3000 uses constitutive and apoplast-induced nutrient assimilation pathways to catabolize nutrients that are abundant in the tomato apoplast. *Molecular Plant-Microbe Interactions*, *21*(2), 269–282. https://doi.org/10.1094/MPMI-

21-2-0269
Schachterle, J. K., & Sundin, G. W. (2019). The leucine-responsive regulatory protein lrp participates in virulence regulation downstream of small RNA ArcZ in Erwinia amylovora. *MBio*, *10*(3). https://doi.org/10.1128/mBio.00757-19
Seaver, S. M. D., Liu, F., Zhang, Q., Jeffryes, J., Faria, J. P., Edirisinghe, J. N., Mundy, M., Chia, N., Noor, E., Beber, M. E., Best, A. A., DeJongh, M., Kimbrel, J. A., D'haeseleer, P., McCorkle, S. R., Bolton, J. R., Pearson, E., Canon, S., Wood-Charlson, E. M., … Henry, C. S. (2021). The ModelSEED Biochemistry Database for the integration of metabolic annotations and the reconstruction, comparison and analysis of metabolic models for plants, fungi and microbes. *Nucleic Acids Research*, *49*(D1), D575–D588. https://doi.org/10.1093/nar/gkaa746
Shao, X., Tan, M., Xie, Y., Yao, C., Wang, T., Huang, H., Zhang, Y., Ding, Y., Liu, J., Han, L., Hua, C., Wang, X., & Deng, X. (2021). Integrated regulatory network in Pseudomonas syringae reveals dynamics of virulence. *Cell Reports*, *34*(13), 108920. https://doi.org/10.1016/j.celrep.2021.108920
Song, M., Kim, H. J., Eun, Y. K., Shin, M., Hyun, C. L., Hong, Y., Joon, H. R., Yoon, H., Ryu, S., Lim, S., & Choy, H. E. (2004). ppGpp-dependent stationary phase induction of genes on Salmonella pathogenicity island 1. *Journal of Biological Chemistry*, *279*(33), 34183–34190. https://doi.org/10.1074/jbc.M313491200
Stauber, J. L., Loginicheva, E., & Schechter, L. M. (2012). Carbon source and cell density-dependent regulation of type III secretion system gene expression in Pseudomonas syringae pathovar tomato DC3000. *Research in Microbiology*, *163*(8), 531–539. https://doi.org/10.1016/j.resmic.2012.08.005
Sturm, A., Heinemann, M., Arnoldini, M., Benecke, A., Ackermann, M., Benz, M., Dormann, J., & Hardt, W.-D. (2011). The Cost of Virulence: Retarded Growth of Salmonella Typhimurium Cells Expressing Type III Secretion System 1. *PLoS Pathogens*, *7*(7), e1002143. https://doi.org/10.1371/journal.ppat.1002143
Subashchandrabose, S., LeVeque, R. M., Wagner, T. K., Kirkwood, R. N., Kiupel, M., & Mulks, M. H. (2009). Branched-chain amino acids are required for the survival and virulence of Actinobacillus pleuropneumoniae in swine. *Infection and Immunity*, *77*(11), 4925–4933. https://doi.org/10.1128/IAI.00671-09
Tang, X., Xiao, Y., Zhou, J., Zheng, X. Y., Spivey, N. W., Zeng, W., Liu, P. P., Fu, Z. Q., Klessig, D. F., He, S. Y., Dong, X., Chatterjee, A. K. A., Cui, Y., Yang, H., Collmer, A., Alfano, J. R., Chatterjee, A. K. A., Djonović, S., Urbach, J. M., … Rahme, L. G. (2006). Regulation of the type III secretion system in phytopathogenic bacteria. *Proceedings of the National Academy of Sciences of the United States of America*, *19 11*(2), 1159–1166. https://doi.org/10.1094/MPMI-19-1159
Tani, T. H., Khodursky, A., Blumenthal, R. M., Brown, P. O., & Matthews, R. G. (2002). Adaptation to famine: A family of stationary-phase genes revealed by microarray analysis. *Proceedings of the National Academy of Sciences of*

the United States of America, *99*(21), 13471–13476. https://doi.org/10.1073/pnas.212510999

Thaw, P., Sedelnikova, S. E., Muranova, T., Wiese, S., Ayora, S., Alonso, J. C., Brinkman, A. B., Akerboom, J., van der Oost, J., & Rafferty, J. B. (2006). Structural insight into gene transcriptional regulation and effector binding by the Lrp/AsnC family. *Nucleic Acids Research*, *34*(5), 1439–1449. https://doi.org/10.1093/nar/gkl009

Thiele, I., & Palsson, B. (2010). A protocol for generating a high-quality genome-scale metabolic reconstruction. *Nature Protocols*, *5*(1), 93–121. https://doi.org/10.1038/nprot.2009.203

Tomassetti, M., Garavaglia, B. S., Vranych, C. V., Gottig, N., Ottado, J., Gramajo, H., & Diacovich, L. (2018). 3-Methylcrotonyl Coenzyme A (CoA) carboxylase complex is involved in the Xanthomonas citri subsp. Citri lifestyle during citrus infection. *PLoS ONE*, *13*(6), 1–23. https://doi.org/10.1371/journal.pone.0198414

Toruño, T. Y., Shen, M., Coaker, G., & Mackey, D. (2019). Regulated disorder: Posttranslational modifications control the RIN4 plant immune signaling hub. *Molecular Plant-Microbe Interactions*, *32*(1), 56–64. https://doi.org/10.1094/MPMI-07-18-0212-FI

Tsuda, K., & Katagiri, F. (2010). Comparing signaling mechanisms engaged in pattern-triggered and effector-triggered immunity. *Current Opinion in Plant Biology*, *13*(4), 459–465. https://doi.org/10.1016/j.pbi.2010.04.006

Tsuda, K., Sato, M., Glazebrook, J., Cohen, J. D., & Katagiri, F. (2008). Interplay between MAMP-triggered and SA-mediated defense responses. *Plant Journal*, *53*(5), 763–775. https://doi.org/10.1111/j.1365-313X.2007.03369.x

Turner, S. E., Pang, Y. Y., O'Malley, M. R., Weisberg, A. J., Fraser, V. N., Yan, Q., Chang, J. H., & Anderson, J. C. (2020). A DeoR-Type Transcription Regulator Is Required for Sugar-Induced Expression of Type III Secretion-Encoding Genes in Pseudomonas syringae pv. Tomato DC3000. *Molecular Plant-Microbe Interactions*, *33*(3), 509–518. https://doi.org/10.1094/MPMI-10-19-0290-R

Verhage, A., Vlaardingerbroek, I., Raaymakers, C., Van Dam, N. M., Dicke, M., Van Wees, S. C. M., & Pieterse, C. M. J. (2011). Rewiring of the Jasmonate signaling pathway in arabidopsis during insect herbivory. *Frontiers in Plant Science*, *2*(SEP), 1–12. https://doi.org/10.3389/fpls.2011.00047

Wallon, G., Yamamoto, K., Kirino, H., Yamagishi, A., Lovett, S. T., Petsko, G. A., & Oshima, T. (1997). Purification, catalytic properties and thermostability of 3-isopropylmalate dehydrogenase from Escherichia coli. *Biochimica et Biophysica Acta - Protein Structure and Molecular Enzymology*, *1337*(1), 105–112. https://doi.org/10.1016/S0167-4838(96)00157-4

Weingart, H., Stubner, S., Schenk, A., & Ullrich, M. S. (2004). Impact of temperature on in planta expression of genes involved in synthesis of the Pseudomonas syringae phytotoxin coronatine. *Molecular Plant-Microbe Interactions*, *17*(10), 1095–1102. https://doi.org/10.1094/MPMI.2004.17.10.1095

Wildermuth, M. C., Dewdney, J., Wu, G., & Ausubel, F. M. (2002). Erratum:

corrigendum: Isochorismate synthase is required to synthesize salicylic acid for plant defence. *Nature*, *417*(6888), 571–571. https://doi.org/10.1038/417571a

Xin, X. F., Kvitko, B., & He, S. Y. (2018). Pseudomonas syringae: What it takes to be a pathogen. In *Nature Reviews Microbiology* (Vol. 16, Issue 5, pp. 316–328). Nature Publishing Group. https://doi.org/10.1038/nrmicro.2018.17

Yamada, K., Saijo, Y., Nakagami, H., & Takano, Y. (2016). Regulation of sugar transporter activity for antibacterial defense in Arabidopsis. *Science*, *354*(6318), 1427–1430. https://doi.org/10.1126/science.aah5692

Yu, I. C., Parker, J., & Bent, A. F. (1998). Gene-for-gene disease resistance without the hypersensitive response in Arabidopsis dnd1 mutant. *Proceedings of the National Academy of Sciences of the United States of America*, *95*(13), 7819–7824. https://doi.org/10.1073/pnas.95.13.7819

Yu, X., Lund, S. P., Scott, R. A., Greenwald, J. W., Records, A. H., Nettleton, D., Lindow, S. E., Gross, D. C., & Beattie, G. A. (2013). Transcriptional responses of Pseudomonas syringae to growth in epiphytic versus apoplastic leaf sites. *Proceedings of the National Academy of Sciences of the United States of America*, *110*(5). https://doi.org/10.1073/pnas.1221892110

Zeier, J. (2013). New insights into the regulation of plant immunity by amino acid metabolic pathways. *Plant, Cell and Environment*, *36*(12), 2085–2103. https://doi.org/10.1111/pce.12122

Zhang, X., Khadka, P., Puchalski, P., Leehan, J. D., Rossi, F. R., Okumoto, S., Pilot, G., & Danna, C. H. (2022). MAMP-elicited changes in amino acid transport activity contribute to restricting bacterial growth. *Plant Physiology*, 1–17. https://doi.org/10.1093/plphys/kiac217

Zhang, X., Tubergen, P. J., Agorsor, I. D. K., Khadka, P., Tembe, C., Denbow, C., Collakova, E., Pilot, G., & Danna, C. H. (2023a). Elicitor-induced plant immunity relies on amino acids accumulation to delay the onset of bacterial virulence. *Plant Physiology*. https://doi.org/10.1093/plphys/kiad048

Zhang, X., Tubergen, P. J., Agorsor, I. D. K., Khadka, P., Tembe, C., Denbow, C., Collakova, E., Pilot, G., & Danna, C. H. (2023b). Elicitor-induced plant immunity relies on amino acids accumulation to delay the onset of bacterial virulence. *Plant Physiology*. https://doi.org/10.1093/plphys/kiad048

Zipfel, C., Robatzek, S., Navarro, L., Oakeley, E. J., Jones, J. D. G., Felix, G., & Boller, T. (2004). Bacterial disease resistance in Arabidopsis through flagellin perception. *Nature*, *428*(6984), 764–767. https://doi.org/10.1038/nature02485